2004-11-09

Geometric Acoustic Modeling of the LDS Conference Center

Heather Smith
Brigham Young University - Provo

GEOMETRIC ACOUSTIC MODELING OF THE

LDS CONFERENCE CENTER

by

Heather M. Smith

A thesis submitted to the faculty of

Brigham Young University

in partial fulfillment of the requirements for the degree of

Master of Science

Department of Physics & Astronomy

Brigham Young University

December 2004

BRIGHAM YOUNG UNIVERSITY

GRADUATE COMMITTEE APPROVAL

of a thesis submitted by

Heather M. Smith

This thesis has been read by each member of the following graduate committee and by majority vote has been found to be satisfactory.

_____	_____
Date	Timothy W. Leishman, Chair
_____	_____
Date	Scott D. Sommerfeldt
_____	_____
Date	Jonathan D. Blotter

BRIGHAM YOUNG UNIVERSITY

As chair of the candidate's graduate committee, I have read the thesis of Heather M. Smith in its final form and have found that (1) its format, citations and bibliographical style are consistent and acceptable and fulfill university and department style require-ments; (2) its illustrative materials including figures, tables, and charts are in place; and (3) the final manuscript is satisfactory to the graduate committee and is ready for submission to the university library.

Date	Timothy W. Leishman Chair, Graduate Committee

Accepted for the Department

Ross L. Spencer Graduate Coordinator

Accepted for the College

G. Rex Bryce Associate Dean, College of Physical and Mathematical Sciences

ABSTRACT

GEOMETRIC ACOUSTIC MODELING OF THE

LDS CONFERENCE CENTER

Heather M. Smith

Department of Physics & Astronomy

Master of Science

This thesis discusses the process of modeling a 21,000 seat fan-shaped auditorium using methods of geometric acoustics. Two commercial geometric acoustics software packages were used in the research: CATT-Acoustic™ 8.0 and EASE™ 4.1. The process first included creating preliminary models of the hall using published absorption coefficients for its surfaces and approximate scattering coefficients based on current best-known techniques. A detailed analysis determined the minimum numbers of rays needed in both packages to produce reliable results with these coefficient values. It was found that 100,000 rays were needed for CATT™ and 500,000 rays were needed for EASE™. Analysis was also done to determine whether the model was sensitive to the scattering coefficients of the seating areas. It was found that most acoustic

parameters were not significantly affected by scattering coefficient variation. The models were subsequently refined by including measured absorption coefficients of dominant surfaces in the hall: the seats, audience and suspended absorptive panels. Comparisons were made between measurements made in the hall and results from the computer models with impulse responses, acoustic parameters, and auralizations. The results have shown that the models have been successful at representing characteristics of the hall at some positions but less successful at representing them at other positions. Comparisons have shown that positions on the rostrum were especially difficult positions to model in this hall. Significant differences were not found between the preliminary models and the refined models. There was not significant evidence showing that either the EASE™ or the CATT™ model was more successful in accurately representing the acoustical conditions of the hall. The results from this research suggest that more work must be done to improve the modeling capabilities of these packages for this application.

ACKNOWLEDGMENTS

- Sarah Rollins for coding many of the acoustic parameters and for other assistance she has given me.

- Members of the ARG for their help with the absorption coefficient measurements, including those who built the surrounding barriers, acted as audience members, moved heavy objects, and taught me how to use the equipment.

- Bengt-Inge Dalenbäck (CATT-Acoustic™ author) for his useful comments made throughout the project.

- My husband, Brandon, for his unfailing support and confidence in me.

- My parents and family for their faith and prayers in my behalf.

Table of Contents

List of Tables

List of Figures

xviii

1   Introduction

An important part of modern room acoustic design and analysis involves computer modeling of a room before it is built. This tool enables both investigation of acoustic characteristics of the hall and qualitative impressions of how it will sound. Unfortunately, such modeling was never completed for the LDS Conference Center prior to its construction. Had it been completed, some of its acoustical problems might have been prevented.

A research project was undertaken by the BYU Acoustics Research Group (ARG) to study the LDS Conference Center auditorium. In connection with this project, computer models were created in an effort to better understand the existing acoustical conditions of the hall as well as to aid in any future improvements of the hall. The purpose of this thesis is to present the research done on the computer modeling portion of this project.

The main construction of the LDS Conference Center was completed by April of 2000. After its construction some acoustical problems were noticed to be present in the hall, including strong perceived echoes near the front of the hall, marginal speech intelligibility, uneven sound coverage, and poor acoustic ensemble for choir and orchestra members. The immense size and shape of the hall are some of the primary causes for these problems.

The Conference Center auditorium is a fan-shaped hall that seats 21,000 people (see Figure 1.1). Large halls (halls with more than 2,500 seats) are typically problematic from an acoustical standpoint because they provide less intimacy, less acoustic energy per listener and less energetic lateral reflections.[1] Fan-shaped halls also cause other acoustical problems, including a poor sense of spatial impression and envelopment for music listening, few lateral reflections except near the rear of the hall, a lack of intermediate reflections (around 40-180 ms), and a poor sense of reverberation.[1] The size and general shape of the Conference Center were nearly unavoidable because it was intended to seat so many people with reasonable sight lines and proximity to speakers. Many of the acoustical problems, however, could have been avoided or at least lessened with greater attention to the acoustical problems associated with the general hall design.

The primary goal of this research was to accurately model the existing acoustical characteristics of the Conference Center auditorium using commercial software packages CATT-Acoustic™ 8.0 and EASE™ 4.1. This research was limited to the use of these two tools. A perfect model of the Conference Center auditorium was not expected because of the known limitations of geometric acoustic modeling, but the goal was to create the best models possible within the capabilities of these packages. A secondary goal in

Figure 1.1. Photograph of the Conference Center of The Church of Jesus Christ of Latter-day Saints,

© Intellectual Reserve, Inc., Reproduced by Permission.[2]

the research was to use physical principles to find accurate absorption and scattering coefficients to input into the models. It was hoped that if the absorption and scattering coefficients were based upon physical principles, a more accurate model of the Conference Center auditorium acoustics would result.

Perhaps the most significant contribution of this research is the computer models themselves. The challenge of creating computer models of such a large, acoustically detailed auditorium is a daunting task that has seldom, if ever, been attempted by acousticians. This research also presents a detailed analysis of the number of rays needed to obtain accurate acoustic parameter values for the hall using both CATT-Acoustic™ and EASE™. Previous published analyses on the number of rays needed for geometric acoustic packages do not contain the depth of this study. Another contribution of the research is a complete study on the sensitivity of the acoustic parameters to the variation of scattering coefficients. This is significant because the extent to which a model shows variation in the results when scattering coefficients are varied demonstrates the level of accuracy at which the scattering coefficients need to be calculated when being used in the model.

This thesis will first present background information, including sections on computer modeling techniques, computer algorithm descriptions, and

measurement techniques used in the research. A description of how the preliminary computer models were created is then presented, followed by a description of the refined computer models. The preliminary and refined models are subsequently compared and results are discussed. Final conclusions are then offered.

2   Computer Modeling Techniques

In the past, an acoustical consultant given the task of designing an auditorium would sit down with a drawing of the room and a pencil to trace sound rays around the room to construct sound reflections.[3] Another well-tried method for the acoustical design of halls was to build a smaller, geometrically scaled model of the hall under consideration. Wave propagation was studied in these scale models in an effort to predict what the actual room would sound like under certain conditions.

These tools are still available for the acoustical design of halls and still used in practice.[4,5,6] However, with the introduction of modern computers, digital simulation of sound propagation in enclosures has become practical. Many authors attribute the invention of computer modeling in room acoustics to Schroeder[7] and the first practical implementation to Krokstad, et al.[8] Since then, numerous authors have developed their own computer algorithms and some even feel that computer simulations are taking over the part of scale modeling in consulting.

The advantages of computer modeling over scale modeling are discussed by Rindel[9] and Kuttruff.[10] One of the advantages is that computer modeling is more flexible than a scale model because it is easier to make

changes to the geometry and the surface materials. Often scale modeling is very expensive and in many ways computer modeling is much more cost effective.

This chapter presents background information on computer modeling techniques used by acousticians. First, the geometric acoustics assumptions will be discussed along with methods used in computer modeling. A discussion on diffuse reflection will follow. Auralization methods will then be presented and finally, the boundary element method will be explained.

2.1   *Geometric Acoustics*

Like other phenomena in physics, sound can be described in different ways. Two of the most common descriptions include the wave and ray model approaches. To describe sound using the wave model approach, solutions to the wave equation are found analytically (when possible) or are approximated using methods such as the Finite Element Method (FEM) or the Boundary Element Method (BEM). The Boundary Element Method will be discussed in more detail later in this chapter. These methods are often not practical for architectural acoustics because the number of modes in a room increases rapidly to an unwieldy value as frequency increases. As a result, these methods are restricted to studying small rooms and low frequencies.[9]

The ray model approach describes sound as a small segment of a spherically diverging wave which originates from a point and propagates in a specified direction.[11] This description has lead to more practical methods for architectural acoustics, namely ray-tracing and image-source methods. These methods fall under the general realm of geometric acoustics. They involve a simplification based on a special solution to the wave equation that is valid when the wavelength of sound is small compared to overall reflecting surface dimensions and large compared to surface irregularities and curvature.[12] Geometric acoustics does not account for diffraction but assumes rays propagate in straight lines.[11] It also assumes absorption at surfaces is independent of angle of incidence.[13] Interference is not taken into account, meaning that when several sound field components are superposed, their phase relationships are not considered. This simplification is valid when the different components are incoherent with respect to each other, which is usually true when the components have broad frequency spectra.[11] In spite of these limitations associated with geometric acoustics, the scheme provides significant and useful information about the sound characteristics of a room.

2.2   *Geometric Acoustics Methods*

Two classical methods are used within the geometric acoustics realm:

ray-tracing and image-source methods. In this section, both are discussed in detail, along with their advantages and disadvantages. Hybrid methods, which combine elements from both methods, are also discussed.

2.2.1   Ray-Tracing Method

In the ray-tracing method, a source emits a large number of rays in various directions (Figure 2.1). The rays propagate around the room, losing energy at each reflection according to the absorption coefficient of the pertinent surface. They are specularly reflected at each surface, meaning their new directions of propagation are determined according to the law of mirrors[14] (i.e., angle of incidence equals angle of reflection). As each ray impinges on a "counter" (a plane or spherical area defined in the region of the receiver) its energy, direction, and arrival time are recorded. After a certain time has elapsed, the temporal distribution of ray impacts is used as an approximation to
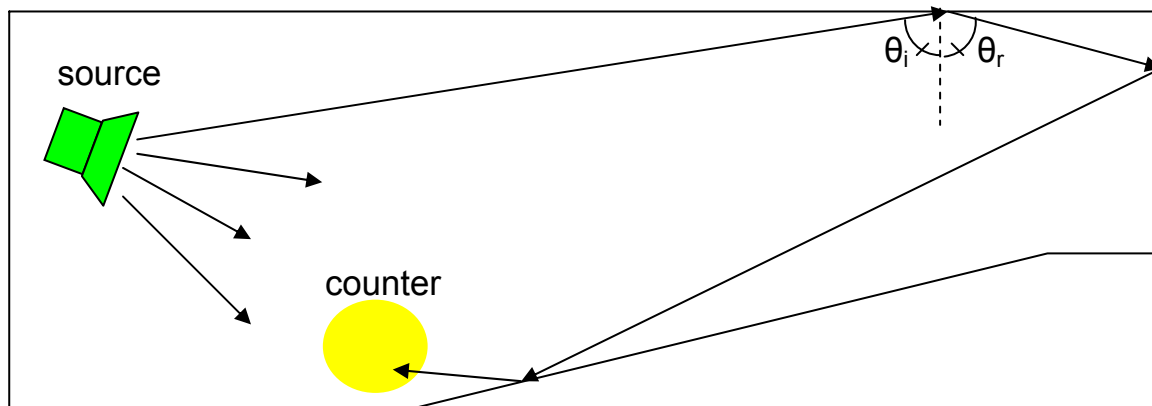
Figure 2.1. Ray-tracing method.[3]

the impulse response of the room.[9,12,15]

Some advantages of this method include its ability to include curved surfaces as well as scattering into the algorithm. Neither of these are possible with the image-source method (as will be discussed later). Another advantage is that the method is fairly quick and easy to calculate. Vorländer[16] gave the following estimation for the calculation time of the ray-tracing method:

$$t_{calc} \approx N\bar{n}(n_w + n_r)t_0 t_{IR},$$

(2.1)

where N is the number of rays, $\bar{n}$ is the mean reflection rate (= $cS/4V$), n_w is the number of walls of the room model, n_r is the number of receivers, c is the sound speed, S is the room surface area, V is the room volume, t_{IR} is the desired length of the impulse response, and t_0 is an elementary time depending on the computer speed. It can be seen from the equation that the calculation time goes up linearly with the length of the impulse response.

The main limitation of this method seems to be its inaccuracy in representing a "true" impulse response. Rindel[9] states that there is a risk that some reflections that are collected will be false reflections while other reflection paths will not be included. Kuttruff[15] argues that the results from the ray-tracing method represent a temporal energy distribution rather than a true impulse response.

2.2.2 Image-Source Method

The image-source or mirror-image method is based on the idea that a sound ray that is reflected from a planar surface can be thought of as originating from a source which is the mirror image of the original sound source as formed by the planar surface (Figure 2.2). The mirroring process can be extended to enclosures with many planar surfaces, yielding higher order reflections due to mirror images of image sources and so forth. In theory, the final infinite pattern of images represents the original room. The sound field in the room can be found by summing the contributions of all free-space image sources. If the original sound source generates a Dirac impulse, this process yields the impulse response of the room.[15]
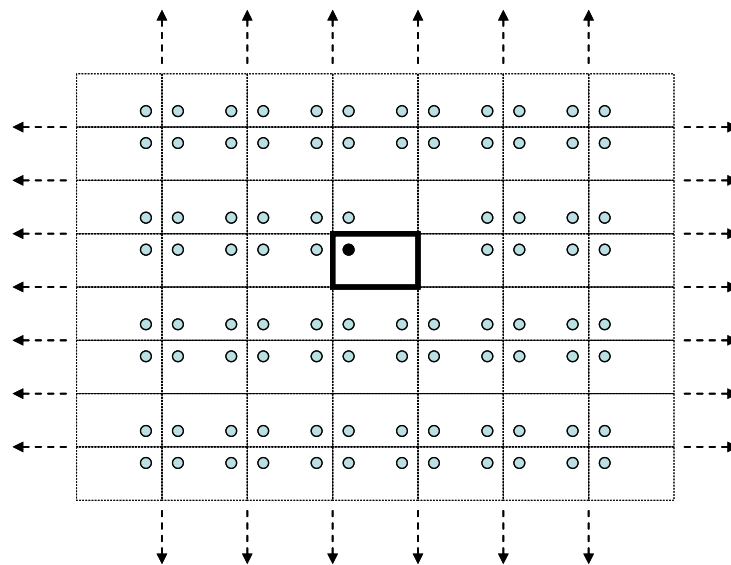
Figure 2.2. 2-D rectangular room (dark box) with source (black circle) and image sources (lighter circles).

Notably, this method assumes each surface is perfectly planar. The number of images grows exponentially with the number of surfaces, number of sound sources, and the desired reflection order. Vorländer[16] also gave an estimation for the calculation time of the image-source method:

$$t_{calc} \approx \frac{n_w}{n_w - 2}[(n_w - 1)^{t_{IR}\bar{n}} - 1]n_r t_0.$$

(2.2)

It can be seen from this equation that the calculation time of the classical image-source model increases exponentially with the length of the impulse response. Thus, required numerical calculations and computation times can easily become unwieldy. In spite of these limitations, the method is very accurate and the impulse response can be calculated with extremely high time resolution.[16] In fact, Kuttruff argues that this method yields more information than is significant from a psychoacoustic point of view.[15]

2.2.3   Hybrid Methods

Because of the inherent limitations in the ray-tracing and image-source methods, hybrid algorithms have been written to incorporate and optimize the positive characteristics of each. These hybrid methods may contain variations on the general methods (e.g., cone, beam or pyramid tracing as opposed to ray-tracing) and are usually optimized to speed up computation time without

serious loss of accuracy. Conversely, they may increase accuracy without serious extension of computation time.

Many hybrid algorithms include a visibility test which uses ray-tracing to determine valid image sources.[16,9] Each ray that is detected by a receiver is associated with a "visible" image source. Often these "visible" sources are found by tracing back from the receiver towards the image source. In order to keep track of the valid image sources used, an 'image tree' is created.

Hybrid methods are frequently divided into early and late reflections with some transition order defined. Often the image-source method is used for the early part of the impulse response (along with a visibility test), while some type of ray-tracing is used for the late part of the impulse response.

Vorländer[16] gave the following estimate for the calculation time of a hybrid algorithm:

$$t_{CALC} = (\frac{4c^2 \overline{nt}_{IR}^3}{r_r^2})(n_w + n_r)t_0 \tag{2.3}$$

where r_r is the receiver volume and all other variables are defined in the paragraph following Eq. (2.1). It should be noted that this is an estimate of the calculation time for only one type of hybrid algorithm and is not general to all hybrid algorithms. It can be seen that the calculation time no longer increases exponentially with t_{IR}. Figure 2.3 shows an example of how the calculation
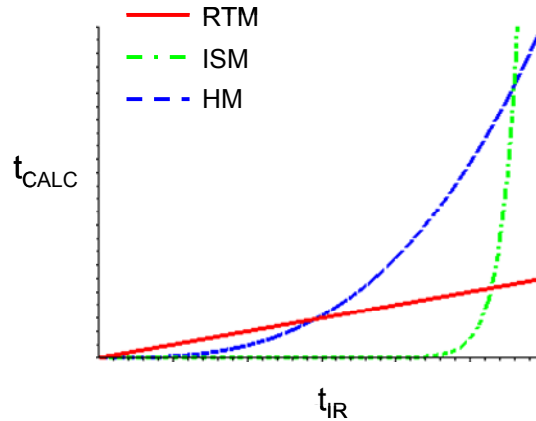
Figure 2.3. Calculation time vs. impulse response time for the ray-tracing method (RTM), image-source method (ISM), and a hybrid method (HM).

time varies with the length of the impulse response for the three methods mentioned.

It can be seen from Figure 2.3 that for large t_{IR}, the ray-tracing method gives the shortest calculation time, the hybrid method gives the next shortest, and the image-source method gives the longest. Because hybrid algorithms optimize the positive characteristics of both the ray-tracing method and the image-source method, most programmers use a hybrid algorithm in their development of room acoustic computer modeling software.

2.3 Diffuse Reflection

Most authors agree that diffuse reflection is important to include in computerized room acoustic predictions. Dalenbäck explains possible problems with using only specular reflections in computerized room acoustic

predictions, including severe overestimation of reverberation time and unnatural decay characteristics in binaural room impulse responses.[17]   The results of a round robin comparison of room acoustic computer simulation programs have also suggested that diffuse reflections are necessary to include in computer modeling packages in order to obtain accurate results.[18]   The author states that only three out of fourteen programs tested produced "unquestionably reliable results."   It was noted that these three programs required neither extremely high calculation times nor extremely detailed room geometries. What all three programs did have in common, however, was the inclusion of diffuse reflection.

Because of this research, most geometric acoustic packages began (or continued) to include diffuse reflections into their algorithms. Subsequently, two coefficients are used to describe diffuse reflections.   The scattering coefficient is used to characterize the degree of scattering due to the roughness of a surface while the diffusion coefficient is used to characterize the uniformity of the scattering from a surface.[19] Many authors agree that it is the scattering coefficient that is appropriate for use in room acoustic computer models.[20,21]

2.3.1   Scattering Coefficient Definition

As depicted in Figure 2.4, Vorlander and Mommertz[22] define the scattering coefficient as the ratio of the non-specularly reflected sound energy to the total reflected energy:

$$\delta = \frac{\text{non-specularly reflected sound energy}}{\text{total reflected sound energy}} \qquad (2.4)$$

If the incident energy is normalized to 1, the total reflected sound energy will be *1-α*, where *α* is the absorption coefficient. The component of the sound energy that is reflected specularly will be *(1-α)(1-δ)* and the component that is reflected non-specularly (or scattered) will be *(1-α) δ*.

2.3.2   Methods of Including Diffuse Reflection in Geometric

Acoustic Packages

Diffuse reflections are included in geometric acoustical packages in
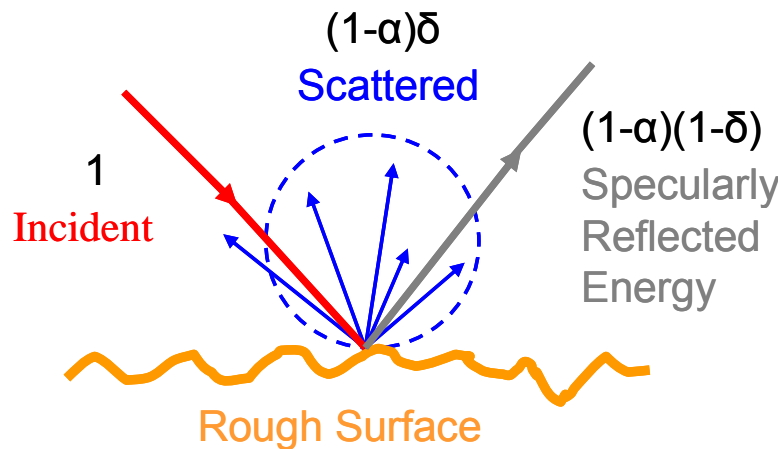
Figure 2.4. Scattering from rough surface.[23]

17

various ways. Dalenbäck[24] explains that a straight-forward approach for including diffuse reflections using a ray-tracing procedure is to let every ray incident upon a diffusing surface create a new source that sends out rays for the diffusely reflected sound. However, because this approach would result in an exponential calculation time dependence, it is not very practical.

Dalenbäck, et al.[25] present a discussion on other methods of including diffuse reflection in computer modeling packages. A description of what is probably the most common method follows. When a ray encounters a surface, a random number (between 0 and 1) is generated. If the number is lower than the scattering coefficient assigned to that surface, the scattered ray direction is randomized (other random numbers are generated to determine its direction); otherwise the ray is reflected specularly. This method is referred to throughout this thesis as the random number method for scattering.

In many cases the scattered energy is randomized according to Lambert's law, an ideal model of totally diffuse reflections.[26] Lambert's law is correct for high frequency, point, incoherent scattering.[27] Assume that an area element dS is illuminated by a bundle of parallel rays of intensity I_0 making an angle θ_0 to the wall normal (see Figure 2.5). Then according to Lambert's law, the intensity of the sound which is scattered in a direction characterized by an angle θ and
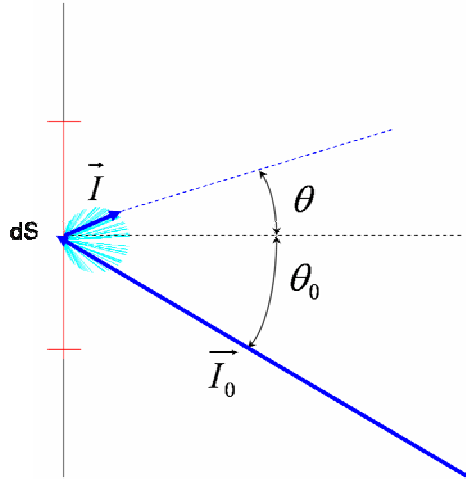
Figure 2.5. Lambert's law for an acoustically rough surface.[26]

measured at a distance r from dS, is given as

$$I(r) = I_0 dS \frac{\cos\theta \cos\theta_0}{\pi r^2}.$$ (2.5)

In Figure 2.5, the lengths of the incoming and outgoing rays are proportional to their intensities. It should be noted that Equation (2.5) holds assuming the wall has no absorption. If it does have absorption, it must be multiplied by the factor $1-\alpha$, where α is the absorption coefficient of the surface.

2.3.3   Methods of Approximating Scattering Coefficients

Unfortunately, there is not a clear relationship between most physical properties of a surface and the scattering coefficient associated with that surface. As a result, scattering coefficients are usually approximated with some ambiguity; different users approximate them using different methods. Lam[28]

showed that scattering coefficients actually depend on the modeling package employed, because all modeling packages use different algorithms for scattering.

The CATT-Acoustic™ manual[29] provides guidelines for approximating the scattering coefficients of surfaces as follows. A minimum of 20% scattering is recommended for average-size, flat, smooth surfaces (10% for larger flat, smooth surfaces). In contrast, 30% to 70% is recommended for an audience (30% for the 125 Hz octave band and increasing up to 70% for the 4 kHz octave band). For rough surfaces, a high value (80%) should be assigned where the roughness scale is of the order of the wavelength (i.e. if the roughness is about 0.3 m, the 1 kHz diffusion should be set high). If in doubt, it is better to assign scattering coefficients too high than too low. Automatic edge diffusion can be applied to reflectors, windows, cupboards, tables, etc. that often are flat and smooth and only give diffusion if their size is small in relation to the wavelength.

ODEON is another numerical acoustic package similar to CATT-Acoustic™. The ODEON manual[30] also gives recommendations for approximating the scattering coefficients. It recommends 10% to be assigned to large surfaces and smooth, rigid surfaces. It recommends 70% to be assigned to scattering surfaces such as the audience area in a concert hall. In general, it

20

recommends keeping the scattering coefficients between 10% and 70%. For rooms such as offices and classrooms, a minimum scattering coefficient of 30% is recommended due to small objects that are not accounted for directly in the models.

Other sources give different guidelines. For example, Gehrke[31] recommends a minimum value of 5% on surfaces. He also gives some recommendations for step-like structures and rectangular structures. Another common method in the literature is to vary the scattering coefficient on the surfaces of the models until the calculated reverberation time matches the measured reverberation time.[32] Cox, et al.[33] give an overview of other methods used to estimate scattering coefficients.

Clearly, various authors give diverging recommendations for approximating scattering coefficients. From this fact alone, it can be concluded that more work needs to be done to establish improved methods of determining these coefficients.

2.4   *Auralization*

After the impulse response of a room has been computed using the methods described in previous sections, it is often desirable to "auralize" the impulse response. Kleiner, Dalenbäck, and Svensson[34] give a definition for

auralization that has been cited in several other papers: "Auralization is the process of rendering audible, by physical or mathematical modeling, the sound field of a source in a space, in such a way as to simulate the binaural listening experience at a given position in the modeled space." A common analogy used to describe auralization is this: as visualization is to light, auralization is to sound.

Møller[35] explains two main techniques of auralizing sound fields (see Figure 2.6). The first technique is the free-field method wherein the sound field is simulated with several spaced loudspeakers arranged around a listener. Sound waves are generated to emanate from nearly the same direction as they would in the field being simulated. The other technique is the binaural method which uses the fact that human hearing creates three-dimensional sound images based only on sound pressures presented to each of the eardrums. On its way to a listener's ears, sound waves undergo diffraction around the
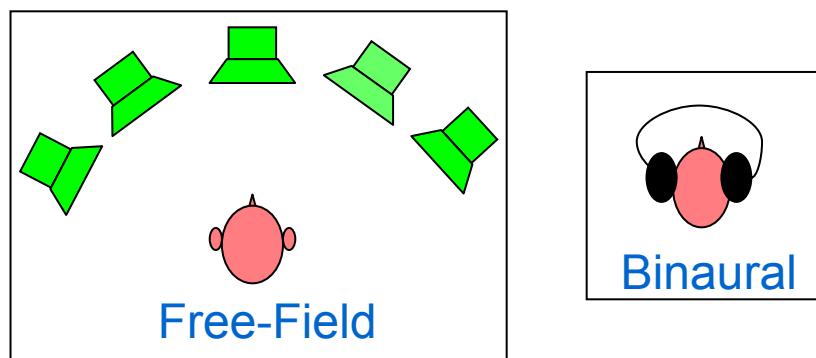
Figure 2.6. Free-field and binaural auralization.

listener's head and body.   The consequent filtering of the sound depends on the direction of the sound arriving at the listener and may include a delay between the two ears.   Human hearing perceives the direction of sound incidence based on this filtering.

In computer models, the binaural method of auralization is typically used because it only involves two signals (for the left and right ears) rather than a whole arrangement of loudspeakers.   In the remainder of this thesis, auralization accordingly refers to the binaural method of auralization only.

Head-related transfer functions (HRTFs) are often incorporated with these signals to enhance binaural listening quality. The diffraction around the head is taken into account in computer auralizations by convolving the calculated impulse responses with measured HRTFs. In reality, each listener has an individual HRTF and measured data for each listener should ideally be used in this process. The convolution of the impulse response with a measured HRTF yields what is called a Binaural Impulse Response (BIR) or Binaural Room Impulse Response (BRIR). As a result of the convolution, two impulse responses are generated for each listening position, one for each ear.

When listening to reproduced sound from computer-generated auralizations, it is desirable to have the sound from the right channel reach only

the right ear and sound from the left channel reach only the left ear. Unfortunately, when listening over loudspeakers in a room, sound from both loudspeakers reaches both ears. The inter-aural cross-talk cancellation (IACC) method uses the HRTFs and the angle to the loudspeakers from the listening position to create filters that effectively cancel the signal from the left channel to the right ear and from the right channel to the left ear (Figure 2.7).

To create an auralization, the BRIR is convolved with anechoically recorded music or speech samples. The auralization is best listened to over headphones or over loudspeakers (with inter-aural cross-talk cancellation) in an anechoic chamber. In this way, the room acoustical effects of the playback environment are minimized in order to enhance the simulation of the modeled room.
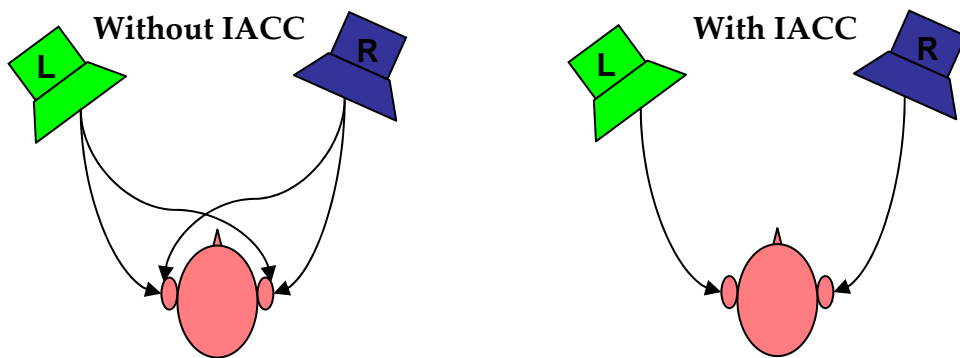
Figure 2.7. Inter-aural cross-talk cancellation.[36]

2.5   *Boundary Element Method*

In this research, the boundary element method (BEM) was used to compute the scattering coefficients of surfaces. This section provides a general description of BEM.   Details of its application to predicting scattering coefficients is given in Section 6.2.2.

Two different approaches are widely used with the Boundary Element Method: direct and indirect.[37]   The direct approach can only be used to investigate closed surfaces, while the indirect approach works for closed and open surfaces.[38]   This research uses the indirect approach, and a brief description of the method will be discussed here.

The indirect approach to the Boundary Element Method is able to solve the internal and external acoustic radiation problem simultaneously. The fluid on both sides of a closed or open surface is taken into account by using layer potential densities μ and σ defined as follows:

$$\mu = p^+ - p^-$$

(2.6)

$$\sigma = \frac{\partial p^+}{\partial n} - \frac{\partial p^-}{\partial n}$$

(2.7)

Here, μ is the difference between the outside and inside pressure on the surface and is called the jump of pressure or the double layer potential. In addition, σ is the difference between the outside and inside normal derivatives

on the surface and is called the jump of normal derivative of pressure or the single layer potential.[39] Finally p is the acoustic pressure, and n is the normal to the surface S. The + and – signs mark the two sides of the boundary.[38]

These layer potential densities are involved in the integral representation of the acoustic pressure at a field point X:[38,39]

$$p(X) = \int_S \left(\mu(Y) \frac{\partial G(X,Y)}{\partial n_y} - \sigma(Y) G(X,Y) \right) dS(Y) \tag{2.8}$$

Here, $\mu(Y)$ and $\sigma(Y)$ are the layer potential densities defined in Equations (2.6) and (2.7) at a point Y on the surface, S. Further, $G(X,Y)$ is the Green's function that is given by

$$G(X,Y) = \frac{e^{-ik|X-Y|}}{4\pi|X-Y|} \tag{2.9}$$

for three-dimensional problems (i.e., a point source) and by

$$G(X,Y) = -\frac{i}{4} H_0^2(k|X-Y|) \tag{2.10}$$

for two-dimensional problems (i.e., a line source). [38,39] Here, H_0^2 is the Hankel function of order 0 of the second kind.

Once the single and double layer potentials are known, the pressure at any point outside or inside the surface can be calculated. The single and double layer potentials are obtained by translating boundary conditions on the surface

S to constraints on the layer potentials. One of the following three boundary conditions is applied on the surface:[39]

1. Given pressure on the surface (Dirichlet boundary condition)

2. Given normal velocity on the surface (Neumann boundary condition)

3. Given normal admittance on the surface (Mixed boundary condition, the relation between pressure and normal velocity on the surface is given)

These boundary conditions are translated into the following conditions for the layer potentials on the surface *S*.[39]

1. Dirichlet boundary condition gives $\mu = 0, \sigma \neq 0$

2. Neumann boundary condition gives $\sigma = 0, \mu \neq 0$

3. Mixed boundary condition gives $\sigma + ik\beta\mu = 0, \mu \neq 0$

Using a variational formulation, the solution is calculated based on the above conditions for the layer potentials. The variational approach used in this calculation is discussed in detail in the SYSNOISE™ Theoretical Manual.[39]

3   Computer Algorithms

This chapter gives a description of the current CATT-Acoustic™ (i.e.,
CATT™) and EASE™ algorithms. Bork[40] describes room acoustic software
packages as "black boxes," in the sense that the user does not have access to the
source code and only has control of some input variables to the software. Little
of what is inside the prediction methods is published due to marketing
competition. This chapter, therefore, explains as much of the algorithms as is
available to users.

3.1   CATT-Acoustic™

As mentioned previously, CATT-Acoustic™ version 8.0 was used in this
research. Throughout the project, upgrades were made to the package by the
developer and the upgrades were incorporated into the research as they were
made available. The geometry input methods of the package are first described
in this section, followed by the prediction algorithms.

3.1.1   Geometry Input

The hall geometry is created using the CATT™ Editor in a text language
and saved as a GEO file. The user inputs points (i.e., vertices, corners, or nodes)
with their x, y, and z coordinates. The points are then connected to form planar

surfaces (faces). The number of corners used in the room is only limited by

available memory while the number of faces is limited to 5000.

The program allows advanced input options for creating and organizing

the GEO file. The options include symbolic constants, math expressions, IF

statements, object rotation, mirrored room symmetry, visual non-acoustical

markers, hierarchal organization of room geometry, planar subdivisions, etc.

The aim of these options is to simplify the method of inputting data needed to

define a room.

The developer emphasizes how important it is that the geometry of the

room be perfectly closed (assuming the room is actually closed), meaning that

there are no leaks in the room where sound can escape. The cut and lock[41]

commands are helpful (and sometimes necessary) to avoid leaks in a room due

to nonplanar surfaces. A debug file can be created which lists the planes

overlapping, the non-planar faces, and the possible reversed planes, all of

which can cause leaks in the room. If the program discovers leaks in the room,

a plot file is created which shows where the leaks are occurring, thus helping

the debugging process.

30

3.1.2   Prediction Methods

CATT-Acoustic™ is a room acoustic prediction program which contains three separate prediction methods. The audience area mapping prediction method uses ray-tracing to color map parameters on the audience area. The Early Part Detailed ISM Prediction Method uses the image-source method (ISM) to calculate the early part of an echogram with qualitative details. An echogram is an approximation to the squared impulse response of a room.[42] The Full detailed calculation prediction method uses Randomized Tail-corrected Cone-tracing (RTC) for a complete echogram calculation which allows for auralization. This discussion will focus on methods used in the Full detailed calculation module because that is the prediction method used in this research.

The RTC[43] method is a hybrid method which combines the features of both cone-tracing, standard ray-tracing and the image-source method. Ray-tracing and the image-source method were explained in Chapter 2. Cone tracing is similar to ray-tracing, except it uses cones instead of rays (see Figure 3.1). Because these cones do not cover the surface of a sphere exactly, they must be overlapped. An algorithm must also be implemented to weight the energy so that the multiple contributions produce (on average) the correct sound level.[44] Only the center ray of the cone is traced in the calculations.[45]
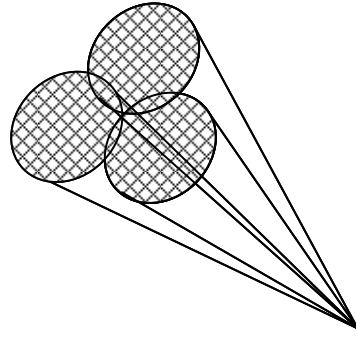
Figure 3.1. Cone tracing with cones overlapping.

The RTC method is used for the full response but handles the direct sound, the first order specular reflection, the first order diffuse reflection, and the second order specular reflection deterministically using the image-source method. The "early part" contains the part of the echogram where details are considered to be valid and the length is dependent on the number of cones traced.

One advantage of RTC is that it requires very few assumptions about the statistical properties of the room under consideration. If the room is closed it assumes that reflection density growth is quadratic over time, which is generally true. If the room is open, the algorithm makes no assumption about the reflection growth.

The RTC handles diffuse reflections in different ways depending on the order of reflection. For first order diffuse reflection, the RTC creates a number of elementary sources on each diffusing surface with a density governed by (1-α)δ, giving hard diffusing surfaces the highest density. The radiated power is

according to Lambert's law (see Section 2.3.2) and is proportional to $(1-\alpha)\delta$, where δ is the frequency-dependent scattering coefficient and α is the absorption coefficient. For the diffuse reflection of order greater than one, the random number method for scattering is used with the scattered ray direction randomized according to Lambert's law (see Section 2.3.2).

The RTC prediction method is used to create a complete echogram. The calculations are done for the octave-band center frequencies (125 Hz to 16 kHz). The echogram is saved and can be post-processed to create a reflection path transfer function and later converted to an impulse response. Post-processing is performed differently depending on the order of reflection. For details on how the post-processing is done see the CATT-Acoustic™ v8 User's Manual.[46]

3.2   EASE™

Multiple versions of EASE™ (3.0, 4.0, and 4.1) were used during the course of the research as upgrades became available. The majority of the research was done using versions 4.0 and 4.1. Only preliminary work was done using version 3.0.

EASE™ is made up of a group of integrated software modules. The main module ties together all other modules. In this section, the details of all modules will not be discussed. Instead, an overview of the geometry input

methods are described, followed by a description of the prediction algorithms used in this research.

3.2.1 Geometry Input

The hall geometry is created using the Edit Project module in EASE™, which includes a GUI interface. The user inputs points by clicking on the screen in the approximate position. A window then pops up for the user to input the x, y, and z coordinates accurate to two decimal places. Each point is shown on the GUI so the user can click on them to connect them and create faces.

Tools have been included in EASE™ to expedite the process of building a 3-D model. These options include entering a series of objects in linear or curved arrays, entering an unevenly spaced series of objects, grouping objects together to allow movement or duplication, and extruding to create 3-D complex shapes.[47] Also included in the package are prototypes of basic shapes as well as common room designs that can be modified and included into the model. These options simplify the method of inputting data needed to define a room. For more detailed information on the EASE™ Project module and the geometry input options, see the EASE™ user's manual[48] and the EASE™ tutorial manual[49].

3.2.2   Prediction Methods

The regular Ray-tracing and Image-source room acoustic prediction methods in EASE™ do not take scattering into account. Due to the importance of including scattering in computer modeling packages, these prediction methods could not be relied on alone to obtain accurate results. Starting with EASE™ version 4.0, the AURA™ module was incorporated into the program, which uses a hybrid method and takes scattering into account. The main algorithm for AURA™ was developed at Aachen University and originally called CAESAR. In this research, the AURA™ prediction method was used to calculate both impulse responses and the room acoustic parameters.

The AURA™ mapping module is used to calculate room acoustic parameters. A ray-tracing method is used to collect energy for each receiver in the form of an echogram. Scattering is taken into account according to the random number method for scattering, and the scattered ray direction is randomized according to Lambert's law (Section 2.3.2). Once the echogram is generated, the parameters are calculated according to ISO 3382.[47]

A more complicated algorithm is used for auralization because the temporal structure of the impulse response is important in order for the auralization to sound natural. As is common in computer modeling algorithms, the generation of the impulse response in the AURA™ response module is

separated into early and late portions. The reflection cutoff order determines the early/late separation time and is specified by the user.

The early specular reflections are calculated using a hybrid mirror image method, where ray-tracing is used to determine the valid images that are visible to the receiver. A fast tree search is used to compare a newly found image source with previously found sources.

The early scattered reflections and the late part of the impulse response are simulated with an energetic ray-tracing algorithm, with a uniform density distribution.[50] The random number method for scattering is used and the ray will scatter according to Lambert's law (Section 2.3.2)[31]. The early and late reflections are combined into the impulse response. For more details on this process see Schmitz, et al.[47]

4 Measurement Techniques

This chapter discusses current experimental measurement techniques used to assess the absorption and scattering coefficients of materials. The techniques are based on the most recent standards available at the time of the research. It also focuses on specific methods of measuring absorption coefficients of audience seating areas.

4.1 Measuring Random-Incidence Absorption Coefficients

The random-incidence absorption coefficient can be defined as the ratio of sound energy absorbed by a surface to the total random-incidence sound energy:

$$\alpha = \frac{\text{sound energy absorbed by a surface}}{\text{total random - incidence sound energy}} \qquad (4.1)$$

It is important to note that this coefficient is independent of the angle of incidence, whereas absorption is generally dependent on the angle of incidence. Absorption is also dependent on frequency, so absorption coefficient measurements are usually made in a series of frequency bands. Absorbed sound includes sound dissipated through the acoustical material and the sound transmitted beyond the material through the substructure to which it is mounted (Figure 4.1).
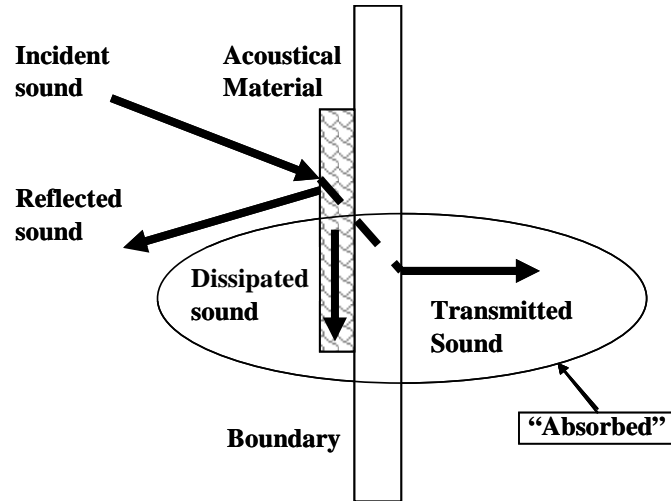
Figure 4.1. Absorbed sound includes the sound dissipated through the acoustical material and the sound transmitted through the surface to which it is mounted.[51]

Techniques for measuring the random-incidence absorption coefficients are based on the Sabine equation:

$$T_0 = \frac{55.3}{c} \frac{V}{S\alpha_0} = \frac{55.3}{c} \frac{V}{A},$$

(4.2)

where V is the volume of the room in m³, T_0 is the reverberation time, S is the surface area of the room boundaries in m², α_0 is the mean absorption coefficient of the boundaries, c is the speed of sound, and A is the total absorption of the boundaries. Sabine's equation can also be written in terms of the decay rate, d, where d is $\frac{60dB}{T_0}$:

$$A = 0.9210 \frac{Vd}{c}$$

(4.3)

Equations (4.2) and (4.3) assume a perfectly diffuse sound field which is not valid in practice, even in a reverberation chamber where random-incidence absorption coefficients are normally measured.

The ASTM C423-00[52] and ISO 354[53] standards give guidelines for the measurement of random-incidence absorption coefficients including specifications on the reverberation room size and shape, the diffusion of the sound field, the temperature and relative humidity, and the number, type and positions of the microphones and sources. The main objective of these guidelines is to ensure that measurement of average decay curves, with and without the test specimen, yields a sufficiently accurate value for the absorption of the test sample. The standards also discuss two different acceptable methods of measuring decay curves: the interrupted noise method and the integrated impulse response method.

Decay curves are measured and then converted to reverberation times for the empty reverberation room (T_1), and the reverberation room with the test specimen in it (T_2). These are used to calculate the absorption area of the test specimen, which follows from Equation (4.2) with additional terms to account for air absorption:

$$A_T = 55.3V(\frac{1}{c_2 T_2} - \frac{1}{c_1 T_1}) - 4V(m_2 - m_1) \tag{4.4}$$

where V is the volume of the room, c_1 and c_2 are the speeds of sound (based in part on temperature measurements), and $4Vm_1$ and $4Vm_2$ are air absorption terms where m is the power attenuation coefficient calculated according to ISO 9613-1[54]. The subscript 1 refers to measurements made in the empty reverberation room and subscript 2 refers to measurements made with the test specimen in the room. From the absorption area, the absorption coefficient is determined using:

$$\alpha = \frac{A_T}{S} ,$$ (4.5)

where S is the surface area of a plane absorber or the equivalent surface area of a specified array of test objects.

4.2   Measuring Audience Seat Absorption in Reverberation Chambers

Audience seating absorption often makes up the majority of the absorption in a hall. It is therefore important that it be estimated accurately when used to predict acoustic parameters of a hall. Tables of audience seat absorption values have been published in the literature by different authors.[55] Davies[56] observes, however, that these values will have to be within 5% of the absorption of the actual seats in order to accurately predict acoustic parameters.

The purpose of measuring random incidence absorption coefficients of a small sample of seats in a reverberation chamber is to use these values to predict the total absorption of a larger area of the same seats when installed in an auditorium. The problem, however, is that the absorption at the edges of the smaller block of seats is overemphasized when it is scaled up to a larger block of seats, and the absorption will be predicted higher than what it actually will be in the auditorium. Kath and Kuhl[57,58] and Bradley[59,60] have proposed two different methods that correct for this error. Because the Kath and Kuhl method has been said to be more efficient than the Bradley method with the same level of accuracy, it was chosen for the seating and audience absorption measurements in this thesis, as discussed in Section 6.1.

The Kath and Kuhl[57,58] method has been explained by different authors.[56,61] It involves placing the seating in the corner of the reverberation chamber in rows with the same row spacing as the actual hall. Stiff, massive barriers are placed around the exposed edges (see Figure 4.2).

The barriers should be at least as high as the seating, and higher if any audience is present for an occupied measurement. Excessive height (e.g., more than 100 mm above the top of the seating for the unoccupied case) should be avoided. The corner placing of the seats is advantageous because the array is mirrored in the adjacent walls of the chamber, thus effectively increasing the
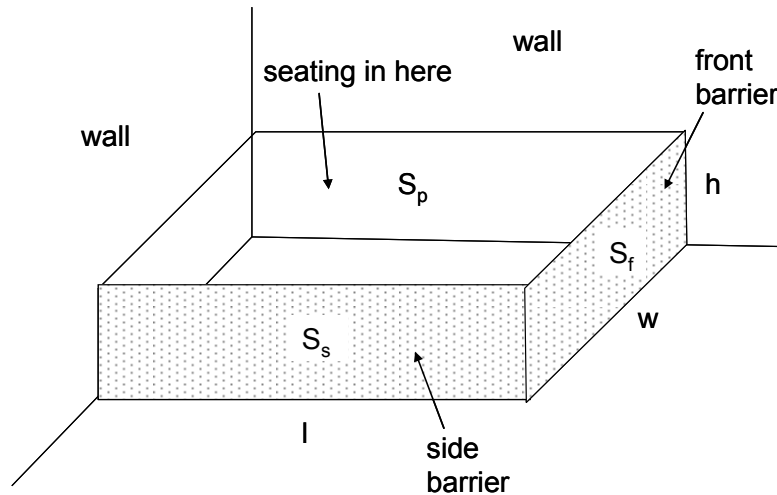
Figure 4.2. Set-up for Kath and Kuhl seating absorption measurements.[61]

size of the seating block. The disadvantage with this arrangement is that the

pressure in a reverberant field is increased at the boundaries so the absorption

coefficients measured are higher than those found when the sample is in the

center of the chamber. To compensate for this, Kath and Kuhl proposed that

the absorber areas used in the calculations should be increased by strips of

width $\lambda/8$. Diffraction effects are still present so the measured absorption

coefficient may still vary with sample size.

Three separate absorption coefficients are measured in order to compute

the total absorption coefficient of the seats or seated audience block. First,

measurements are made with both side and front barriers surrounding the

audience, yielding an absorption coefficient α_∞:

$$\alpha_\infty = \frac{A_1}{(l+\lambda/8)(w+\lambda/8)}, \qquad (4.6)$$

where A_1 is the horizontal plane absorption area of the sample with both barriers in place, λ is the wavelength of the center frequency in the octave band, and l and w are defined in Figure 4.2.

Next, measurements are made with only the side barrier present, yielding an absorption coefficient for the front edges, α_f:

$$\alpha_f = \frac{A_2 - A_1}{h(w + \lambda/8)}, \tag{4.7}$$

where A_2 is the vertical absorption area of the sample with only the side barrier present, and h is the barrier height.

Measurements are then made with only the front barrier present, yielding an absorption coefficient for the side edges, α_s:

$$\alpha_s = \frac{A_3 - A_1}{h(l + \lambda/8)}, \tag{4.8}$$

where A_3 is the vertical absorption area of the sample with only the front barrier present.

If the areas of the fronts (S_f), sides (S_s) and plan (S_p) are known for the hall, the total absorption coefficient of the audience block is then:

$$\alpha = \alpha_\infty + \alpha_f \frac{S_f}{S_p} + \alpha_s \frac{S_s}{S_p}. \tag{4.9}$$

4.3   *Measuring Random-Incidence Scattering Coefficients*

Section 2.3.1 gives the definition of the scattering coefficient. It is important to note that this coefficient is independent of the angle of incidence, where in general, scattering from a surface is actually dependent on the angle of incidence. The scattering coefficient does not contain any information about the direction of the scattered energy. Instead, this is contained in the diffusion coefficient which is not typically used in computer modeling packages. Because scattering is also, in general, dependent on frequency, scattering coefficient measurements are usually made in a series of frequency bands.

The principles that govern the measurement of scattering coefficients were proposed by Vorländer and Mommertz.[22] In Figure 4.3, three bandpass filtered pulses are shown, each of which were reflected from a rough surface sample at different orientations. It can be seen that the initial parts of the reflections are highly correlated, while the later parts are not in phase and depend strongly on the specific orientation of the sample. The early part of each reflection took the path with the shortest delay (Fermat's principle) and is related to the specular component of the reflection. The energy in the "tail" of the reflected pulse contains the scattered part.
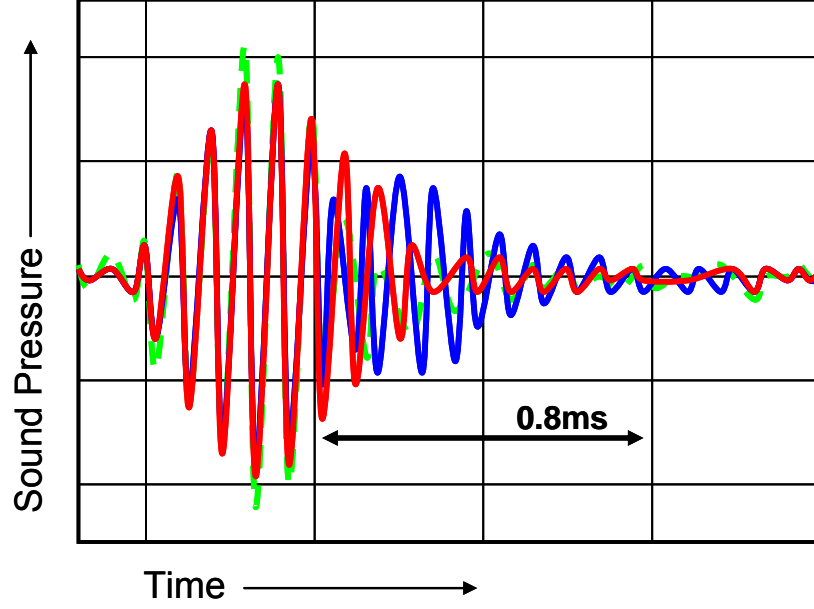
Figure 4.3. Sound pressure in time domain for three orientations of the same rough surface sample.[23]

When normalized with respect to a reflection from a rigid reference plane the energies can be expressed in terms of the specular absorption coefficient (a) and the total absorption coefficient (α):

$$E_{spec} = (1-\alpha)(1-\delta) = (1-a),$$ (4.10)

$$E_{total} = (1-\alpha),$$ (4.11)

where E_{spec} is the specular component of the energy and E_{total} is the total energy. Then, from the definition of the scattering coefficient in Equation (2.4),

$$\delta = \frac{a-\alpha}{1-\alpha} = 1 - \frac{E_{spec}}{E_{total}}.$$ (4.12)

In this method, the scattering coefficient is found by extracting the specular component E_{spec} from the reflected pulses. This is done by phase-lock

averaging the pulses obtained for different sample orientations as illustrated in Figure 4.4. While the specular components of the energy add up in phase, the scattered energy is incoherent and thus interferes destructively.

The preliminary ISO/DIS 17497-1 standard[62] was created based on these principles. The scattering sample is placed on a turntable in a reverberation chamber and the impulse responses of the chamber are taken for different orientations of the sample with fixed source and receiver positions (Figure 4.5). For an ideal plane surface, impulse responses will be perfectly correlated as the sample is rotated to different positions. However, for a rough surface, the correlation decreases with increasing time.

In the measurement process, according to ISO/DIS 17497-1, decay rates are measured without and with the test sample following one of the methods given in ISO 354[53] (see Section 4.1) then converted to reverberation times T_1 and
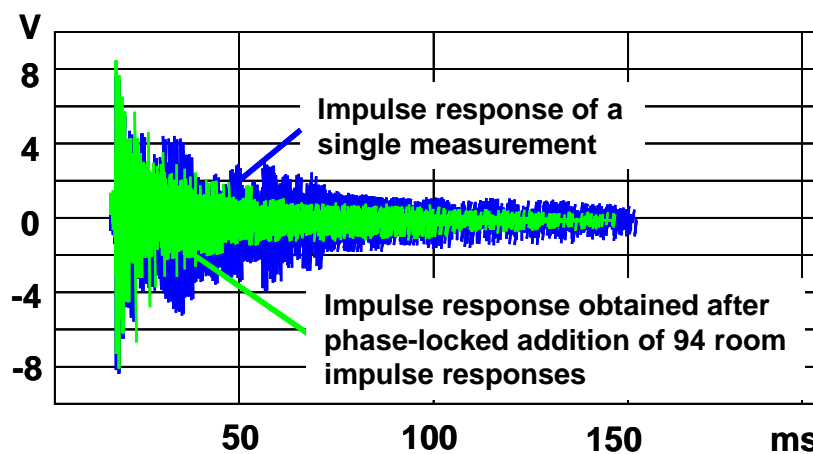
Figure 4.4. Impulse responses measured in a reverberation room.[63]

46
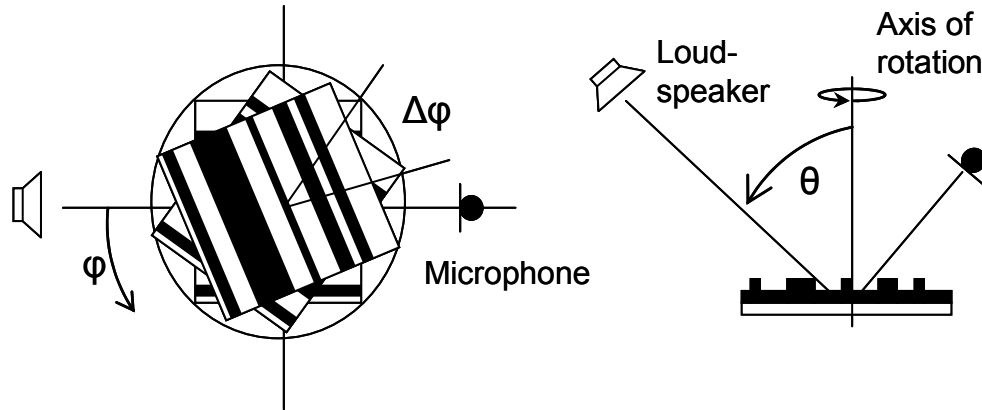
Figure 4.5. Orientation of the sample on the turntable.[63]

T_2 respectively. Measurements are then made with the turntable rotating, without and with the sample. For a rotating turntable, phase-locked averaging of the measurements is required to obtain the time-invariant response. This is then converted to the reverberation times for the rotating turntable without the test sample (T_3) and for the rotating turntable with the test sample (T_4). The measurements are summarized in Table 4.1.

The random-incidence absorption coefficient can be calculated according to Equations (4.4) and (4.5). Similarly, the specular absorption coefficient can be

Table 4.1. The measurement conditions for the four different reverberation times.

Reverberation Time	Test Sample	Turntable
T_1	Not Present	Not Rotating
T_2	Present	Not Rotating
T_3	Not Present	Rotating
T_4	Present	Rotating

calculated as follows:

$$a = 55.3\frac{V}{S}(\frac{1}{c_4 T_4} - \frac{1}{c_3 T_3}) - \frac{4V}{S}(m_4 - m_3),$$ (4.13)

where the subscripts in these equations now refer to the measurement conditions found in Table 4.1. From the absorption coefficient and the specular absorption coefficient, the scattering coefficient is then calculated using Equation (4.12).

5   Preliminary Models

The process of computer modeling a hall usually begins by converting two-dimensional drawings of the hall into a three-dimensional model. In this research, two-dimensional AutoCAD™ files of the Conference Center were provided by architects who designed the hall. They included floor plans and elevation drawings for different levels of the hall.

As explained in Chapter 3, the three-dimensional models are created by connecting vertices into planar faces. Curved surfaces have to be approximated by a series of planar faces.

After the models are created, each planar face is assigned material properties, namely, absorption and scattering coefficients. Absorption coefficients for materials are often taken directly from tables in the literature. If a specific material cannot be found, computer modelers often approximate them with a material that closely resembles the actual material or an average of two or more closely related materials. Values for scattering coefficients, on the other hand, are normally estimated because values for most surfaces cannot be found in the literature. Current methods for estimating them are listed in Section 2.3.3.

This chapter explains the design procedure for preliminary models created in EASE™ and CATT™. First, the geometry methods will be explained. The process of determining the absorption and scattering coefficients will then follow. Finally, analyses will be presented to show the number of rays needed in the models and the sensitivity of the models to scattering coefficients.

5.1   Geometry

Several computer models of the Conference Center have been made since the beginning of this research. First, a preliminary model was made in EASE™ using basic floor plans and elevation drawings of the hall. The model was simple, including only a very general level of detail. It aided in learning the computer modeling software as well as providing an understanding of some of the special issues associated with the modeling of such a large hall.

After receiving more detailed floor plans and elevation drawings, the EASE™ model was refined and redrawn to include a high level of detail – especially in the rostrum and choir areas (see Figure 5.1). There are 4,492 faces in this model.

Because of the complexity of the hall, it was anticipated that the model would need a high level of detail in order to accurately predict its acoustical
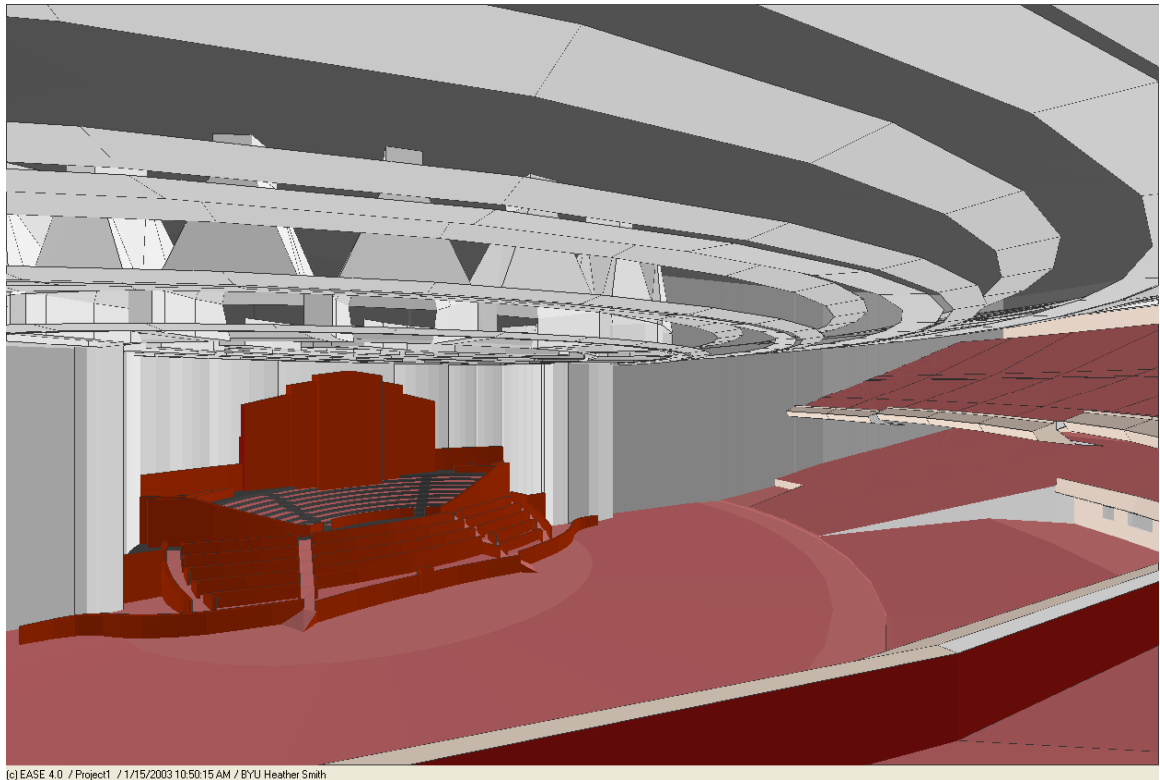
Figure 5.1. Detailed EASE™ preliminary model.

properties. After researching the literature, however, it was found that high levels of detail do not necessarily lead to better accuracy. In fact, Bork[40] argues that too high of a geometrical resolution could even reduce the accuracy of the calculation. Bradley[64] studied the effect of model detail on room acoustic computer simulations and found that, for the extent that he varied it, levels of detail did not seem to affect accuracy of predictions. Naylor[65] gives a guideline indicating that one should aim for a replication of the general proximities and forms in the room, while avoiding unnecessary small surfaces. The detailed model was abandoned because of these reasons and the impractical computation times it required.

A third EASE™ model was then created by simplifying the detailed model (Figure 5.2). This was done to decrease the number of surfaces (1,777 faces) making them more manageable, without losing the overall accuracy of the model. Including the correct level of detail in the models is one of the major challenges of modeling the Conference Center auditorium. The models need to be detailed enough that the basic characteristics that set this room apart from other rooms are considered, but not so detailed that the computation time is too long due to a large number of faces.

A program was written to convert models from EASE™ to the format of CATT-Acoustic™. As mentioned in Section 3.1.1, it is important that the

(c) EASE 4.1 / Conference Center 3D audience areas / 7/16/2004 10:58:20 AM / BYU BYU Acoustics
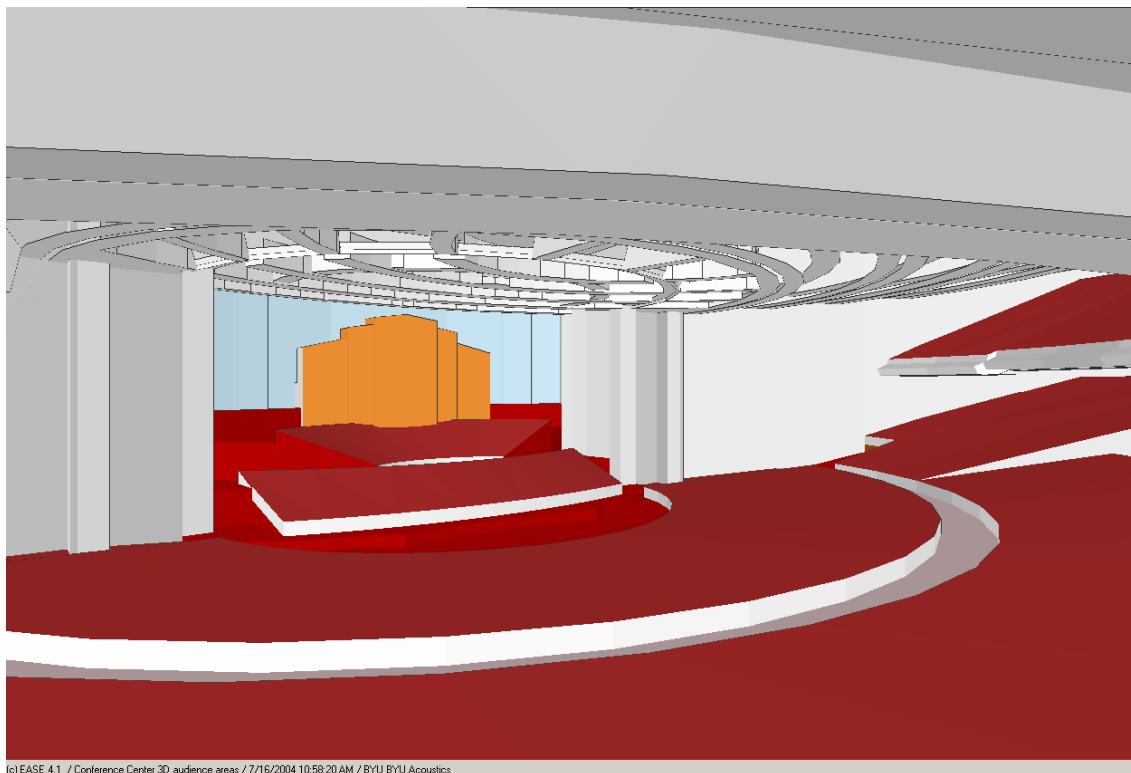
Figure 5.2. Simplified EASE™ preliminary model.

geometry in the CATT™ model be perfectly airtight. EASE™, on the other hand, does a check for nonplanar surfaces, but the airtight requirements are less rigorous. The default tolerance for planar surfaces in EASE™ is 0.1 meters, whereas the tolerance in CATT™ is 0.0001 meters[45]. While the tolerance in EASE™ can actually be changed, the user is limited to input vertices to the nearest 0.01 meters. In CATT™, there is no limit to how accurately the user may input the vertices. As a result, the EASE™ model will generally not satisfy the requirements CATT™ has for room closure. The idea of converting the model from EASE™ to CATT™ was accordingly abandoned. Instead, a model was created directly inside CATT-Acoustic™ (Figure 5.3). This model has 1,670 faces. Although differences exist due to the stricter requirements of CATT™ for room closure, the basic geometries of the models are essentially the same.

Getting the Conference Center model airtight in CATT™ was difficult because of the large number of curved surfaces found in the hall. This was especially true for curved faces sloping upward at an angle, such as the audience areas. The easiest way to define a perfectly planar surface of this type is shown in Figure 5.4. Points 1 and 2 are located on an arc with a radius R1 centered about C1. Points 3 and 4 are located on an arc with a radius R2 also centered about C1. Points 1 and 2 must have the same height, but can be different from the height of points 3 and 4 (which must have the same height).
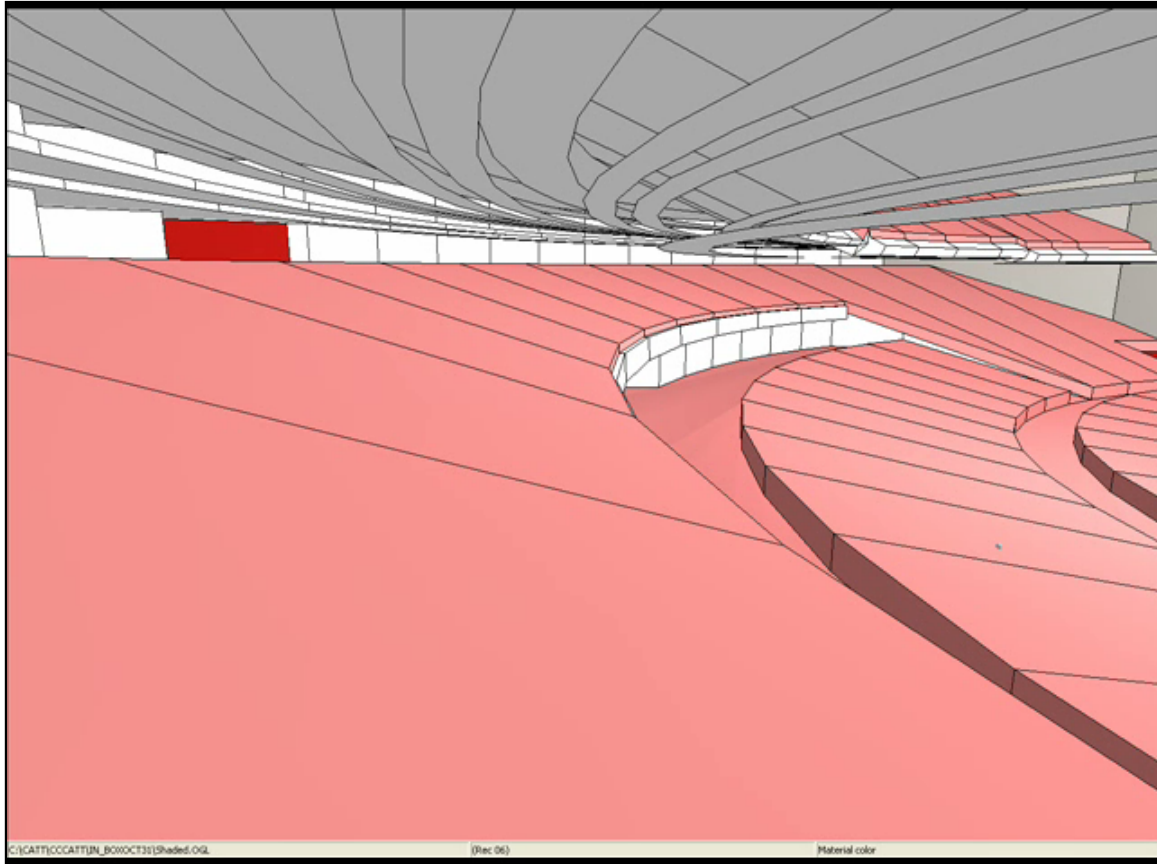
Figure 5.3. CATT-Acoustic™ preliminary model.

Point 3 must lie along the line connecting point 1 with C1. Point 4 must lie along the line connecting point 2 with C1. The plane F1 is defined by
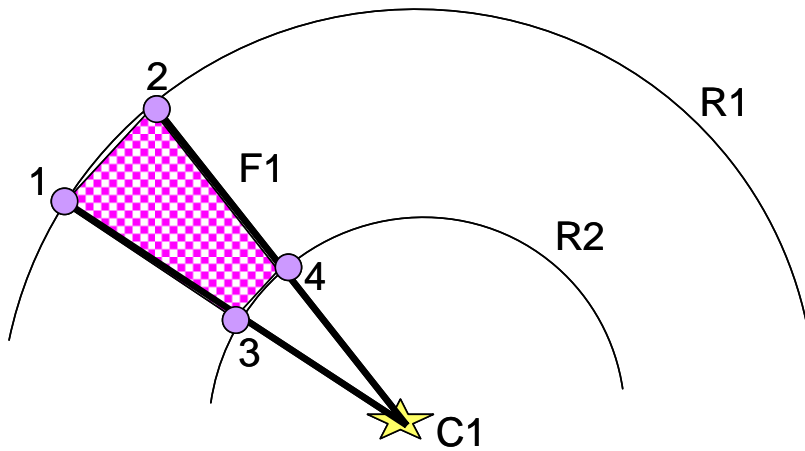
Figure 5.4. Defining plane from sloped curved surfaces in CATT™.

connecting points 1, 2, 3, and 4. This method was used to create a majority of the audience areas in the CATT™ model.

The last two models mentioned (the simplified EASE™ preliminary model and the CATT™ preliminary model) were used to compute impulse responses, auralizations, and acoustic parameters to compare with measurements made in the hall (see Chapter 7).

Some general simplifications were made in order to minimize the number of faces in the models. The vertical aisles between the seats were not included and the windows on the back of the main floor were not modeled explicitly (although absorption values were taken into account). The various structures and rooms located above the ceiling canopy were not modeled explicitly (although higher scattering coefficients were applied to the surfaces to take them into account). In addition, the organ pipes were not modeled explicitly (although higher scattering coefficient values were given to their casing).

5.2   *Absorption Coefficients*

Basic absorption coefficients were applied to surfaces in the preliminary model using published absorption coefficients values. These coefficients were taken from the following references: Beranek[66], Beranek and Hidaka[55], Davis[67],

and Everest and Shea[68]. When published values were not obtainable for certain surfaces, coefficients were estimated using values for materials with similar absorption properties or averages of a few materials with similar absorption properties. Some surfaces in the model are actually made up of more than one surface material in the hall. For surfaces of this type, an average of the different material types was used. Detailed tables of the absorption coefficients used in the preliminary models can be found in Appendix A.

The absorption area for each material was found by multiplying its frequency-dependent absorption coefficient by its surface area. The absorption areas were then added in a cumulative manner to create a total absorption area curve. In this way, the contributions for each type of material to the total absorption can be visualized (Figure 5.5). The total absorption curve can be compared to the measured total absorption curve. Measured reverberation times were calculated from octave-band filtered impulse response measurements made using the TEF 20 analyzer and the Maximum Length Sequence (MLS) module. The measured total absorption curve was found by determining the average absorption coefficient from measured reverberation times and the Eyring equation,

$$T_{60} = -0.163 \frac{V}{S \ln(1 - \bar{\alpha}) - 4mV} ,$$ (5.1)
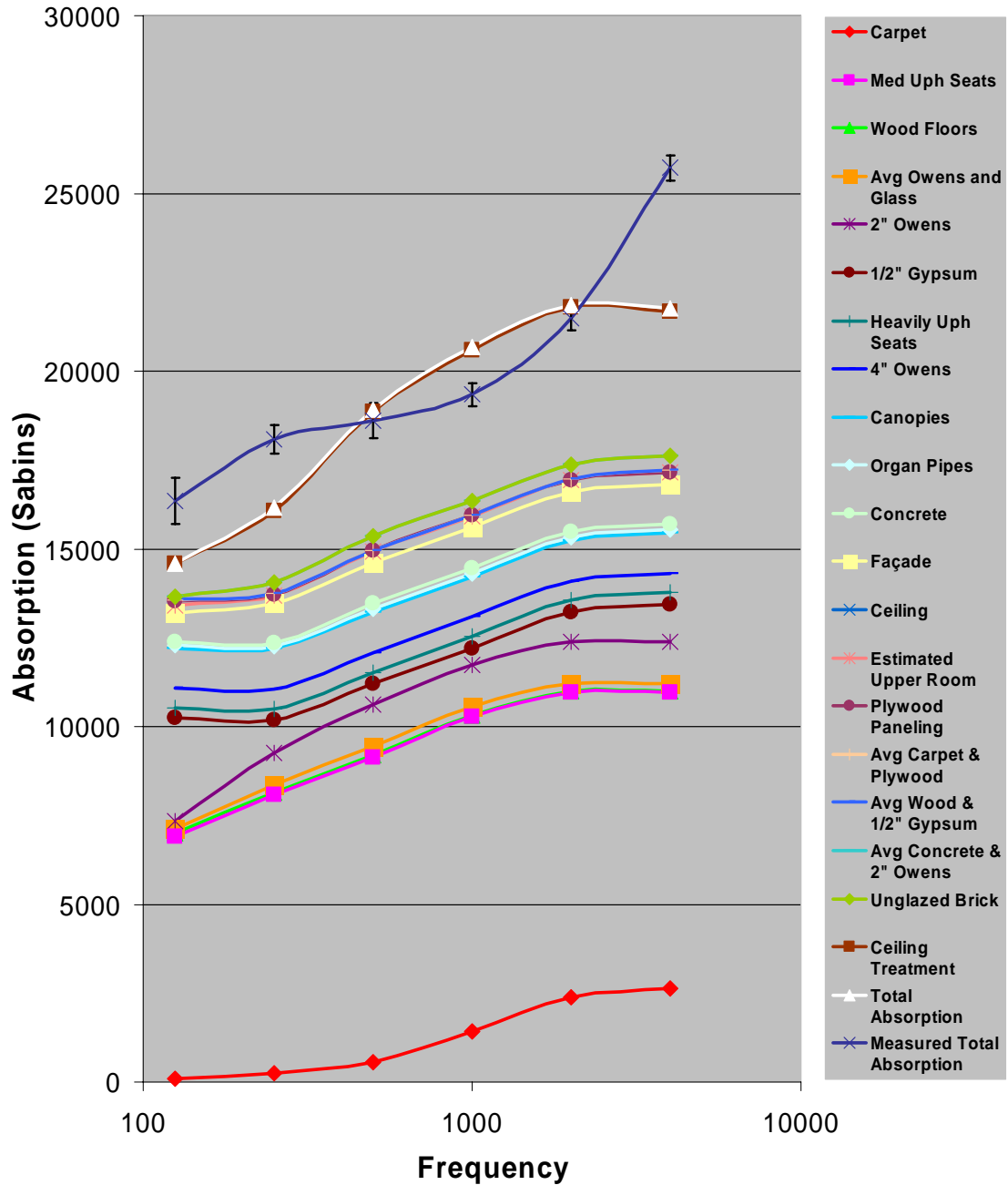
Figure 5.5. Cumulative absorption curves for preliminary model.

then multiplying by the total surface area in the hall. Seven different measurements of the reverberation time on the main floor were averaged for use in computing the measured total absorption curve. The error bars on the

curve indicate the standard deviation in the measurements.

The absorption curves were made specifically from the CATT™ preliminary model, but the EASE™ preliminary model would have similar curves because of their similarity. It can be seen from Figure 5.5 that the measured total absorption curve provides reasonable agreement to the total absorption curve from the model. The most significant differences seem to be the overall shape of the curve and the large underestimate of the model absorption at 4 kHz.

It also can be seen from the figure that the surfaces which contribute the most to the total absorption are the medium upholstered seats and the absorptive ceiling treatment above the canopy (see Figure 6.3a). It was expected that if these absorption coefficients could be determined more accurately, the total absorption curve in the model would more closely match the measured total absorption curve and produce more accurate modeling predictions. As explained in Section 6.1, these coefficients were then measured in a reverberation chamber for input into refined CATT™ and EASE™ models.

5.3   *Scattering Coefficients*

The scattering coefficients for the preliminary models were determined using the best-known approximation techniques available. Some methods for

approximating scattering coefficients were given in Section 2.3.3. Because the most comprehensive method seemed to be that proposed by Dalenbäck in the CATT™ user's manual[29], it was used for the preliminary models. For surfaces that were not perfectly flat, measurements were made of their dimensions and scattering coefficient values were approximated as Dalenbäck outlined. Scattering coefficients of curved surfaces were increased slightly because of other recommendations of Dalenbäck.[45] Edge diffraction was applied to small, hard surfaces. Detailed tables of the scattering coefficients used in the preliminary models can be found in Appendix B.

5.4 *Quantifying the Number of Rays to Use*

It is obvious that the accuracy of the ray-tracing method must depend on the number of rays traced. Kulowski[69] observed that in numerous cases, the number of rays (although large) is chosen rather arbitrarily without any analysis as to whether this number is sufficient for the room being studied. For the Conference Center preliminary models, research was done to quantify the number of rays to trace in order to produce reliable results.

Authors have suggested various methods of determining the number of rays to use. Giner[70] states that the number of rays depends on the computer

program, the shape of the room, the number and size of the receptors, and the absorption distribution, among other factors.

The EASE™ 4.1 user's manual gives a few guidelines for the number of rays to use in EASE™. It specifies that the greater number of rays used, the greater the accuracy and the greater the calculation time. It recommends 1,000 or less rays for studies of basic reflection patterns and 100,000 or more rays for auralization and more detailed investigations.[71]

Dalenbäck[72] gives the guideline that at least 5,000 rays must be used for good results in CATT™. He seldom uses more than 50,000 rays and for a typical hall he uses between 10,000 and 20,000 rays.[45] He mentions that even with as few as 1,000 rays, estimated parameters should not vary more than the difference limen from run to run unless the statistical properties are very special.[73] He suggests that it may be necessary to perform test runs on new halls to determine the number of rays needed to give sufficiently repeatable results.[73] CATT™ has an option wherein the user can have the program calculate the number of rays to use, called "auto number." This number is generated by taking the larger of the following two calculated numbers:

1) A number is calculated that corresponds to 1 ray per square meter arriving 80 ms after the direct sound for all positions (this number gives a good

sampling of parameters for D50, C80, and LF, see Appendix C for parameter definitions).

2) A number is calculated which corresponds to 1 ray for every 4 square meters at the longest hall dimension (this number will be higher than the number in 1) for very large halls. It allows for a determination of some detailed reflections from far away surfaces).[72]

The method that was used in this research is similar to a method proposed by Kulowski[69] to analyze the fluctuations in the results. Gomes[74] published results from similar studies, but they were not as detailed as the studies performed in this research. In this research, not only were the number of rays varied, but multiple runs (or simulations) at each different ray count were taken. The average value from run to run was computed in order to ensure the data showed variations in the parameter as a function of the number rays rather than the variation associated from run to run (because of random fluctuations).

Table 5.1 and Table 5.2 list the number of rays used with their corresponding calculation times for EASE™ and CATT™ respectively (the calculation times were based on a machine with dual 2.4 GHz Intel Xeon™

Table 5.1. EASE™ v4.1 number of rays used and calculation times.

# rays	1,000	5,000	10,000	25,000	50,000	100,000	250,000	500,000	1,000,000
Calc. time	5 min	12 min	15 min	½ hr	45 min	2 hr	4 hr	8 hr	18 hr

Table 5.2. CATT™ v8.0c number of rays used and calculation times.

# rays	100	500	1,000	5,000	10,000	25,000	50,000	100,000	250,000	500,000
Calc. time	3 min	5 min	8 min	½ hr	1 hr	2-1/4 hr	4 hr	8 hr	19-1/2 hr	40 hr

processors and 4 GB of RAM). Ray counts greater than those listed were not used due to the long computation times.

The number of rays necessary to obtain accurate results was determined for each package by using the difference limens (DLs) or just noticeable differences (JNDs) for the acoustic parameters. Difference limens are values that have been published that correspond to the smallest difference in the acoustic parameters that listeners can perceive. Different authors have published different values for individual parameters. Table 5.3 gives the parameters with their various difference limens and references. For those parameters which had more than one published difference limen, it was decided to use the maximum and

Table 5.3. Difference limens (or JND's) for acoustic parameters.

	Cox[75]	Vorländer[18]	Bork[40]	Bork[76]	Farina[77]	Howarth[78]	Bradley[79]	Bistafa[80]
T30	—	5 %	5 %	0.05 s	0.07 s	—	—	—
EDT	—	5 %	5 %	0.05 s	0.05 s	5%	—	—
D50	—	5 %	5 %	5 % s	5 %	—	—	—
C80	0.67 dB	0.5 dB	1 dB	1 dB	0.5 dB	0.5 dB		—
G	—	1 dB	1 dB	1 dB	1 dB	1 dB	—	—
LF	—	5%	5%	5%	5%	5%	—	—
LFC	—	5%	5%	5%	5%	5%	—	—
IACC	0.075	—	0.2	0.08	—	—	—	—
C50	—	—	—	—	—	—	1 - 3 dB	1.1 dB
STI	—	—	—	—	—	—	0.03 –0.1	0.03
SPL	—	—	—	—	—	—	—	1 dB

62

minimum difference limens for the rest of the analysis.

It should be noted that difference limens are generally frequency dependent. However, because only single values are typically published in the literature, frequency dependence was likewise ignored in this study.

For this research, 50 different consecutive runs were made for each number of rays (with the exception of the 1,000,000 ray count used in EASE[TM], where only 26 consecutive runs were run because of long computation times). After the simulations were run, it was determined whether the number of consecutive runs was sufficient using statistical methods. It is important to take enough samples for the standard deviation to be within at least one difference limen of the mean value. Hence, the confidence interval was set equal to the difference limen as follows:[81]

$$t * \frac{s}{\sqrt{n}} = DL \qquad (5.2)$$

In this equation $t*$ is the critical-t value which depends on the degrees of freedom and the confidence level you are interested in, s is an estimate of the population standard deviation, n is the sample size, and DL is the difference limen for the parameter of interest.

Equation (5.2) was solved for the critical-t value (assuming a sample size of 50) to determine the confidence level. Table 5.4 shows the minimum critical-t

value (for the highest ray count number) needed. This was done for the highest

ray count number because it assumed that at the highest ray count the

parameter has converged enough to actually be able to give a fairly accurate

estimate of the mean.

It can be seen from Table 5.4 that for all of the parameters, the sample

size of 50 runs seemed to be sufficient except for the EASE™ EDT (DL=0.05 s),

the EASE™ T30 (DL=0.05 s), and the CATT™ EDT (DL=0.05 s). These

parameters (with their corresponding difference limens) correspond to

confidence levels of less than 90%. Because the standard deviation depends

heavily on the number of rays, the analysis cannot conclude that for the EASE™

EDT (DL=0.05 s), the EASE™ T30 (DL=0.05 s), and the CATT™ EDT (DL=0.05 s)

the number of runs has not been sufficient. Rather it must conclude that either

the number of runs has not been sufficient or that the ray count has not been

Table 5.4. Critical t* value and confidence level for fifty runs.

	DL	EASE™ min t * value	EASE™ confidence level	CATT™ min t * value	CATT™ confidence level
C50	1 dB	11.46	~100%	9.79	~100%
	3 dB	34.37	~100%	29.38	~100%
C80	0.5 dB	5.77	~100%	4.17	~100%
	1 dB	11.54	~100%	8.35	~100%
LFC	5 %	17.63	~100%	15.53	~100%
LF	5 %	49.69	~100%	19.71	~100%
G	1 dB	22.059	~100%	20.55	~100%
SPL	1 dB	1.2E+14	~100%	21.17	~100%
EDT	0.05 s	1.33	~83%	0.99	~68%
	5 %	1.88	~92%	2.31	~97%
T30	0.05 s	1.18	~75%	2.72	~99.3%
	5%	3.19	~99.65%	6.35	~100%

sufficient enough to see convergence to within the difference limen. It was not practical to extend this study to higher numbers of rays due to excessively long computation times. However, the study shows that fifty runs was certainly sufficient for most of the parameters.

Fifty different runs were subsequently used in the analysis for each number of rays. The mean values of the parameters vs. the number of rays used for the octave band center frequencies in EASE™ are shown in Figure 5.6 through Figure 5.13. The mean values of the parameters vs. the number of rays used for the octave band center frequencies in CATT™ are shown in Figure 5.14 through Figure 5.21. Error bars indicate the standard deviation in the mean value for each number of rays.

From these figures, it is seen that some parameters are more easily estimated than others for all numbers of rays (such as SPL). Also, the convergence for the parameters is more apparent with the EASE™ plots. At low ray counts, there are a lot of random fluctuations and the standard deviations are large. As the ray count increases, the standard deviation decreases and the parameter seems to converge to some value. The CATT™ plots, on the other hand, do not seem to show the same trend, with the exception of the T30
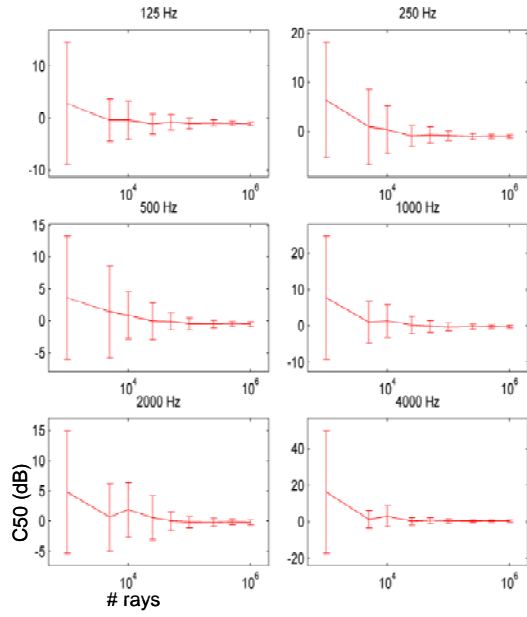
Figure 5.6. EASE™ C50 vs. number of rays.
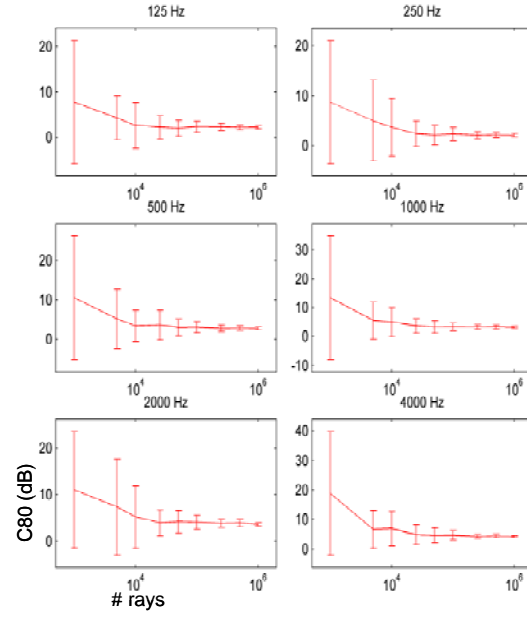
Figure 5.7. EASE™ C80 vs. number of rays.
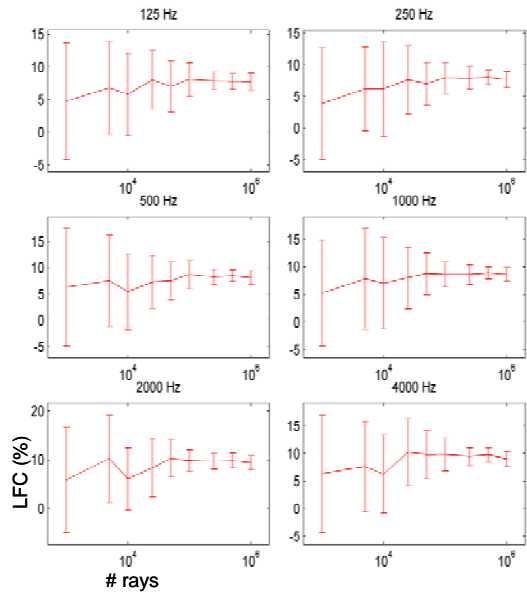
Figure 5.8. EASE™ LFC vs. number of rays.
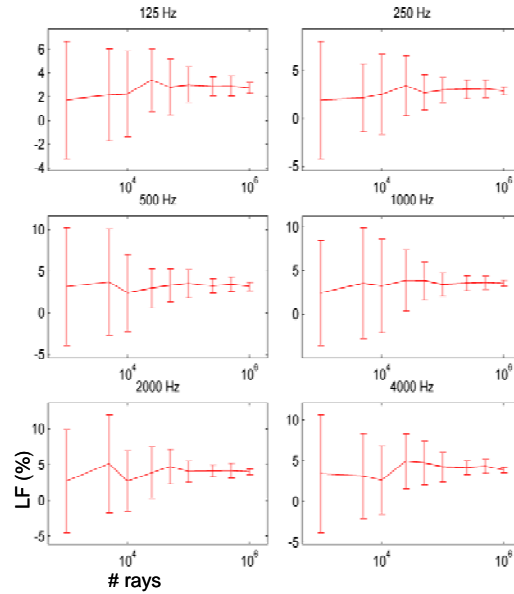
Figure 5.9. EASE™ LF vs. number of rays.
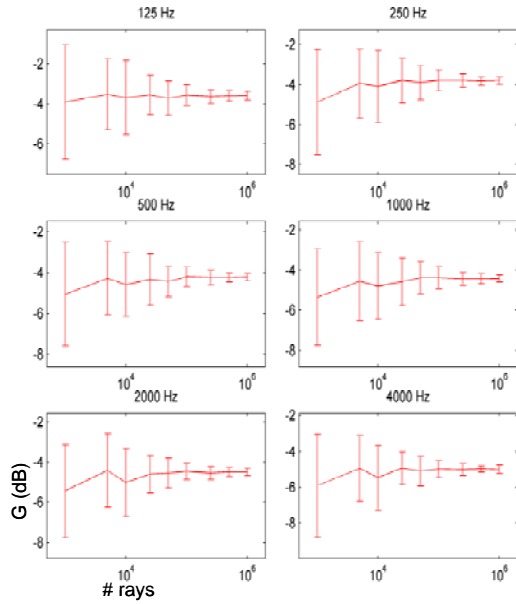
Figure 5.10. EASE™ G vs. number of rays.
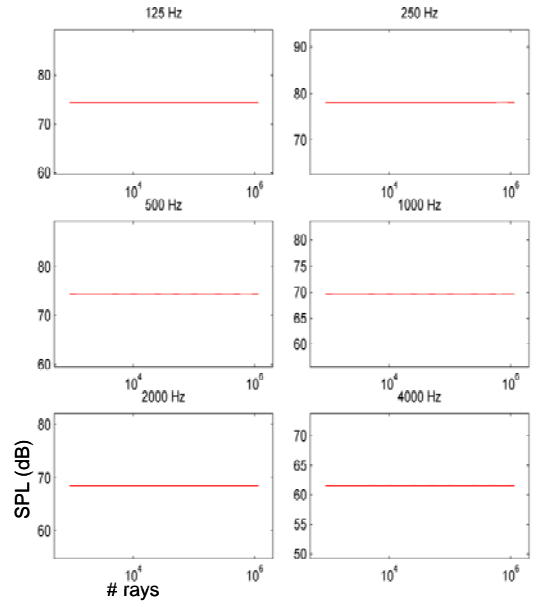
Figure 5.11. EASE™ SPL vs. number of rays.
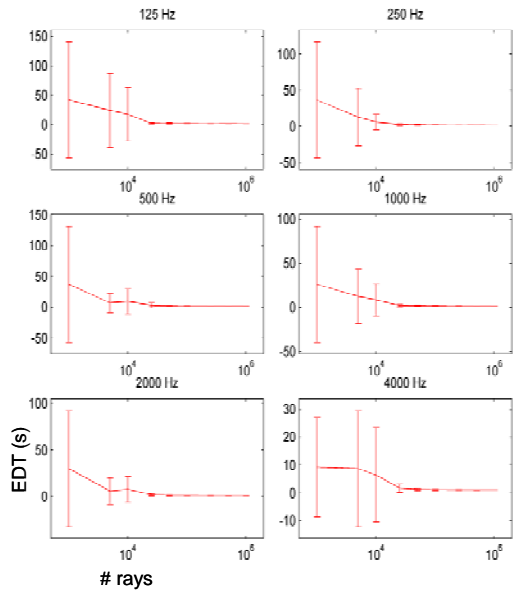
Figure 5.12. EASE™ EDT vs. number of rays.
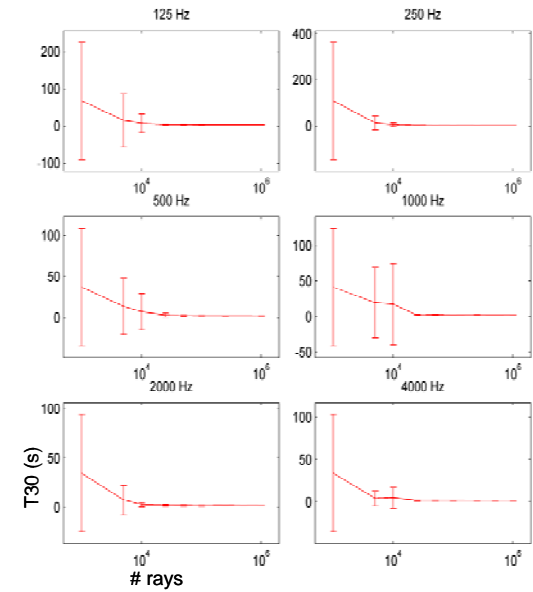
Figure 5.13. EASE™ T30 vs. number of rays.

67
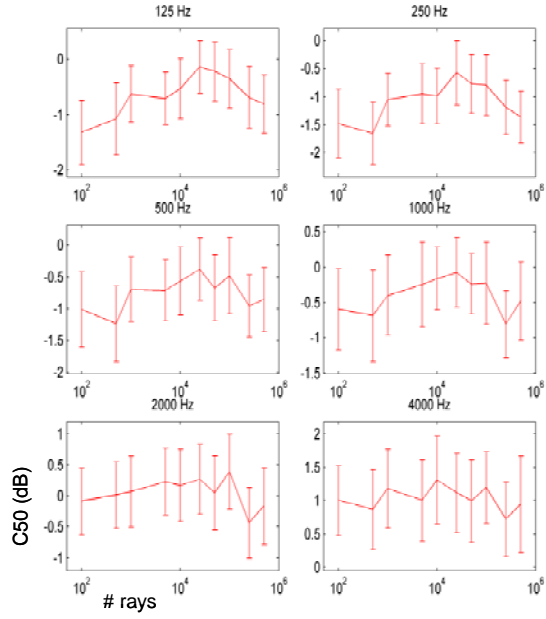
Figure 5.14. CATT™ C50 vs. number of rays.
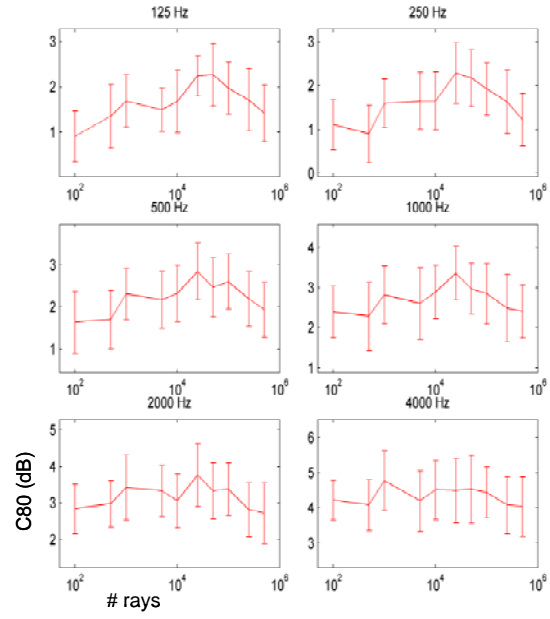
Figure 5.15. CATT™ C80 vs. number of rays.
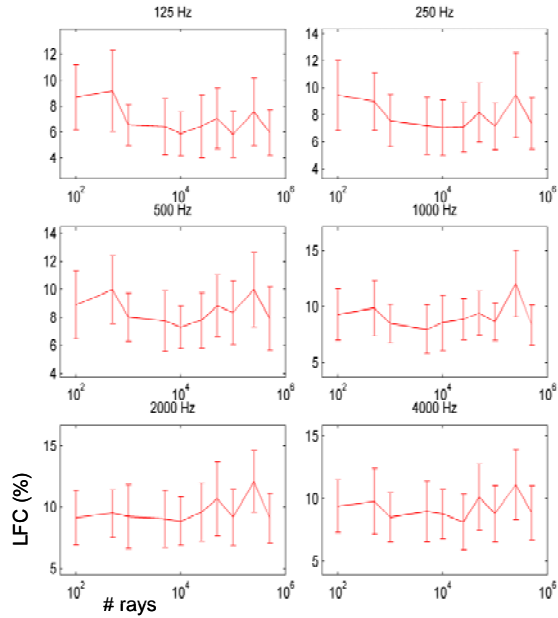
Figure 5.16. CATT™ LFC vs. number of rays.
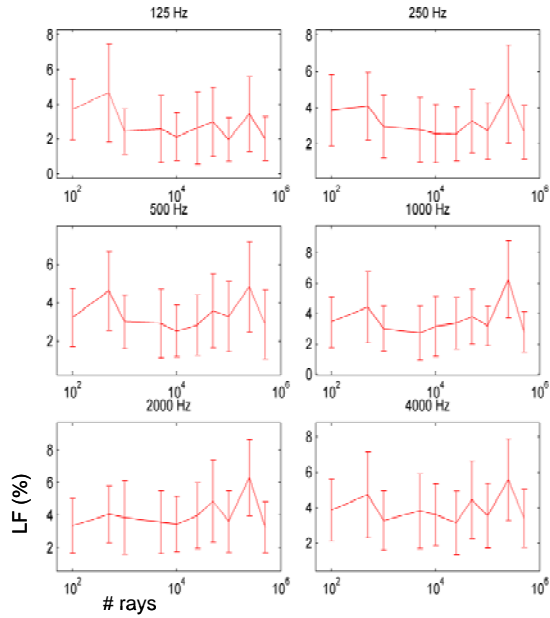
Figure 5.17. CATT™ LF vs. number of rays.

68
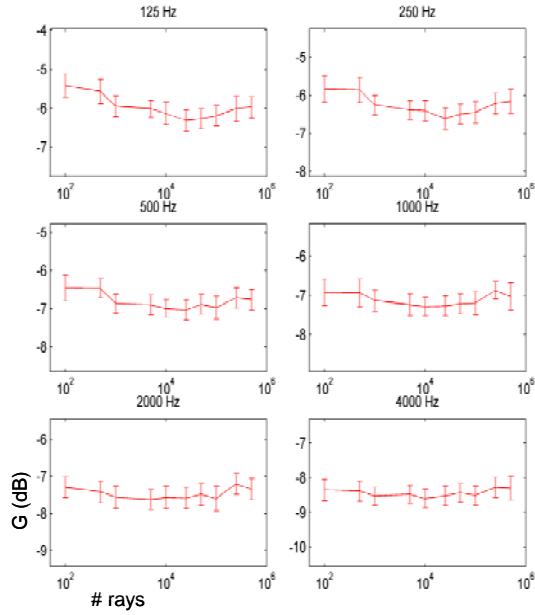
Figure 5.18. CATT™ G vs. number of rays.
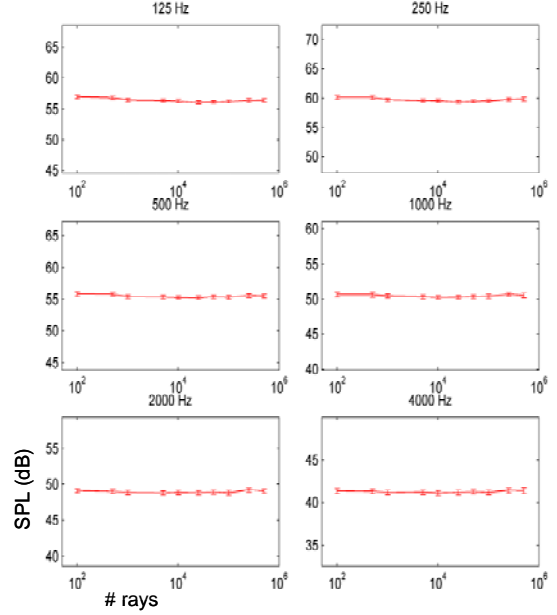
Figure 5.19. CATT™ SPL vs. number of rays.
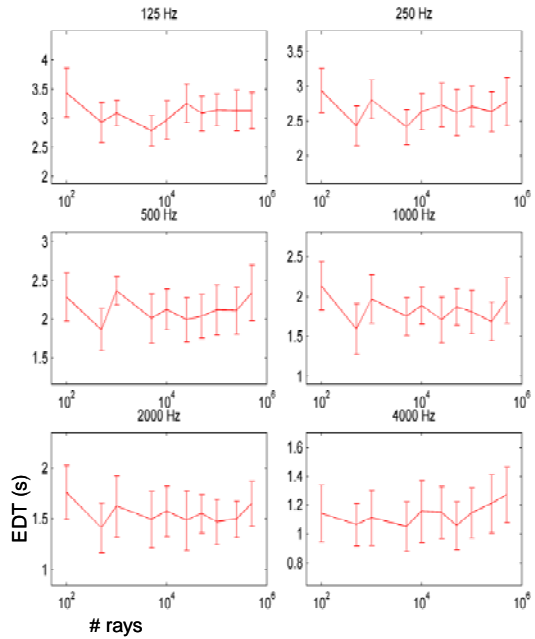
Figure 5.20. CATT™ EDT vs. number of rays.
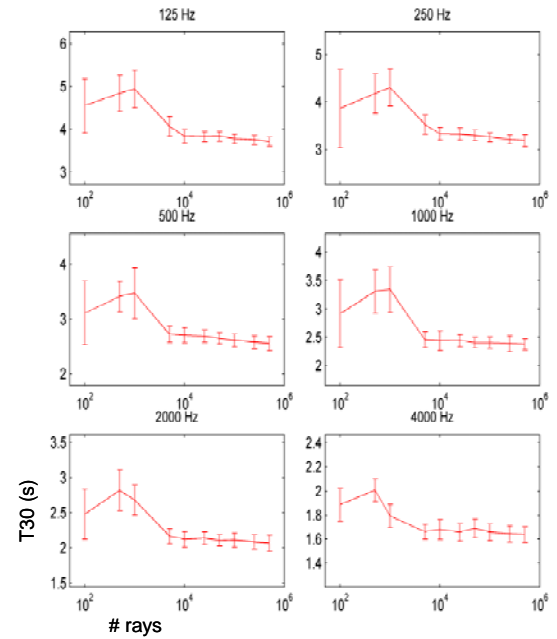
Figure 5.21. CATT™ T30 vs. number of rays.

parameter. Instead, the CATT™ plots seem to exhibit random fluctuations that are seemingly independent of the number of rays. It is unclear from these plots

69

whether this behavior is simply because the parameter has already converged to some value (below the minimum number of rays allowed by the program) or whether the parameter has not yet converged to some value. Further studies were therefore done to determine the number of rays needed in each of the packages to obtain accurate results.

A factor that affects this accuracy is whether the variation in the parameter from run to run (with a given number of rays) is less than the difference limen for that parameter. This was studied by looking at the standard deviation over the different runs as a function of the number of rays for each different parameter. Figure 5.22 through Figure 5.29 show the standard deviation of the parameter vs. the number of rays used for the octave band center frequencies in EASE™. Figure 5.30 through Figure 5.37 show the standard deviation of the parameter vs. the number of rays used for the octave band center frequencies in CATT™. The maximum and minimum difference limens corresponding to each parameter are also shown in the figures.

It can be seen that in the EASE™ plots the standard deviation is greater than the difference limen at low ray counts (with the exception of SPL), and as the number of rays grows larger, the standard deviation decreases to below (or close to below) the difference limen for the parameter. For the CATT™ plots, on
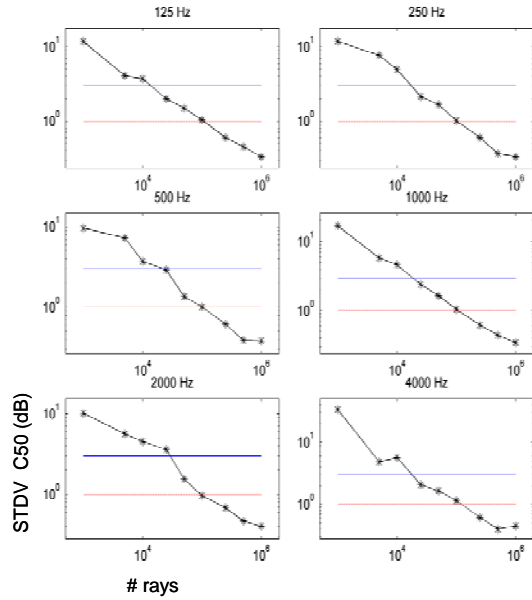
Figure 5.22. EASE™ C50 standard deviation vs. number of rays (*), DL=3 dB (–), DL=1 dB (..).
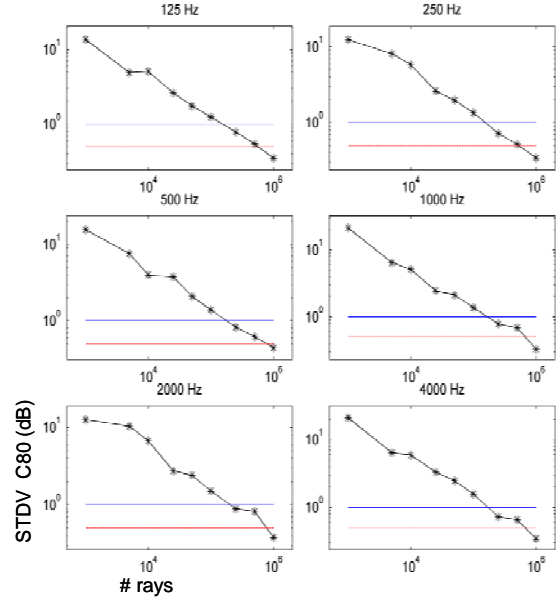
Figure 5.23. EASE™ C80 standard deviation vs. number of rays (*), DL=1 dB (–), DL=.5 dB (..).
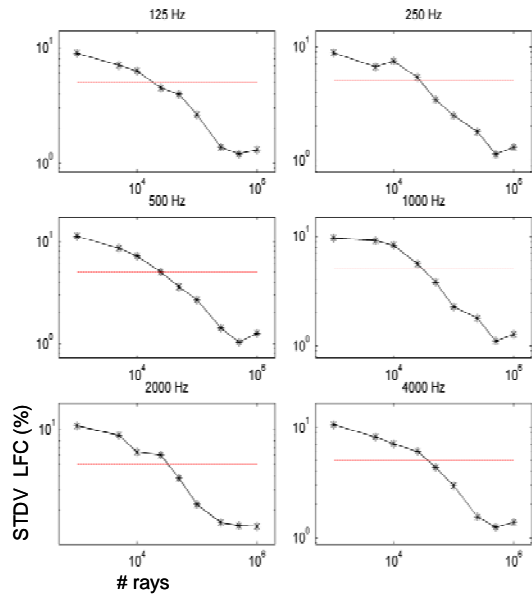
Figure 5.24. EASE™ LFC standard deviation vs. number of rays (*), DL=5 % (..).
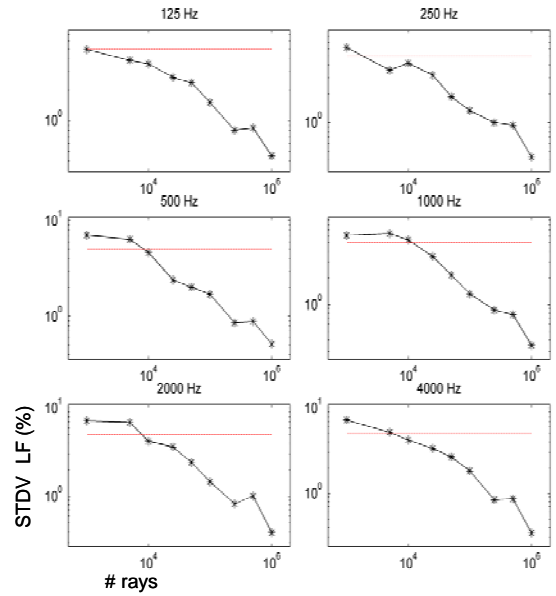
Figure 5.25. EASE™ LF standard deviation vs. number of rays (*), DL=5 % (..).
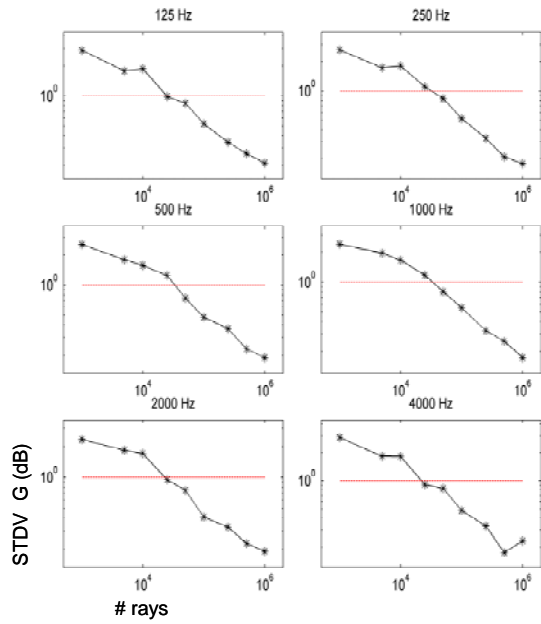
Figure 5.26. EASE™ G standard deviation vs. number of rays (*), DL=1 dB (..).
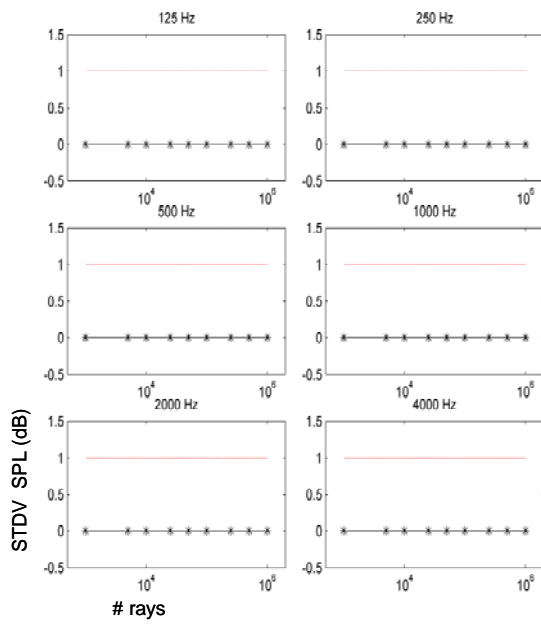
Figure 5.27. EASE™ SPL standard deviation vs. number of rays (*), DL=1 dB (..).
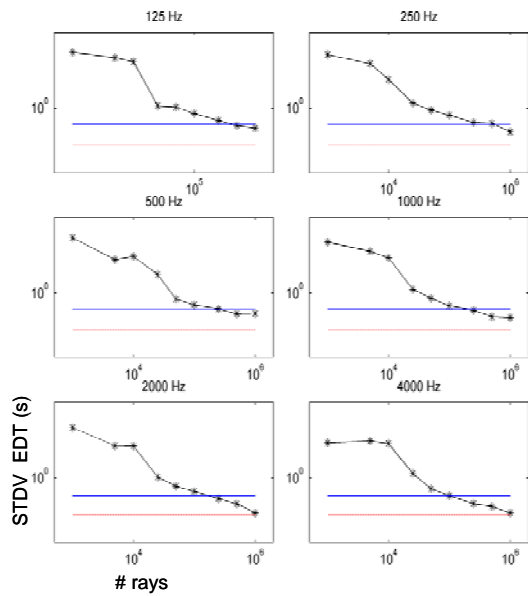
Figure 5.28. EASE™ EDT standard deviation vs. number of rays (*), DL=5 % (–), DL=.05 s (..).
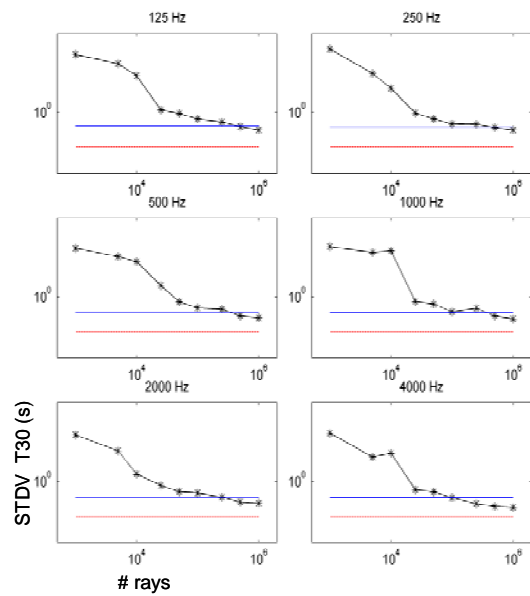
Figure 5.29. EASE™ T30 standard deviation vs. number of rays (*), DL=5 % (–), DL=.05 s (..).

72
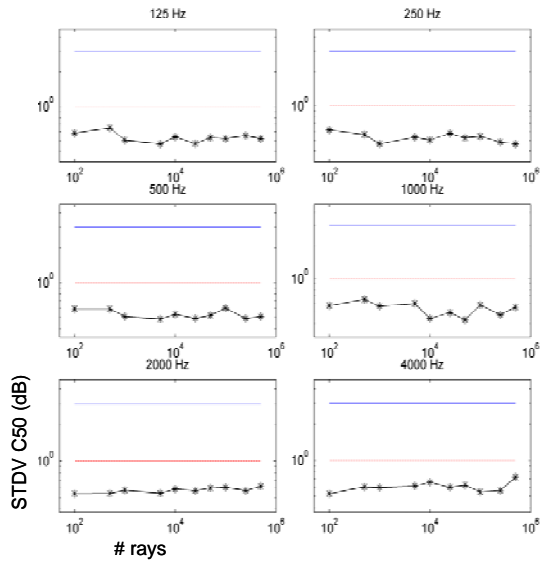
Figure 5.30. CATT™ C50 standard deviation vs. number of rays (*), DL=3 dB (–), DL=1 dB (..).
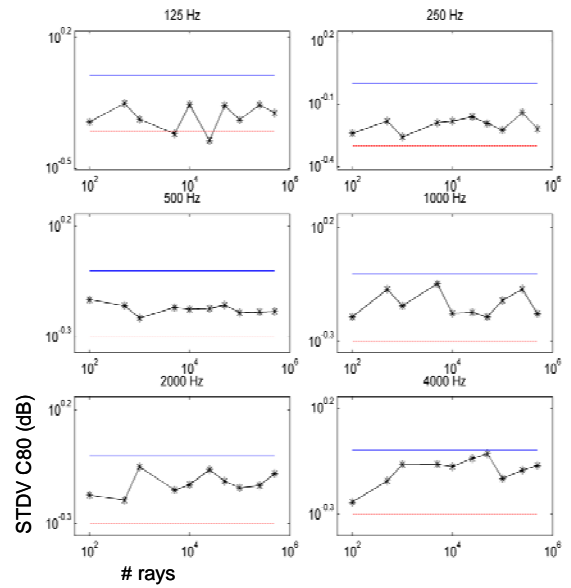
Figure 5.31. CATT™ C80 standard deviation vs. number of rays (*), DL=1 dB (–), DL=.5 dB (..).
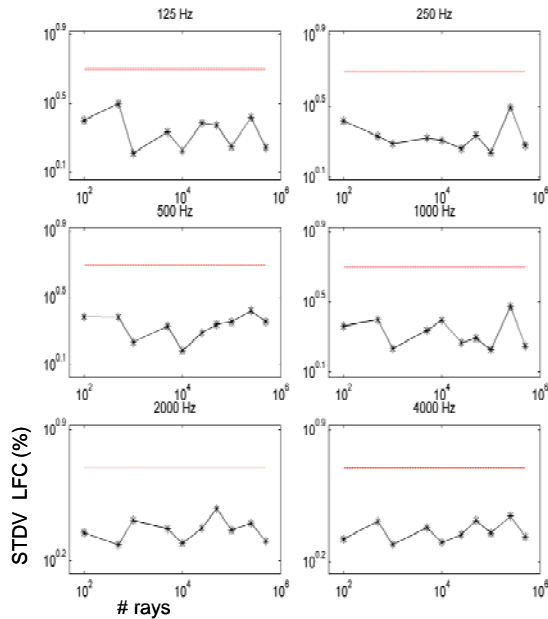
Figure 5.32. CATT™ LFC standard deviation vs. number of rays (*), DL=5 % (..).
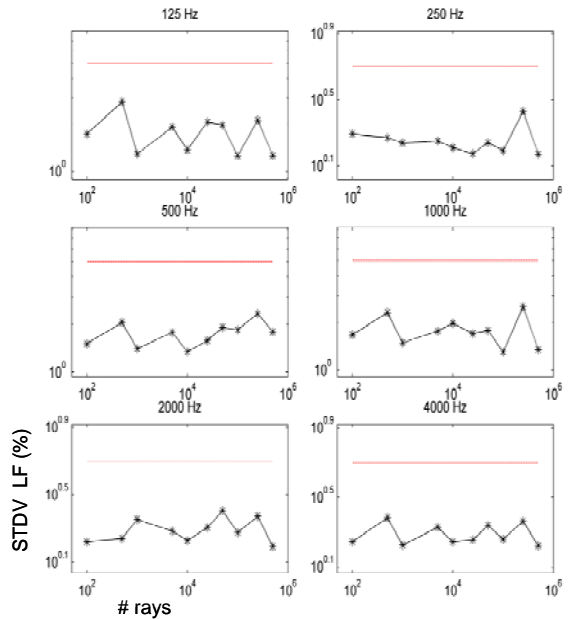
Figure 5.33. CATT™ LF standard deviation vs. number of rays (*), DL=5 % (..).
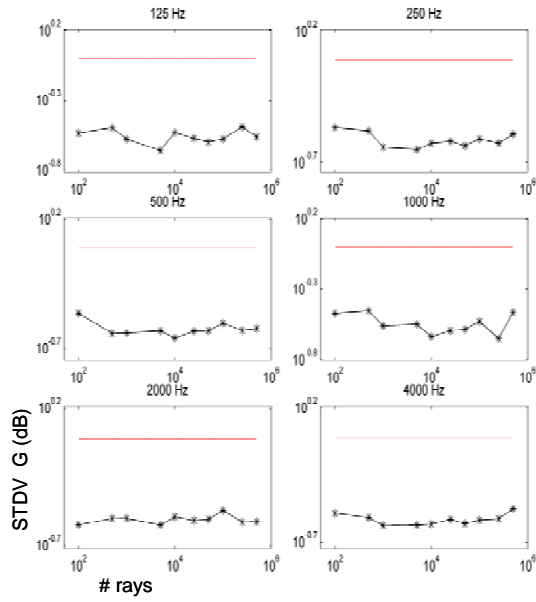
Figure 5.34. CATT™ G standard deviation vs. number of rays (*), DL=1 dB (..).
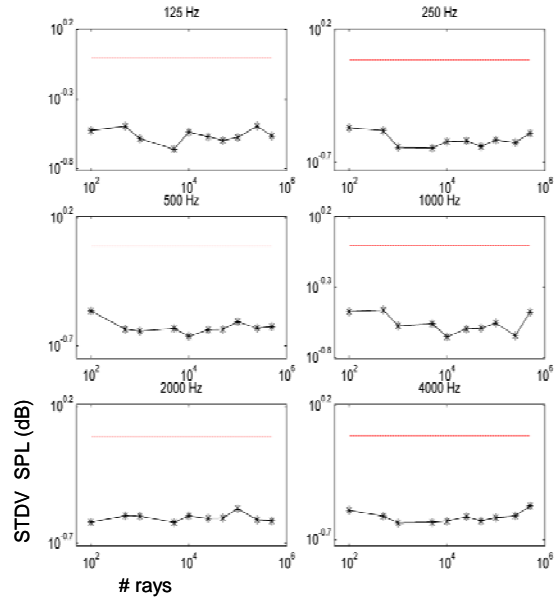
Figure 5.35. CATT™ SPL standard deviation vs. number of rays (*), DL=1 dB (..).
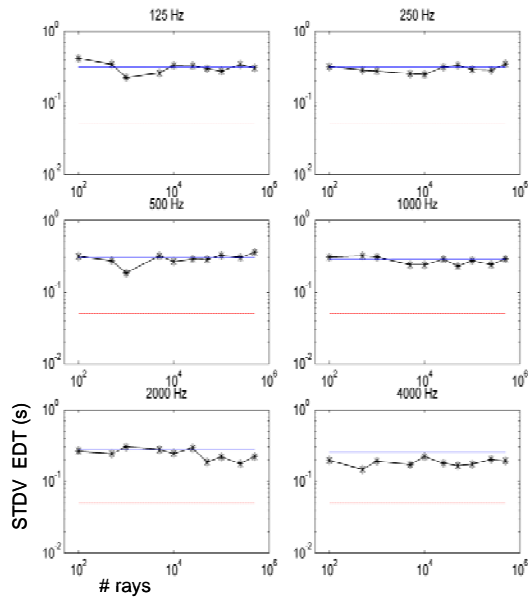
Figure 5.36. CATT™ EDT standard deviation vs. number of rays (*), DL=5 % (–), DL=.05 s (..).
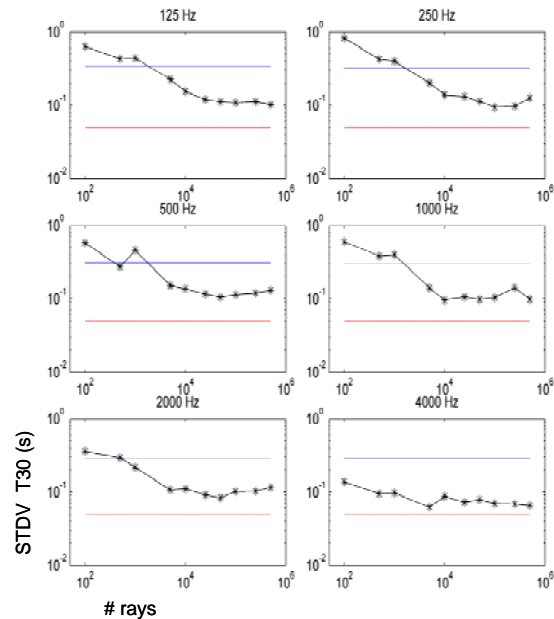
Figure 5.37. CATT™ T30 standard deviation vs. number of rays (*), DL=5 % (–), DL=.05 s (..).

the other hand, the standard deviation starts out below the difference limen for most of the parameters (with the exception of the T30 and EDT) and stays

74

below the difference limen, independent of the number of rays. The results from these figures can be summarized by showing the number of rays at which the standard deviation falls below (and stays below) the difference limen for each parameter, as shown in Table 5.5 for EASE™ and Table 5.6 for CATT™.

It can be seen from the tables that for most parameters, the CATT™ standard deviation falls below the difference limen for lower numbers of rays than the EASE™ standard deviation. Perhaps this result is evidence that the CATT™ program has actually converged (for most of the parameters). It also can be seen from both tables that for some parameters, the programs appear to have not yet converged to a value. These are shown with the > symbol and rows highlighted in the tables correspond to parameters that have not shown convergence at all frequencies.. Ray counts higher than those values have not been studied due to excessively long computation times. It should be noted

Table 5.5. EASE™ number of rays where the standard deviation falls below the difference limen.

	DL	125 Hz	250 Hz	500 Hz	1000 Hz	2000 Hz	4000 Hz
C50	1 dB	250,000	250,000	250,000	250,000	100,000	250,000
	3 dB	25,000	25,000	25,000	25,000	50,000	25,000
C80	0.5 dB	>1x10^6	>1x10^6	>1x10^6	>1x10^6	>1x10^6	>1x10^6
	1 dB	250,000	250,000	250,000	250,000	250,000	250,000
LFC	5 %	25,000	50,000	50,000	50,000	50,000	50,000
LF	5 %	1,000	5,000	10,000	25,000	10,000	10,000
G	1 dB	25,000	50,000	50,000	50,000	25,000	25,000
SPL	1 dB	1,000	1,000	1,000	1,000	1,000	1,000
EDT	0.05 s	>1x10^6	>1x10^6	>1x10^6	>1x10^6	>1x10^6	>1x10^6
	5 %	500,000	>1x10^6	500,000	250,000	250,000	100,000
T30	0.05 s	>1x10^6	>1x10^6	>1x10^6	>1x10^6	>1x10^6	>1x10^6
	5 %	500,000	500,000	500,000	500,000	500,000	100,000

Table 5.6. CATT™ number of rays where the standard deviation falls below the difference limen.

	DL	125 Hz	250 Hz	500 Hz	1000 Hz	2000 Hz	4000 Hz
C50	1 dB	100	100	100	100	100	100
	3 dB	100	100	100	100	100	100
C80	0.5 dB	>500,000	>500,000	>500,000	>500,000	>500,000	>500,000
	1 dB	100	100	100	100	100	100
LFC	5 %	100	100	100	100	100	100
LF	5 %	100	100	100	100	100	100
G	1 dB	100	100	100	100	100	100
SPL	1 dB	100	100	100	100	100	100
EDT	0.05 s	>500,000	>500,000	>500,000	>500,000	>500,000	>500,000
	5 %	>500,000	>500,000	>500,000	>500,000	50,000	100
T30	0.05 s	>500,000	>500,000	>500,000	>500,000	>500,000	>500,000
	5 %	5,000	5,000	5,000	5,000	1,000	100

that standard deviations for at least two consecutive ray counts had to fall below the difference limen in order to be counted, otherwise one cannot assumed the program has converged.

Along with the standard deviation, another thing that is important is the variation in the parameter from one ray count to the next. This can be summarized by plots showing the absolute value of the difference in the average values produced by each ray count and those produced by the largest ray count (1,000,000 for EASE™ and 500,000 for CATT™). The largest ray count was chosen as the reference because it is expected that the variation from one ray count to the next should become progressively smaller due to convergence at large ray counts. It is expected that, for a given parameter, when these differences become less than the difference limen, convergence is starting to

occur. The results for EASE™ are given in Figure 5.38 through Figure 5.45. Those for CATT™ are given in Figure 5.46 through Figure 5.53.

The difference in mean values for the highest ray counts for each package are not seen in these figures because the highest ray counts were used as a reference for this analysis. It can be seen from the figures that the difference in mean values for each ray count and those for the largest ray count in EASE™ follow a trend for most parameters: at larger ray counts the difference is generally less than at smaller ray counts. This trend, however, is not present with the CATT™ plots. Instead, the difference of mean values seemingly fluctuates, independent of the ray count. The results from these figures can be summarized by showing the number of rays at which the difference in mean
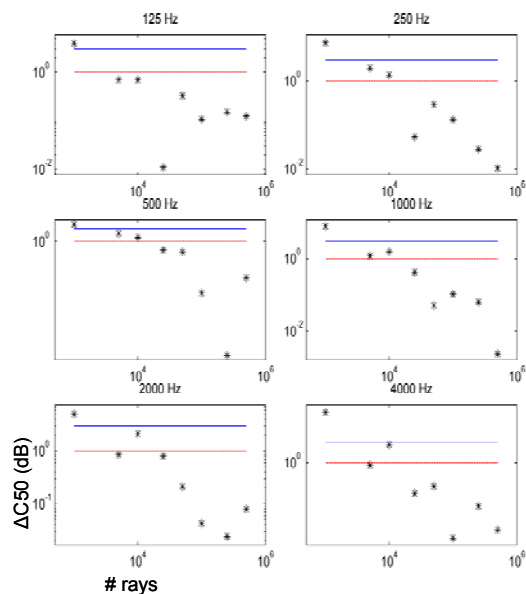
Figure 5.38. EASE™ difference in C50 vs. number of rays (*), DL=3 dB (–), DL=1 dB (..).
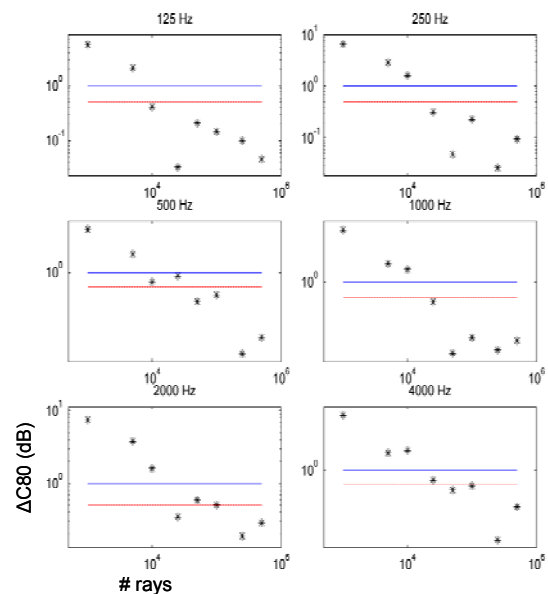
**Figure 5.39. EASE™ difference in C80 vs. number of rays (*), DL=1 dB (–), DL=.5 dB (..).**
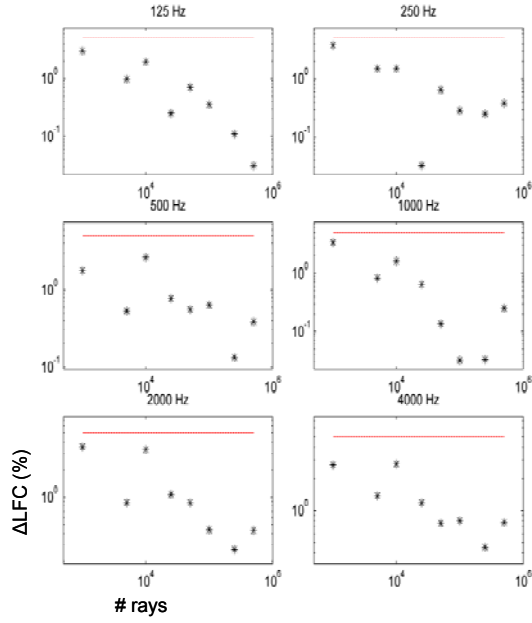
Figure 5.40. EASE™ difference in LFC vs. number of rays (*), DL=5 % (..).
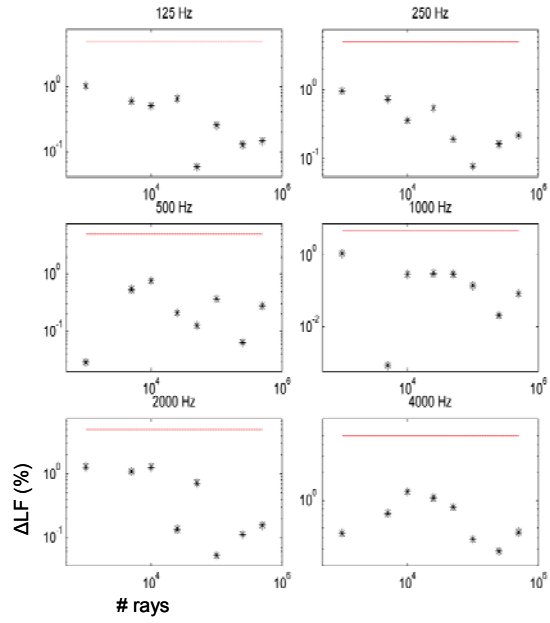
Figure 5.41. EASE™ difference in LF vs. number of rays (*), DL=5 % (..).
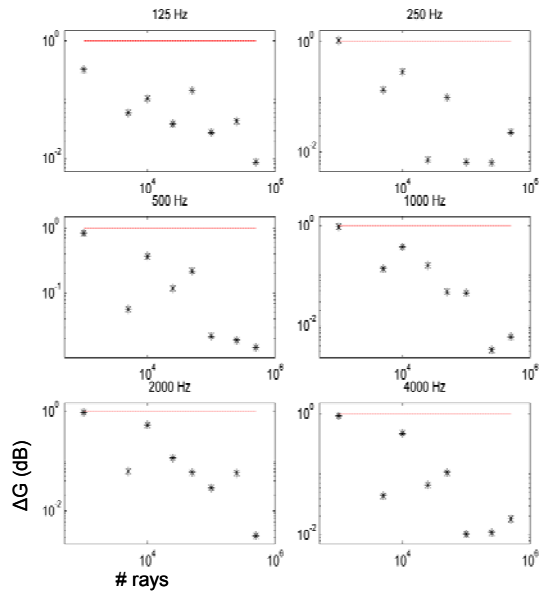
Figure 5.42. EASE™ difference in G vs. number of rays (*), DL=1 dB (..).
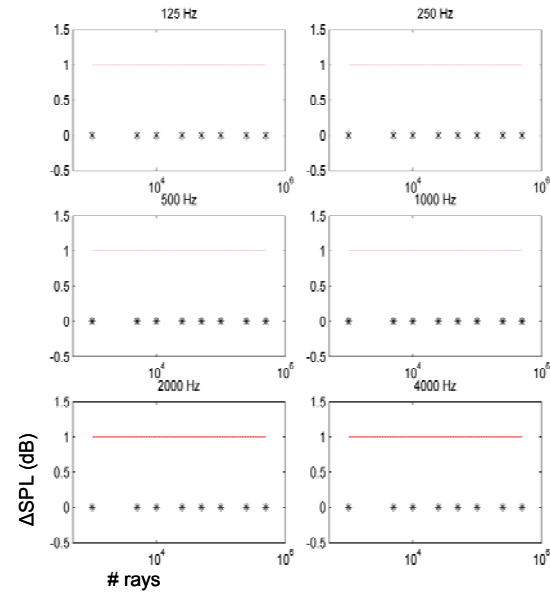
Figure 5.43. EASE™ difference in SPL vs. number of rays (*), DL=1 dB (..).

78
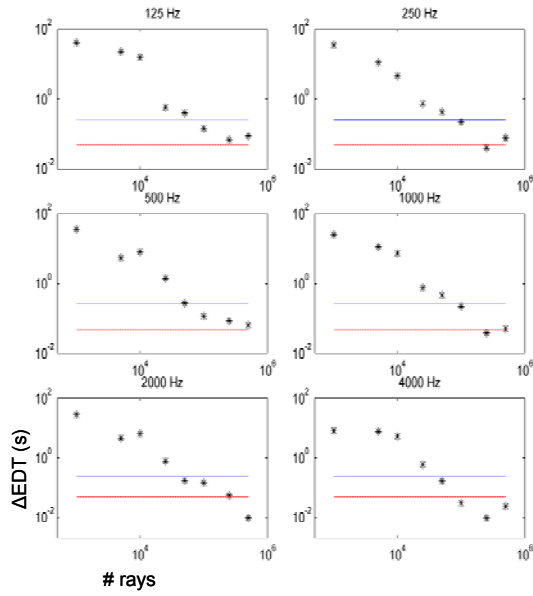
Figure 5.44. EASE™ difference in EDT vs. number of rays (*), DL=5 % (–), DL=.05 s (..).
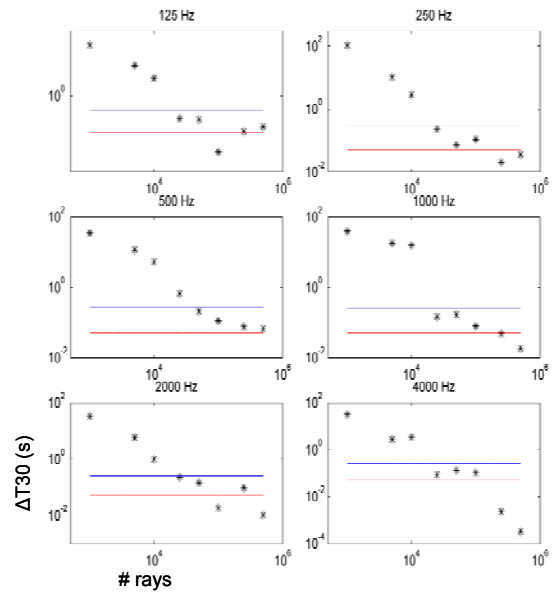
**Figure 5.45. EASE™ difference in T30 vs. number of rays (*), DL=5 % (–), DL=.05 s (..).**
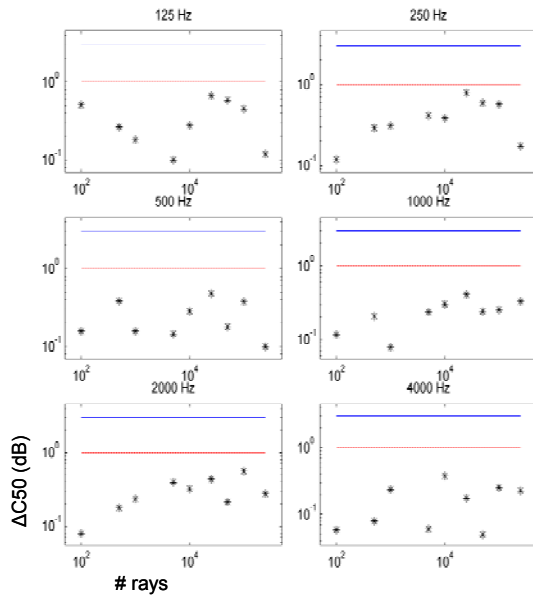
Figure 5.46. CATT™ difference in C50 vs. number of rays (*), DL=3 dB (–), DL=1 dB (..).
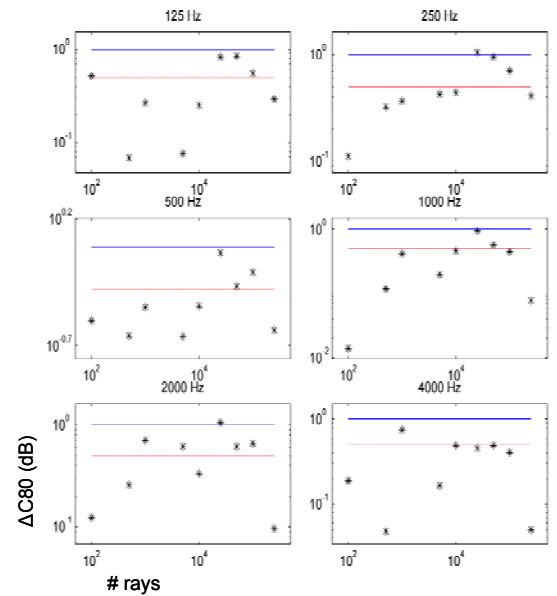
**Figure 5.47. CATT™ difference in C80 vs. number of rays (*), DL=1 dB (–), DL=.5 dB (..).**
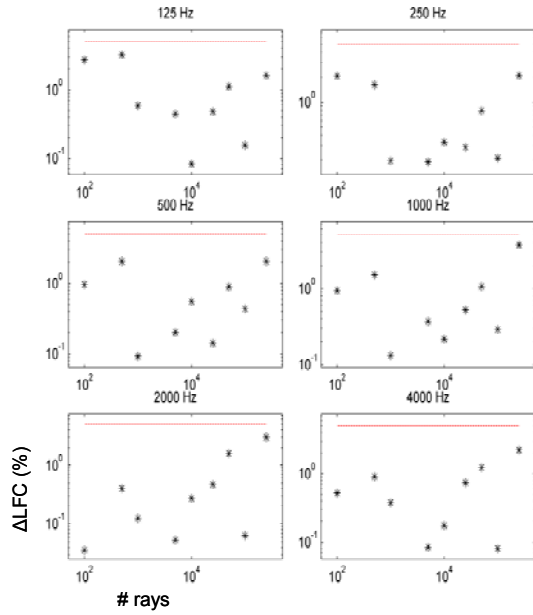
Figure 5.48. CATT™ difference in LFC vs. number of rays (*), DL=5 % (..).
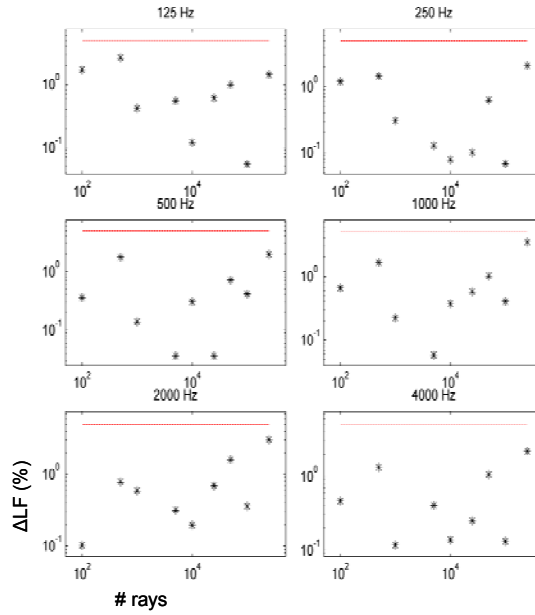
Figure 5.49. CATT™ difference in LF vs. number of rays (*), DL=5 % (..).
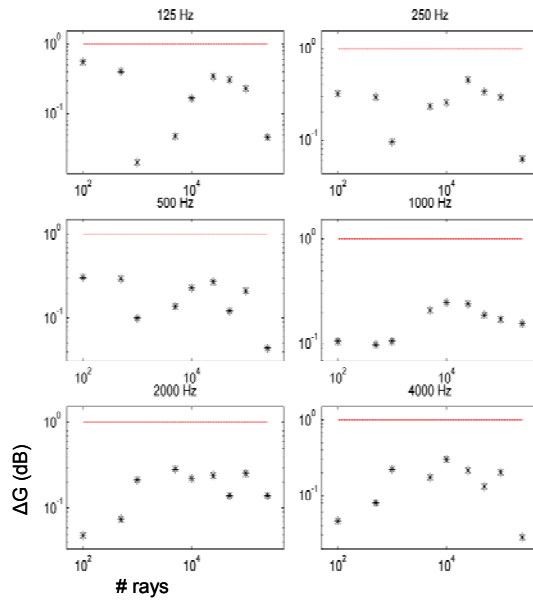
Figure 5.50. CATT™ difference in G vs. number of rays (*), DL=1 dB (..).
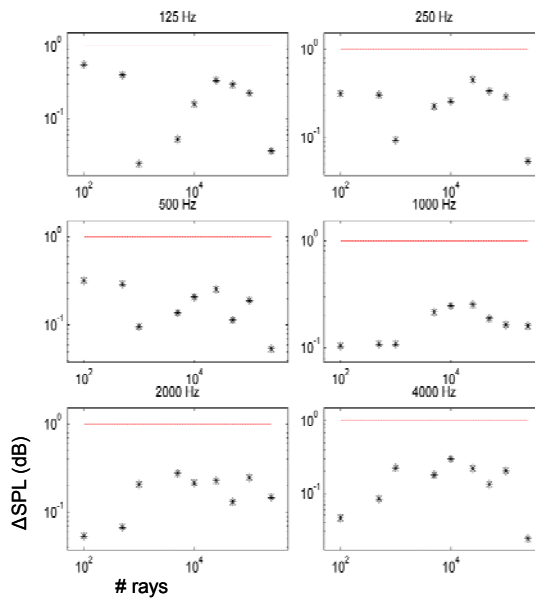
Figure 5.51. CATT™ difference in SPL vs. number of rays (*), DL=1 dB (..).
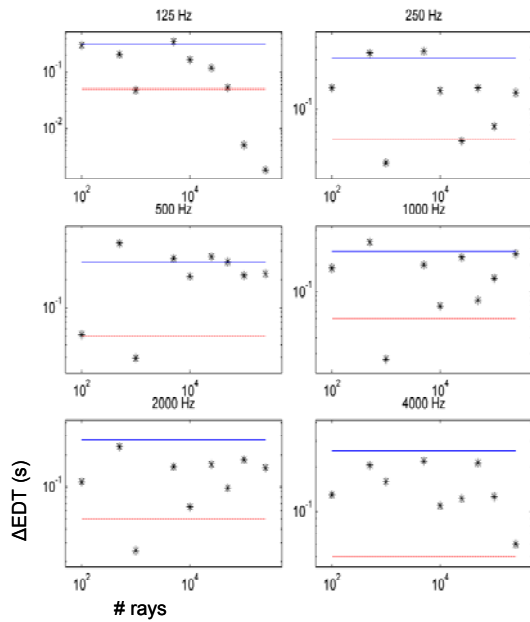
Figure 5.52. CATT™ difference in EDT vs. number of rays (*), DL=5 % (–), DL=.05 s (..).
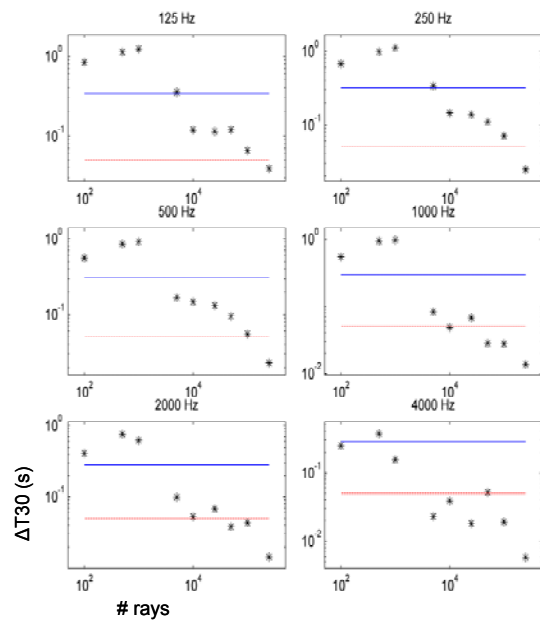
Figure 5.53. CATT™ difference in T30 vs. number of rays (*), DL=5 % (–), DL=.05 s (..).

values falls below (and stays below) the difference limen for each parameter (see Table 5.7 for EASE™ and Table 5.8 for CATT™).

It can be seen from the tables that for most parameters, the CATT™ difference in mean values falls below the difference limen at lower ray counts

Table 5.7. EASE™ number of rays where the difference in mean values falls below the difference limen.

	DL	125 Hz	250 Hz	500 Hz	1000 Hz	2000 Hz	4000 Hz
C50	1 dB	5,000	25,000	25,000	25,000	25,000	25,000
	3 dB	5,000	5,000	5,000	5,000	5,000	5,000
C80	0.5 dB	10,000	25,000	50,000	25,000	250,000	50,000
	1 dB	10,000	25,000	10,000	25,000	25,000	25,000
LFC	5 %	1,000	1,000	1,000	1,000	1,000	1,000
LF	5 %	1,000	1,000	1,000	1,000	1,000	1,000
G	1 dB	1,000	5,000	1,000	1,000	1,000	1,000
SPL	1 dB	1,000	1,000	1,000	1,000	1,000	1,000
EDT	0.05 s	>500,000	>500,000	>500,000	>500,000	>500,000	100,000
	5 %	100,000	100,000	100,000	100,000	50,000	50,000
T30	0.05 s	>500,000	250,000	>500,000	250,000	>500,000	250,000
	5 %	25,000	25,000	50,000	25,000	25,000	25,000

Table 5.8. CATT™ number of rays where the difference in mean values falls below the difference limen.

	DL	125 Hz	250 Hz	500 Hz	1000 Hz	2000 Hz	4000 Hz
C50	1 dB	100	100	100	100	100	100
	3 dB	100	100	100	100	100	100
C80	0.5 dB	>250,000	>250,000	>250,000	100,000	>250,000	5,000
	1 dB	100	50,000	100	100	50000	100
LFC	5 %	100	100	100	100	100	100
LF	5 %	100	100	100	100	100	100
G	1 dB	100	100	100	100	100	100
SPL	1 dB	100	100	100	100	100	100
EDT	0.05 s	100,000	>250,000	>250,000	>250,000	>250,000	>250,000
	5 %	10,000	10,000	100,000	1,000	100	100
T30	0.05 s	>250,000	>250,000	>250,000	50,000	50,000	100,000
	5 %	10,000	10,000	5,000	5,000	5,000	1,000

than does the EASE™ difference in mean values. This result may be further evidence that the CATT™ program has actually converged (for most parameters). It also can be seen from both tables that for some parameters, the programs appear to have not yet converged to a value. These are shown with the > symbol, and rows highlighted in the tables correspond to parameters that have not shown convergence at all frequencies. Once again, ray counts higher than those values have not been studied due to excessively long computation times. It should be noted that the difference in mean values for at least two consecutive ray counts had to fall below the difference limen in order to be counted, otherwise one cannot assume the program has converged.

Some conclusions can be drawn from the results shown in this section about the number of rays necessary for each modeling package. According to

the difference limens published for these parameters, both EASE™ and CATT™

produced parameter values which had not yet shown convergence at the

highest ray counts used in the calculations. However, continuing to increase

ray counts to find their convergence was considered impractical because of

extremely long computation times. The optimum number of rays needed for

the programs was then based on the parameters that had shown convergence

within the ray counts studied.

The number of rays needed in the packages is based upon the data shown

in Table 5.5 through Table 5.8. Excluding the rows that are highlighted in the

table, the maximum number of rays was determined for each table. For each

package, the greater number of rays was chosen from the two tables as the

number of rays needed in the packages to obtain reliable results. For EASE™,

the number of rays needed is 500,000 and for CATT™ the number of rays

needed is 100,000. These values were used for the remainder of the research.

Thus, the EASE™ recommendation of a minimum of 100,000 rays for

auralization and more detailed investigations was shown to be insufficient for

the calculation of parameters in this hall. Dalenbäck's observation that the

parameters should not vary more than the difference limen, even with 1,000

rays, was shown to be true for most of the parameters in CATT™. However,

some parameters definitely needed many more rays (see Table 5.6 and Table

5.8). It is interesting to note that the number of rays calculated by the "auto number" in CATT™ was 127,101 rays, which is in reasonable agreement with the 100,000 rays determined from this research.

5.5   Sensitivity of Model to Scattering Coefficients

Research was also conducted to determine whether the model was sensitive to scattering coefficients. It was expected that the scattering from the seats and audience would be the most significant scattering contribution in the model due to the large proportion of surface area taken up by the audience areas and their large scattering coefficients predicted by many authors. Thus, the focus of this research phase was to determine how sensitive the models would be to scattering from the seating areas.

Rathsam[82] conducted a similar study on how sensitive a few models were to scattering coefficients on all surfaces of a room. He studied three different computer models in ODEON, four acoustic parameters (EDT, T30, C80, and LF) and five different scattering coefficient values (0%, 10%, 30%, 50%, and 80%). He determined the number of JNDs, with reference to a scattering coefficient of 0%, for each parameter at each scattering coefficient value. All parameters fell below 2 JNDs for all scattering coefficient values except T30. He consequently

concluded that T30 appeared to be the most sensitive parameter to scattering coefficient variation in his models.

In this investigation, the scattering coefficient for the seating area was varied from 10% to 99% in 10% increments (and one 9% increment) within the CATT™ model. The scattering coefficient was assumed to have the same value for all frequencies of interest. Eight different parameters were predicted for this investigation. An omnidirectional source was positioned in the soprano section of the choir (position S) and twelve receivers were located throughout the model (see Figure 5.54). Due to random fluctuations from run to run in the package itself, thirty-eight different runs were averaged for each seating position and each scattering coefficient value. Previous research detailed in
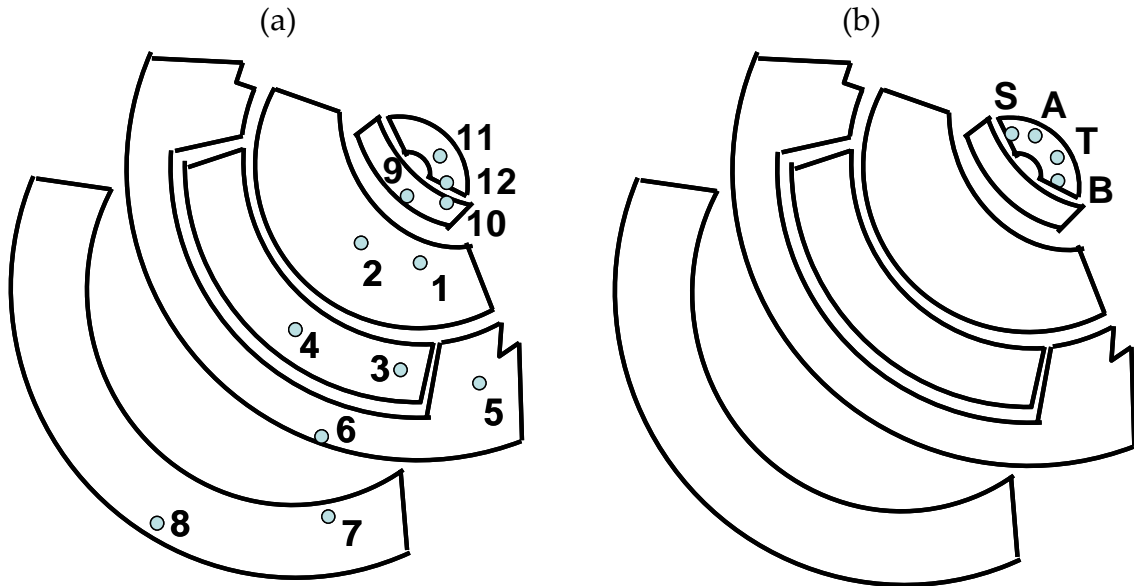
Figure 5.54. Receiver (a) and source (b) positions.

85

Section 5.4 showed that most parameters gave close to a 100% confidence level

when 50 runs were averaged (see Table 5.4). Because a confidence level of less

than 100% is still acceptable, it was expected that thirty-eight runs would give a

good sampling of the random fluctuations from run to run. The scattering

coefficient of 10% was arbitrarily chosen as a reference value. However, it was

verified that with a reference value of 99% the results were not significantly

different. The absolute value of the difference between the parameter at each

scattering coefficient value and the parameter at the reference scattering

coefficient value was first computed. It was then divided by the difference

limen for that parameter to determine the number of difference limens (or

JNDs) the parameter had varied because of the scattering coefficient variation.

Figure 5.55 shows the results for seat number 1 in the form of bar graphs. The

results for seat numbers 2 through 12 are given in Appendix D.

For each parameter, a group of bar plots are seen which correspond to the

difference limens for scattering coefficient values of 20% up to 99%. For

parameters with more than one group of bar plots (i.e., C50, C80, EDT, and

T30), the group closer to the left is the lower published value of difference

limen.

The data in these plots can be summarized by taking the maximum

number of difference limens for each parameter grouping (for each seat) and
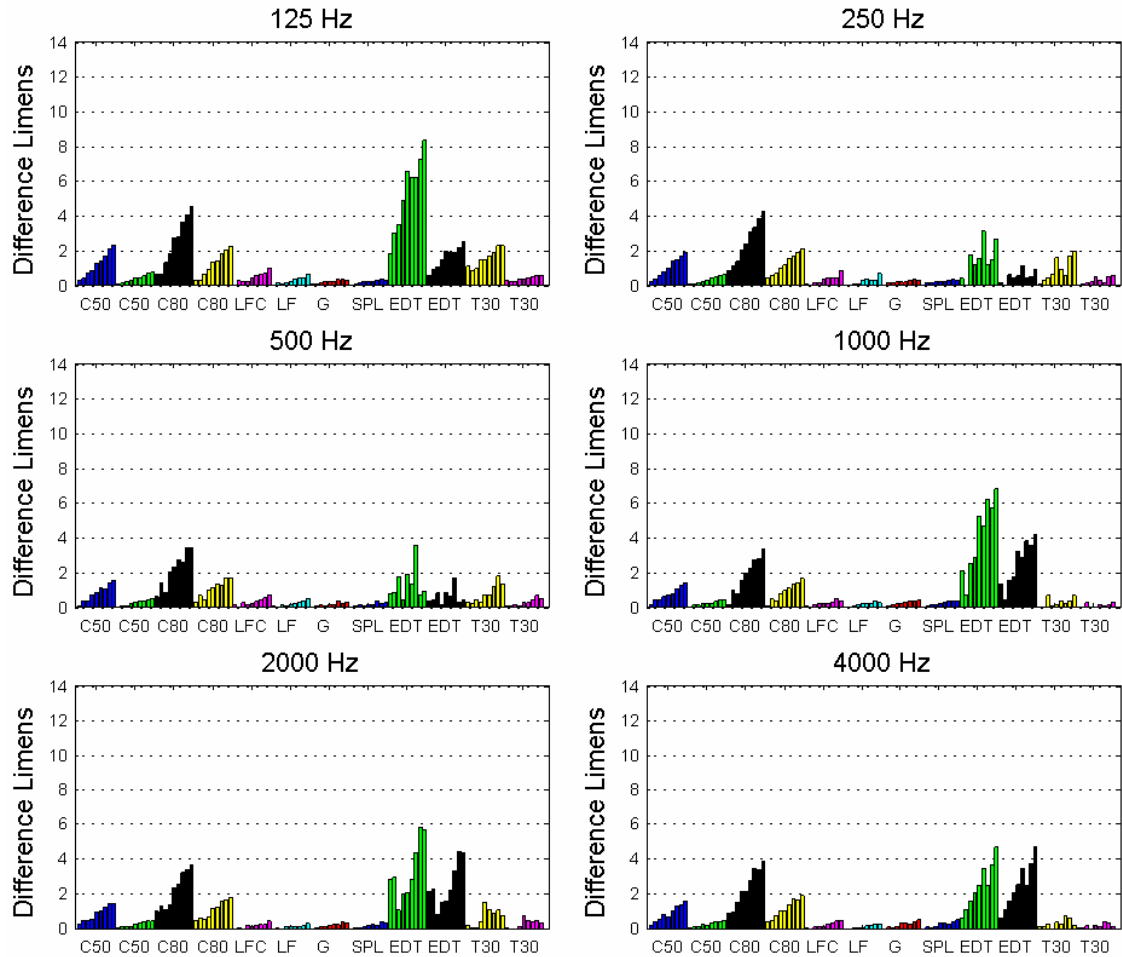
Figure 5.55. Difference limens for variations in the scattering coefficient value for seat number 1.

averaging those values over all twelve seats (see Table 5.9). This effectively gives a worst-case average for each parameter.

Vorländer[18] compared predicted parameter values with measured values in a round robin and stated that the prediction was not totally useless if the accuracy was less than the subjective limen. He pointed out, however, that a difference of more than two subjective limens would produce excessive uncertainty. The highlighted values in Table 5.9 correspond to variations of

Table 5.9. Number of difference limens of variation for each parameter.

	DL	125 Hz	250 Hz	500 Hz	1000 Hz	2000 Hz	4000 Hz
C50	1 dB	1.3395	1.1821	1.1667	1.0799	1.1062	1.128
	3 dB	0.4465	0.394	0.3889	0.36	0.3687	0.376
C80	0.5 dB	2.2149	2.0535	1.9921	1.818	1.9443	1.8693
	1 dB	1.1075	1.0268	0.9961	0.909	0.9721	0.9346
LFC	5 %	1.4518	1.2728	1.1284	0.8878	0.8628	0.92
LF	5 %	1.1256	0.9907	0.8573	0.6823	0.6508	0.7047
G	1 dB	0.5846	0.5283	0.4811	0.5287	0.5296	0.6882
SPL	1 dB	0.5833	0.5283	0.4836	0.5285	0.5285	0.6895
EDT	0.05 s	7.7513	6.2421	4.9851	4.6105	3.8961	2.8934
	5 %	3.2031	3.1004	3.3123	3.3741	3.483	3.1605
T30	0.05 s	2.3601	2.3969	2.2487	2.0184	1.7592	1.0667
	5%	0.6406	0.7232	0.8318	0.7999	0.8358	0.6542

more than two subjective limens. It can be seen that the parameters that show significant sensitivity at some frequencies in the variation of scattering coefficients include C80 (DL = 0.5 dB), EDT (DL = 0.05 s, DL = 5 %), and T30 (DL= 0.05 s). It should be noted, however that according to Table 5.4, thirty-eight runs is not sufficient for EDT (DL=0.05 s), so the large difference limen values could still represent a variation associated from run to run rather than a variation associated with the changes in the scattering coefficient.

Significantly, the investigation has shown that most of the acoustic parameters are *not* sensitive to variations in the scattering coefficient of the seating areas in this model. This seems to suggest that scattering coefficients for the seating areas do not need to be estimated with a high degree of accuracy. Since variation in the scattering coefficient does not significantly affect most acoustic parameters, it should be feasible to obtain accurate results

with only a rough estimate for the scattering coefficients. Further work could be done to determine whether the impulse responses and auralizations are sensitive to variations in the scattering coefficient, and to determine whether some source and receiver positions are more sensitive than others.

6 Refining the Models

The previous chapter discussed the methods that were used to create preliminary models of the Conference Center auditorium. It was hoped that by refining key absorption coefficients of these preliminary models, based on more scientific methods, better predictions would result. It was shown in Section 5.5 that the model was not sensitive to variation in the scattering coefficients for the seating areas, for most parameters. Thus, it was expected that scientific optimization of these coefficients might not strongly affect the modeling results.

This chapter first discusses absorption coefficient measurements made for two dominant surfaces in the hall. It then discusses methods (based on physical principles) that were used in attempts to determine more accurate scattering coefficients of the seating areas. However, these methods did not produce scattering coefficients that were incorporated into the refined models.

6.1   Absorption Coefficients

As mentioned in Section 5.2, the agreement between measured and predicted total absorption curves for the preliminary model was reasonable, with slight differences in their shapes. In this phase of the research, absorption coefficient measurements were made in a reverberation chamber for the surfaces that most strongly affected the total absorption curves. Figure 5.5

shows that these surfaces were the absorptive panels above the canopy ceiling and the empty seats (or seated audience). It was hoped that new absorption coefficient values would yield total absorption curves that better matched measured curves and produced better modeling predictions.

Before making any measurements, it was important that the reverberation room be qualified for sound absorption measurements. The procedure for qualifying the reverberation chamber will first be discussed. Measurements of the two surfaces will then be discussed. Finally, the new cumulative absorption curves will be presented and the measured and predicted total absorption curves will be compared.

6.1.1   Reverberation Chamber Qualification Procedure

Two reverberation chambers were recently built at BYU. The large chamber size and shape meets the ISO 354[53] standard for absorption coefficient measurements, while the small chamber does not. The large chamber was accordingly used for all of the measurements.

The large chamber dimensions are approximately 5 m x 6 m x 7 m, with a volume of 210 m^3 and a total surface area of 214 m^2. It is rectangular in shape, meeting the following ISO 354 criteria:

$$I_{max} < 1.9 V^{1/3},$$ (6.1)

where I_{max} is the length of the longest straight line fitting within the room boundaries (i.e., in a rectangular room, it is the major diagonal), and V is the volume of the room.

In order to create a sufficiently diffuse sound field, diffusers were hung throughout the room (see Figure 6.1). The ISO 354 qualification procedure was used to determine the number of diffusers needed.

For the qualification procedure, the absorption coefficient of a 2.74 m x 3.66 m sample of 5.1 cm-thick Owens Corning 703 semi-rigid fiberglass insulation panel was measured using different numbers of diffusers. The absorption coefficient (averaged over both frequency and space) was then plotted versus the surface area of the diffusers in place. Once the average

Figure 6.1. Diffusers being hung to satisfy the ISO 354 qualification procedure for reverberation chamber measurements.

absorption coefficient leveled off, the number of diffusers was sufficient to set up a diffuse field in the chamber. Figure 6.2 shows the absorption coefficient versus the area of diffusers in the chamber. It can be seen that with the final number of diffusers used, the absorption coefficient had already leveled off, and thus, a sufficiently diffuse sound field had been produced.

The diffusers used for these measurements were .64 cm-thick acrylic panels of various sizes bent into various shapes. Fifteen total diffusers were hung from the ceiling throughout the room in a randomized fashion. Table 6.1 lists the number of diffusers of different areas that were used in the final configuration.
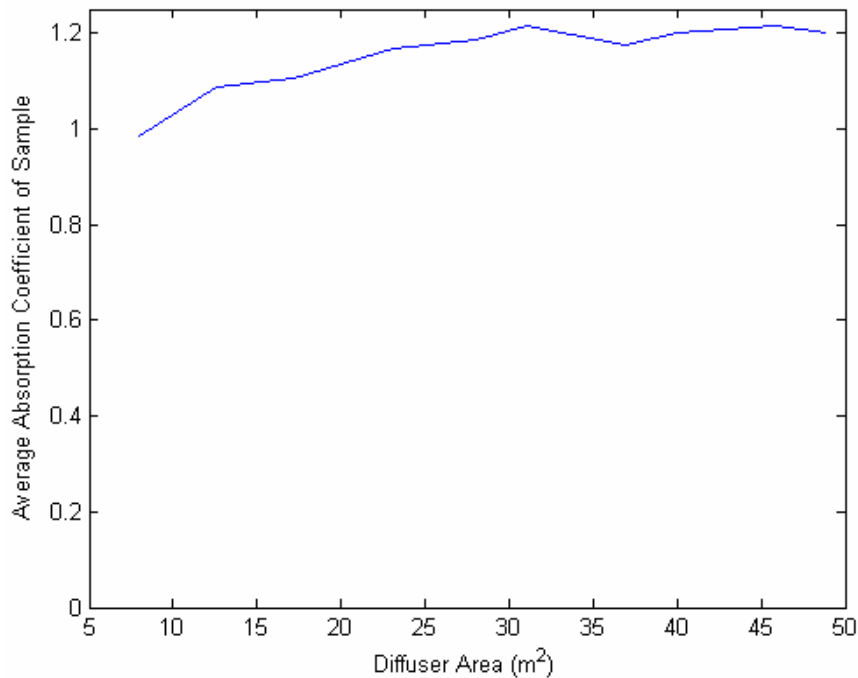
Figure 6.2. Absorption coefficient of sample vs. area of diffusers.

Table 6.1. Area and quantity of diffusers.

Area of Diffuser (m²)	1.89	2.68	2.97	3.03	5.94
Quantity	4	2	3	4	2

6.1.2   Absorptive Ceiling Panel Measurements

Figure 6.3 shows the T-grid set up of absorptive panels in the Conference Center above the canopy ceiling and a similar T-grid sample set up in the reverberation chamber. The floor-plan view of the reverberation chamber in Figure 6.4 shows the microphone and source positions used in its measurement, following ISO 354 guidelines.

The T-grid frame used for the reverberation chamber measurements was 3.66 meters wide by 3.05 meters long. Eight absorptive panels (0.61 meters wide by 1.22 meters long each) were placed in a checkerboard pattern in the T-grid. The absorption area was calculated using Equation (4.4) and the average of twelve reverberation time measurements (according to ISO 354[53]) with and without the absorptive panels in place (see Section 4.1). However, because there was one more absorptive panel than there was empty space in the grid, extra empty space area (equivalent to the area of one absorptive panel) was included in the calculations to obtain an accurate value for the absorption coefficient of the equal-area checkerboard arrangement in the Conference Center. Octave band absorption coefficients were determined by averaging the
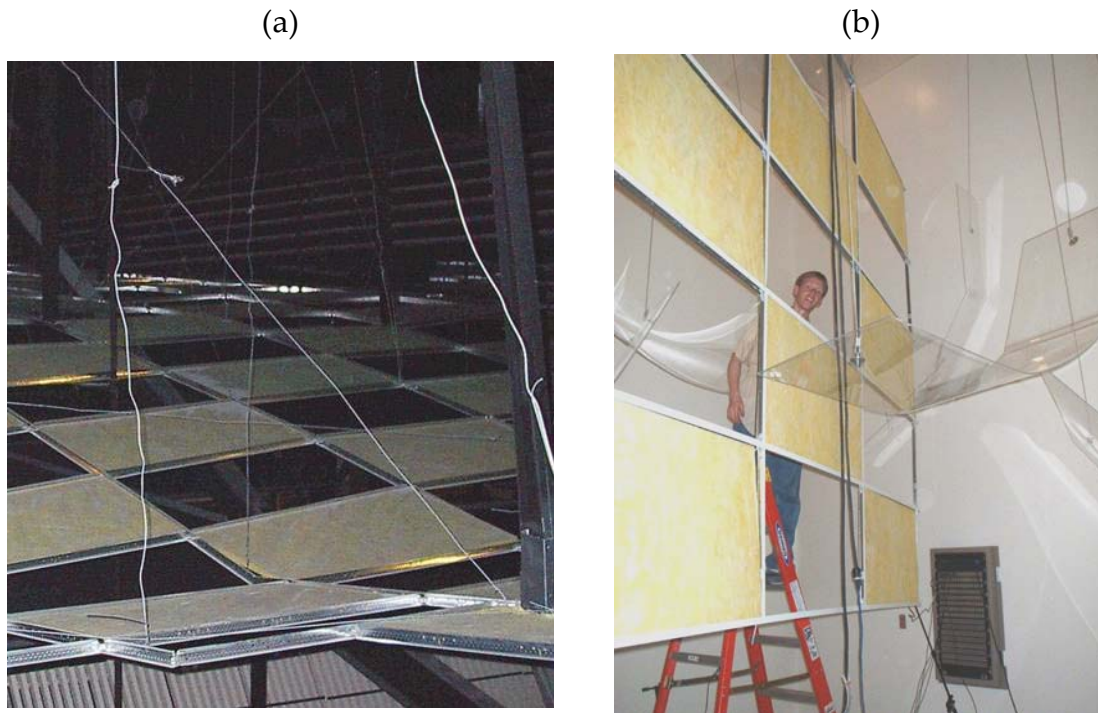
Figure 6.3. T-grid set up in the Conference Center above the canopy ceiling (a) and similar T-grid sample set up in the reverberation chamber (b).
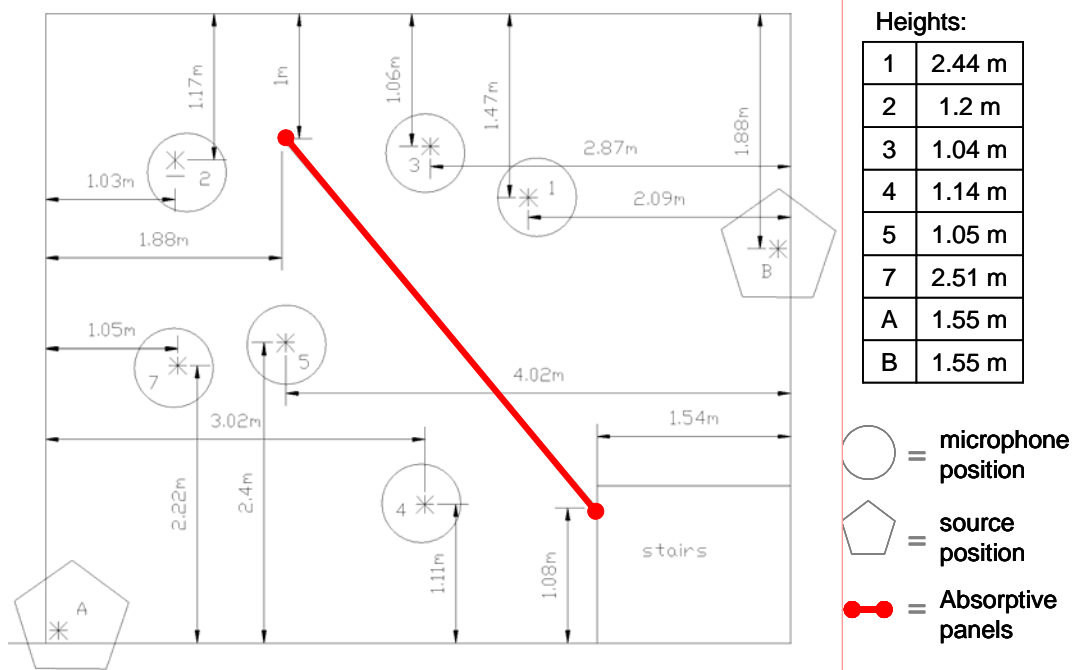
Figure 6.4. Floor plan of reverberation chamber for absorptive panel measurements.

three 1/3 octave band absorption coefficients within each octave band as directed in ISO 354.

It was estimated that the T-grid arrangement only takes up about two-thirds of the ceiling surface area in the Conference Center. Because the ceiling treatment surface in the model takes up the majority of the ceiling area, the absorption coefficient measured for the T-grid should be multiplied by two-thirds in order to obtain a reasonably accurate absorption coefficient for the ceiling treatment in the model.

The absorption coefficients were determined by considering the surface area of both sides of the T-grid and finding the absorption coefficient per side. This is consistent with how the coefficients are entered into the computer models. Absorption coefficients are entered on both sides of a flat plane in the models in order to represent the T-grid.

A graph of the measured octave band absorption coefficients for the ceiling treatment in the Conference Center model is given in Figure 6.5. Also shown in this figure are the absorption coefficients that were estimated using data from the literature and used in the preliminary models before the measurements were carried out. The octave-band values are also listed in Table 6.2 for clarity.

The Schroeder frequency is a rough frequency above which measurements
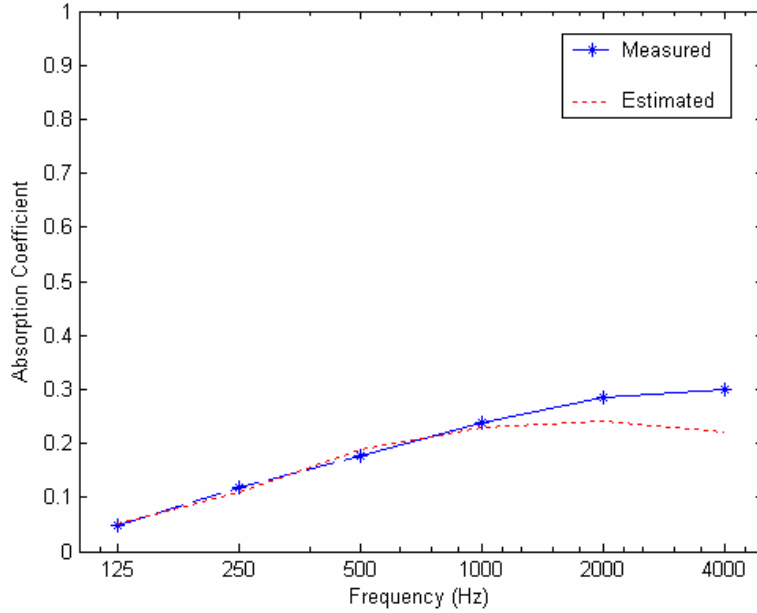
Figure 6.5. Octave band absorption coefficient values for T-grid of absorptive panels.

made in the reverberation chamber are valid, being based on the assumption of a sufficiently diffuse field. It can be calculated using

$$f_s = 2000\sqrt{\frac{T_{60}}{V}} ,$$ (6.2)

where V is the volume of the room in m³ and T_{60} is the reverberation time (measured in the closest third octave band to the Schroeder frequency).

For the room with the absorptive panels in it, the Schroeder frequency was calculated to be 283 Hz. Thus, for these measurements, the 125 Hz and 250 Hz octave band absorption coefficients were considered questionable. Values

Table 6.2. Octave band absorption coefficient values for T-grid of absorptive panels.

Frequency	125 Hz	250 Hz	500 Hz	1000 Hz	2000 Hz	4000 Hz
α measured	0.05	0.12	0.18	0.24	0.29	0.30
α estimated	0.05	0.11	0.19	0.23	0.24	0.22

that were estimated from the literature for these two frequencies were used in the refined computer models instead.

It should be noted that ISO 354[53] requires that the temperature and humidity be recorded for each measurement and included in the calculation of the absorption area, as given in Equation (4.4). However, it was shown with previous measurements that changes in temperature and humidity were negligible over a period of 3 or 4 hours. The entire process for measuring the absorption of the absorptive panels was completed in three hours on a single day. Thus, it was considered safe to ignore humidity and temperature variations in the absorption area calculations.

6.1.3   Unoccupied Chair Measurements

The absorption of the unoccupied chairs from the Conference Center was measured using the Kath and Kuhl method explained in Section 4.2. Nine chairs were placed in a corner of the reverberation chamber with .91 meter high surrounding barriers made of 1.9 cm-thick medium density fiberboard (MDF). The entire measurement process was performed with and without carpet placed underneath the chairs. Although the carpet used in the measurements was not exactly the same as the carpet in the Conference Center, its absorption properties were considered similar. The setup for these measurements is

Figure 6.6. Setup in the reverberation chamber for measuring the absorption of empty chairs.

shown in Figure 6.6. Figure 6.7 provides a floor-plan view of the chamber

configuration showing microphone and source positions used in the

Heights:	
1	2.53 m
2	2.17 m
3	2.45 m
4	1.12 m
5	1.04 m
7	2.59 m
A	1.55 m
B	1.55 m

○ = microphone position

⬠ = source position

●━● = Seating block
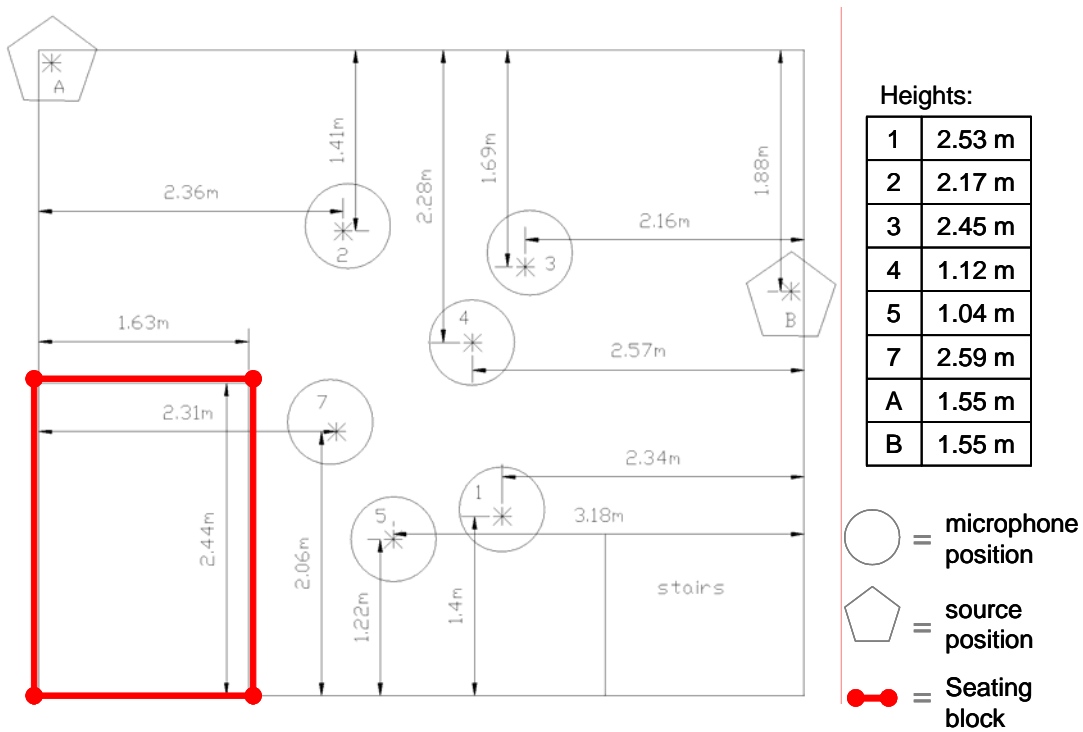
Figure 6.7. Reverberation chamber setup for seating and audience measurements.

measurements.

The procedure explained in Section 4.2 was followed by measuring the reverberation time for the chairs with both barriers in place, with only the rear barrier in place, with only the side barrier in place, and with the room empty. From these reverberation time measurements, the absorption areas A_1, A_2, and A_3 could be calculated, and α_∞, α_s, and α_f could be derived according to Equations (4.6), (4.7), and (4.8). The absorption coefficients could then be calculated for the seats in the Conference Center according to Equation (4.9) by knowing the areas S_s, S_f, and S_p. Based on this approach, Figure 6.8 shows the measured absorption coefficient estimates for the empty chairs with and without carpet in the Conference Center configuration. Also shown in this
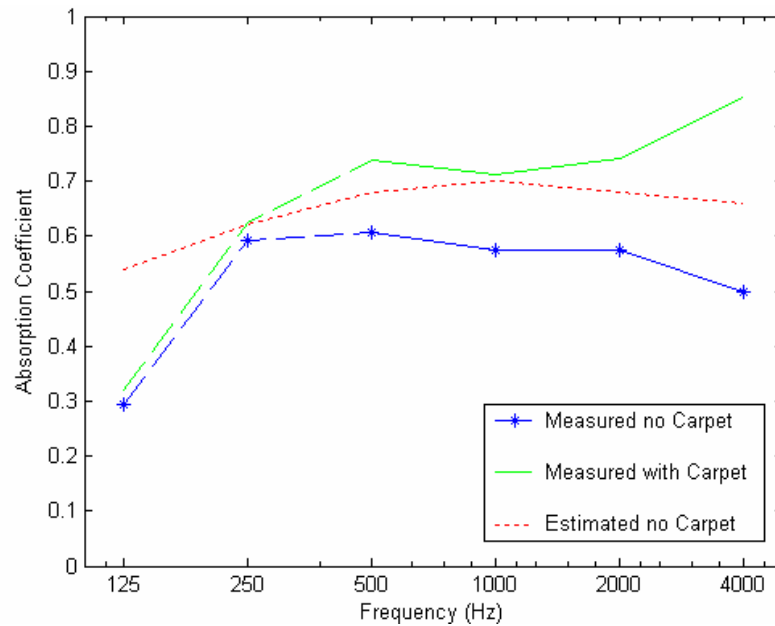
Figure 6.8. Octave band absorption coefficient values for empty chairs.

figure are the absorption coefficient values that were estimated from the literature for the empty chairs without carpet. Table 6.3 lists values for the absorption coefficients of the empty chairs at octave-band center frequencies.

The Schroeder frequency that was calculated according to Equation (6.2) for the empty chairs without carpet is 300 Hz, and for the empty chairs with carpet it is 296 Hz. Once again, because the Schroeder frequency is so high, the 125 and 250 Hz octave band absorption coefficients could not be considered accurate. The values used in the refined computer models were the measured values with carpet, except at 125 Hz and 250 Hz, where the estimated values without carpet were used. As seen in Figure 6.8, carpeting attributes very little at these lower frequencies.

The temperature and humidity were measured using a LI-COR temperature and humidity sensor and recorded using the LI-I400 Datalogger. These measurement values were used to calculate the sound absorption areas according to ISO 354[53] and are given in Appendix E.

Table 6.3. Octave band absorption coefficient values for empty chairs.

Frequency	125 Hz	250 Hz	500 Hz	1000 Hz	2000 Hz	4000 Hz
α measured with carpet	0.32	0.62	0.74	0.71	0.74	0.85
α measured no carpet	0.29	0.59	0.61	0.57	0.58	0.50
α estimated no carpet	0.54	0.62	0.68	0.7	0.68	0.66

6.1.4   Audience Measurements

The absorption of the audience seated in the chairs was also measured using the Kath and Kuhl method explained in Section 4.2. Nine individuals were seated in the chairs with 1.22-meter-high surrounding barriers made of 1.9 cm-thick medium density fiberboard (MDF). These measurements were only taken with carpet underneath the chairs. The setup for the measurements is shown in Figure 6.9. The floor-plan setup for microphones and sources was the same as that shown in Figure 6.7.

Brigham Young University policy requires that researchers obtain permission through the Institutional Review Board (IRB in the Office of Research and Creative Activities) for any research done using human subjects.

Figure 6.9. Setup in the reverberation chamber for measuring the audience absorption.

Permission was granted for this research through the IRB as an exempt research project, but audience members were still required to fill out a consent form before participating in measurements (see Appendix F).

The same procedure used to measure the absorption coefficients of the unoccupied chairs was followed for these measurements. Figure 6.10 shows the absorption coefficient estimates for the seated audience with carpet in the Conference Center configuration. Also shown in this figure are the absorption coefficient values that were estimated from the literature for the seated audience without carpet. Table 6.4 also lists the values.

The Schroeder frequency that was calculated for the audience seated in chairs using Equation (6.2) was 283 Hz. Again, the Schroeder frequency is
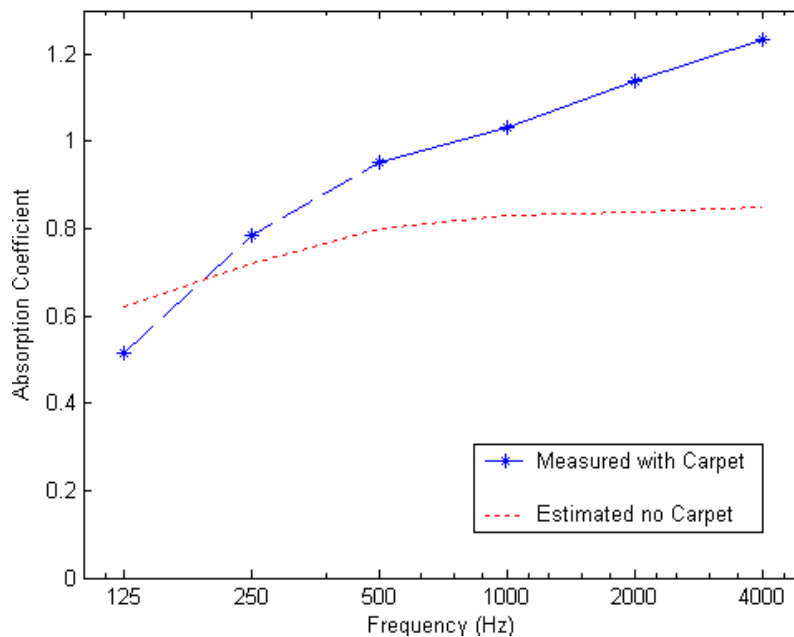
Figure 6.10. Octave band absorption coefficient values for seated audience.

Table 6.4. Octave band absorption coefficient values for seated audience.

Frequency	125 Hz	250 Hz	500 Hz	1000 Hz	2000 Hz	4000 Hz
α measured with carpet	0.52	0.79	0.95	1.03	1.14	1.23
α estimated no carpet	0.62	0.72	0.80	0.83	0.84	0.85

higher than the 125 Hz and 250 Hz octave band center frequencies so the absorption coefficient measurements made in these bands were not considered reliable.

Temperature and humidity values were again measured and used to calculate the sound absorption areas according to ISO 354. They are given in Appendix E.

It is noticed in Figure 6.10 that the audience absorption coefficient values are greater than one for higher frequencies. It is possible that this is due to an assumption of the measurement method that the surface area is only the planar surface on top of the audience box. However, further work should be done to determine the cause of these high absorption coefficients.

6.1.5   Total absorption curves

Figure 6.11 provides the new cummulative absorption curves obtained by using the measured absorption coefficients for the absorptive ceiling panels and the unoccupied seats with carpet (along with the other coefficients from the
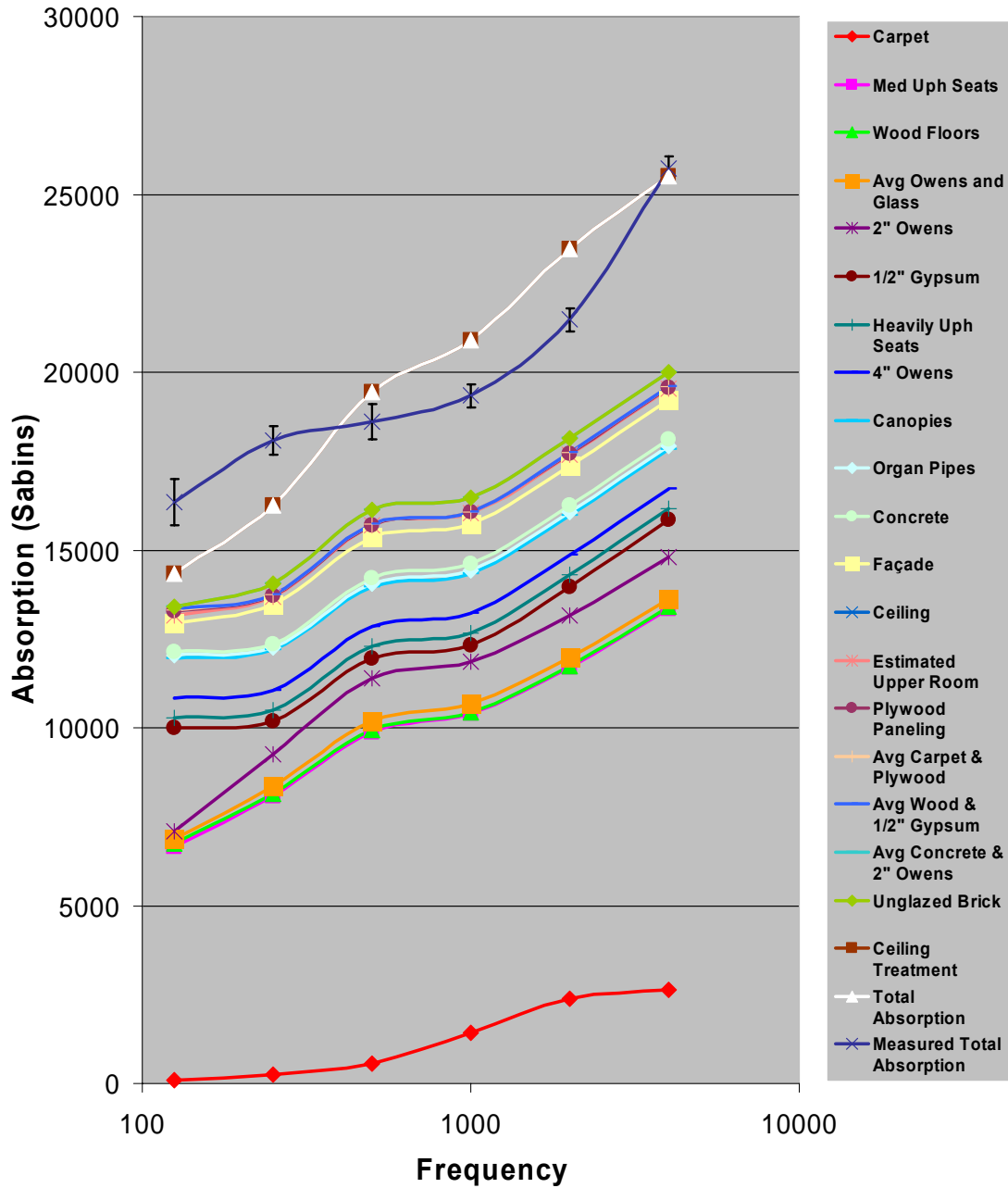
Figure 6.11. Cumulative absorption curves for refined model.

preliminary model). It can be seen that the total absorption curves match much better at 4 kHz than the previous curves (see Figure 5.5). Low frequency values were not predicted any better from these measurements. Measurements made at 125 Hz and 250 Hz were not used.

106

6.2   Scattering Coefficients

Two methods will be discussed in this section that were investigated in hopes of estimating scattering coefficients for the seats and the seated audience. Both were based on physical principles. The first method was to measure the scattering coefficients in a reverberation chamber as explained in Section 4.3. The second method was to predict the scattering coefficients using the Boundary Element Method.

Although the methods did not lead to significant results for the scattering coefficients of seating areas, it was shown in Section 5.5 that the computer models were not sensitive to scattering coefficients of seating areas for most parameters. Thus, the approximations for the scattering coefficients given in Appendix B were used for the refined computer models.

6.2.1   Measuring Scattering Coefficients of Seating

Section 4.3 discusses the current method for measuring random-incidence scattering coefficients in a reverberation chamber. It was hoped that the scattering coefficients of seating could be measured using the current standard: ISO 17497-1.[62] However, after studying the standard more closely, it was found that it was not suitable for measuring the scattering coefficients of seating areas.

The standard requires that the structural depth h of a sample meet the requirement $h \le d/16$, where d is the diameter of the turntable. The seated height of the audience is roughly 1.22 m. In order to meet this condition, the diameter of the turntable would have to be greater than 19.5 meters! Obviously, this condition could not be met in a typical reverberation chamber.

The standard also states that the measurement method has been shown to produce unreliable results for samples with a high absorption coefficient. The absorbent must be present in the test specimen. An equation is given for the standard deviation of the measured scattering coefficient which depends on the absorption coefficient of the sample. The standard specifies that the absorption coefficient of the test specimen should not exceed a value of $\alpha_s = 0.50$. As demonstrated already in Section 6.1.4, the absorption coefficient of the audience is indeed larger than 0.50 at higher frequencies.

Thus, it has been shown that the measurement of the chair and audience scattering coefficients using the current standard is not possible, so other methods were examined to determine the scattering coefficients.

6.2.2   Using BEM to Predict the Seating Scattering Coefficients

Mommertz[83] proposed an equation which determines the scattering coefficient from free-field calculations or measurements:

$$\delta = 1 - \frac{\left| \sum_{i=1}^{n} p_1(\theta_i) p_0^*(\theta_i) \right|^2}{\sum_{i=1}^{n} |p_1(\theta_i)|^2 \sum_{i=1}^{n} |p_0(\theta_i)|^2} \, , \tag{6.3}$$

where $p_1(\theta)$ is the complex amplitude of the pressure scattered at an angle θ by the surface under test, and $p_0(\theta)$ is the complex amplitude of the pressure scattered at an angle θ by a flat reference surface with the same size and shape. This equation is used to determine the scattering coefficient in a two dimensional field, and θ_i are discrete, evenly spaced angles along a two dimensional arc. The equation thus evaluates the directional distribution of a reflection over the surface under test with reference to the directional distribution of a reflection over a flat panel of the same size.

Gomes[63] used the Boundary Element Method to determine the scattered pressure of a surface at various angles θ_i with a given angle of incidence β_i. If the calculations are done for a scattering surface and a flat reference surface, Equation (6.3) can be used to calculate the scattering coefficient for a given angle of incidence $\delta(\beta_i)$.

After calculating the scattering coefficients, $\delta(\beta_i)$, for different angles of incidence, β_i, Paris' formula[84] is used to convert free field scattering coefficients to a random-incidence scattering coefficient:

$$\delta_{random} = \int_0^{\pi/2} \delta(\beta)\sin(2\beta)d\beta \qquad (6.4)$$

$$\delta_{random} \approx \sum_{i=0}^{N} \delta(\beta_i)\sin(2\beta_i)\Delta\beta . \qquad (6.5)$$

Equation (6.4) gives the general Paris formula while Equation (6.5) gives an approximation to the Paris formula for discrete angles of incidence β_i.

This method was used in this phase of the research to roughly predict the seating and audience scattering coefficient values using the BEM in the commercial software program, SYSNOISE™. However, instead of modeling an entire audience, only a single sphere was modeled as a rough approximation to a chair or a person seated in a chair. The sphere was modeled as completely rigid in both baffled and unbaffled configurations.

To determine the radius of the sphere that best approximates a person seated in a chair, three different calculations were averaged. The first two calculations assumed that an average person seated in a chair has a height of 1.12 meters, a depth of 0.63 meters, and a width of 0.6 meters. The first calculation takes the average of the three dimensions, which is 0.8 meters. The second calculation determines the equivalent volume by treating the person seated in a chair as a cube and then finding the equivalent radius of a sphere with the same volume, which is 0.47 meters. The third calculation assumes the density of an average body is 1050 kg/m³ and the average body mass is 68 kg

(150 lbs). From these the average body volume is computed and the radius of a sphere with the equivalent volume is calculated, which is 0.25 meters. When these three calculations were averaged, a radius of 0.5 meters is obtained, which is the radius of the sphere used in this research.

Only two-dimensional scattering was looked at because symmetry was assumed. A plane wave was incident upon the sphere at fifteen degree increment angles along an arc and the pressure was measured in five degree increments along the arc (see Figure 6.12).

The reference surface used for these calculations was a round, perfectly rigid disc with the same radius as the sphere. The same setup shown in Figure 6.12 was used.

The random incidence scattering coefficients of the sphere in both baffled and unbaffled cases were determined using Equations (6.3) and (6.5) and are
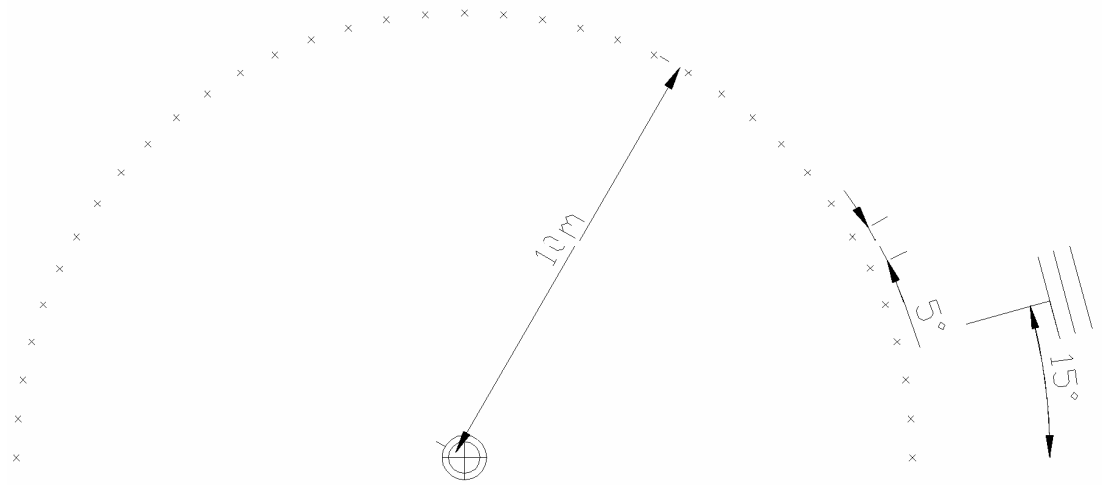
Figure 6.12. Setup for sphere scattering coefficient calculation in SYSNOISE™.

given in Table 6.5. Also shown in this table are the audience scattering coefficients used in the models based on values recommended by Dalenbäck (see Section 2.3.3).

It can be seen that scattering coefficients calculated for the baffled and unbaffled sphere are similar to the values recommended by Dalenbäck at some frequencies. It is expected that if these methods were extended to modeling rows of spheres or rows of seats, that the scattering coefficients calculated would be good estimates of the actual scattering properties of an audience. However, this method was not extended to surfaces that better resemble an audience because of excessively large computation times.

Table 6.5. Scattering coefficient values calculated for baffled and unbaffled sphere using BEM and audience scattering coefficients recommended by Dalenbäck.

	125 Hz	250 Hz	500 Hz	1000 Hz	2000 Hz	4000 Hz
δ Unbaffled	0.20	0.37	0.78	0.90	0.95	0.96
δ Baffled	0.73	0.63	0.70	0.67	0.76	0.56
δ Audience (from Dalenbäck)	0.30	0.40	0.50	0.60	0.70	0.70

7   Comparison of Results

In this chapter, comparisons are made between preliminary and refined models, EASE™ and CATT™ models, and models and measurements. They are made using impulse responses, various acoustic parameters, and auralizations.

The same source and receiver positions are used for the comparisons throughout this chapter. Figure 5.54 shows floor plans of the Conference Center and labels the receiver and source positions used. Each combination is referred to by combining the source position with the receiver position. For example, if the source is in the soprano section and receiver number 1 is used, the source receiver combination is referred to as S1.

7.1   *Comparison of Impulse Reponses*

To facilitate visualization and comparisons, log-squared impulse responses ($10\log[h^2(t)]$) are compared throughout this section. The impulse responses begin at the direct sound arrival at the receiving position. This representation first shows that the models predicted some source-receiver responses better than others. For example, compare Figure 7.1, which shows broadband impulse responses for combination S1, and Figure 7.2, which shows impulse responses for combination S2. For combination S1, there seems to be only minor agreement between the measured impulse response and the

Figure 7.1. Impulse response comparison between measured (M), CATT™ preliminary (CP), EASE™ preliminary (EP), CATT™ refined (CR), and EASE™ refined (ER) for S1.
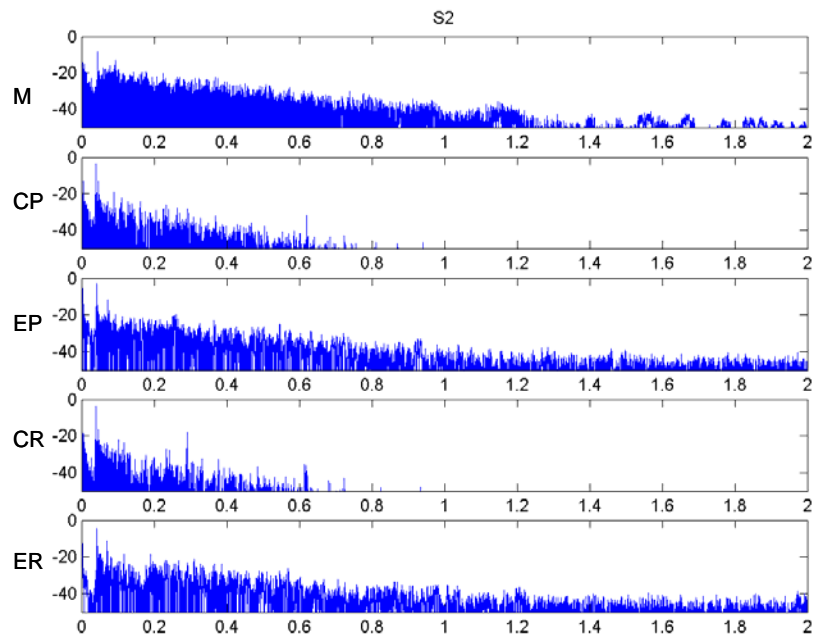
Figure 7.2. Impulse response comparison between measured (M), CATT™ preliminary (CP), EASE™ preliminary (EP), CATT™ refined (CR), and EASE™ refined (ER) for S2.

modeled impulse responses. Greater similarities are seen in the measured

impulse responses and the modeled impulse responses for combination S2.

Another thing to notice about these figures is that the CATT™ impulse

responses tend to have a faster decay than either the measured or EASE™

impulse responses. This trend is typical of impulse responses at all the source

and receiver positions.

The plots do not seem to show that impulse responses at a given source

or receiver position are easier to predict than others. Rather, there are different

receiver positions for which there is some agreement between measured and

model impulse responses for each source position. Responses at receiver

positions 9 and 10 are not predicted well for any source position used in the

models (see Figure 7.3). Both of these receiver positions are located on the

rostrum.

There is not a noticeable trend showing which software package seems

to predict the impulse responses better. At some positions the early portions of

the responses appears to be predicted better by CATT™ (Figure 7.4), at other

positions, it is better predicted by EASE™ (Figure 7.5). At some positions it is

predicted well by both, and at other positions it is not predicted well by either.

The late portions of the curve are consistently predicted better by EASE™. This
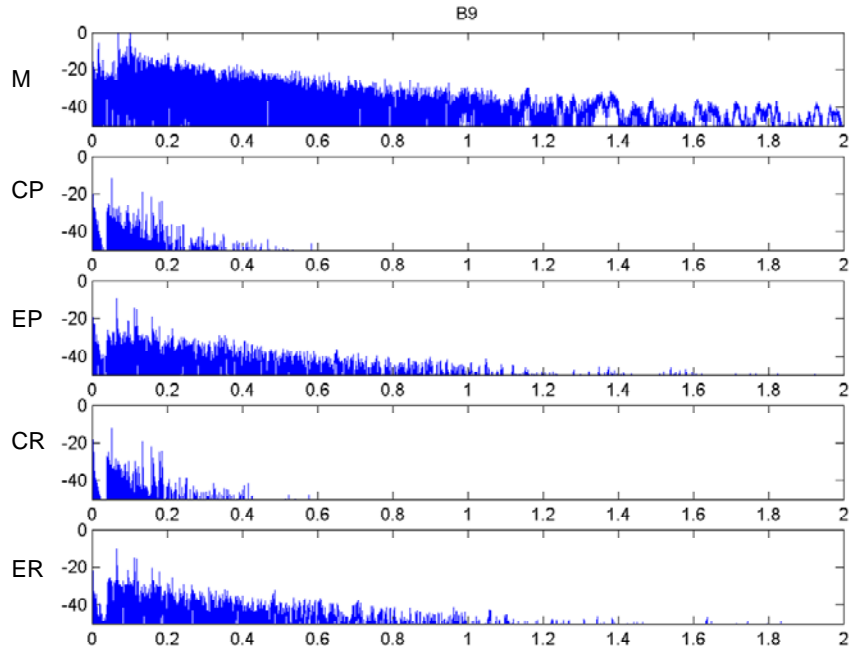
Figure 7.3. Impulse response comparison between measured (M), CATT™ preliminary (CP), EASE™ preliminary (EP), CATT™ refined (CR), and EASE™ refined (ER) for B9.
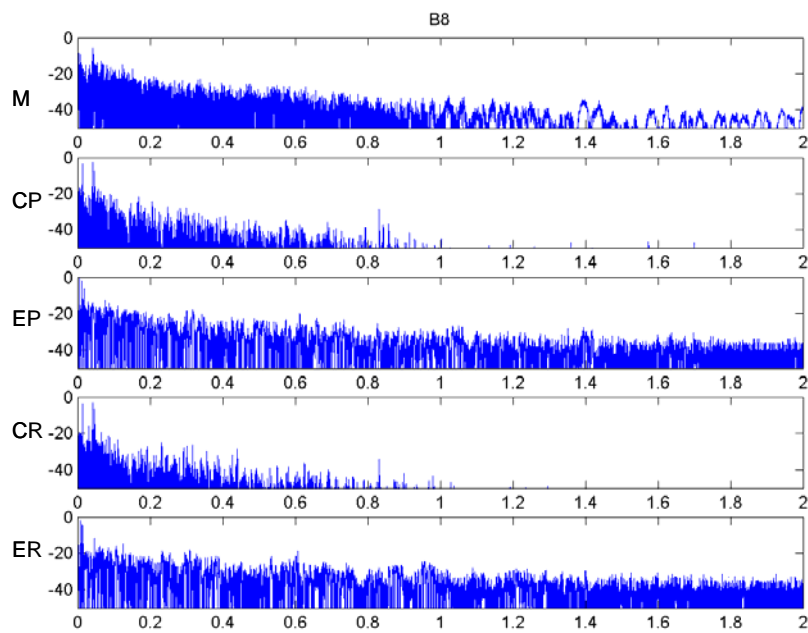
Figure 7.4. Impulse response comparison between measured (M), CATT™ preliminary (CP), EASE™ preliminary (EP), CATT™ refined (CR), and EASE™ refined (ER) for B8.
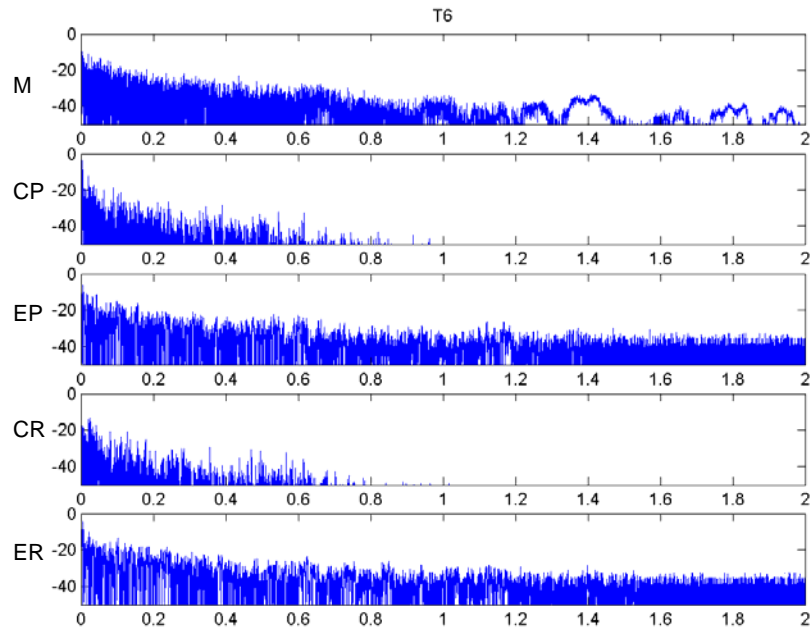
Figure 7.5. Impulse response comparison between measured (M), CATT™ preliminary (CP), EASE™ preliminary (EP), CATT™ refined (CR), and EASE™ refined (ER) for T6.

result is not extremely important, however, as many perceptions of room

acoustics are determined in the earlier part of the impulse response.

The impulse response plots do not seem to show that the refined models

(either EASE™ or CATT™) have significantly improved the predictions. In most

cases, there is little noticeable difference in the plots of the preliminary models

and the refined models. For some positions the preliminary models actually

appear to be closer to the measured impulse response plots than the refined

models.

7.2   Comparison of Acoustic Parameters

The acoustic parameters that are compared in this section include C50, C80, EDT, and T30 (see Appendix C for parameter definitions). The parameters were calculated from octave-band filtered impulse responses using the MATLAB™ code given in Appendix G.

When comparing acoustic parameters derived from measurements and the models, it was seen that some seats showed better agreement than others. Some parameters also show better agreement than others. For example, Figure 7.6 shows the C50 calculation at position B9. The error bars on the measured curve indicate the difference limen for this parameter. The difference limens
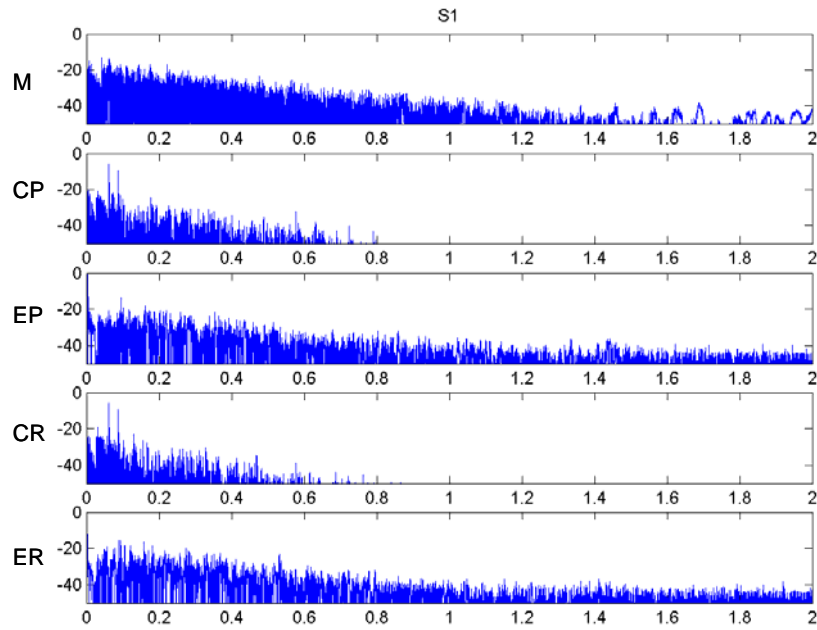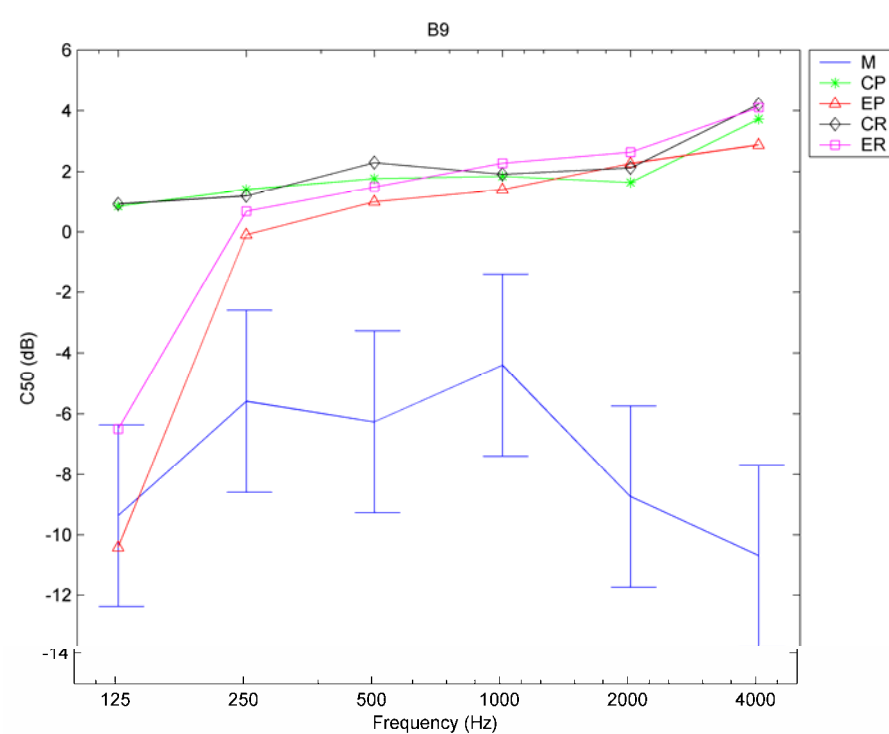

Figure 7.6. C50 comparison (with DL=3dB) between measured (M), CATT™ preliminary (CP), EASE™ preliminary (EP), CATT™ refined (CR), and EASE™ refined (ER) for B9.

that were used in this section are the maximum difference limens for each parameter, from the published values given in Table 5.3. It can be seen that for this position, the model curves do not match the measured curve very well at all.

However, Figure 7.7 shows the C50 calculation at position S6. It can be seen that in this case the model curves match the measured curve much better.

For further comparison, the differences between the measured and predicted parameter values were calculated at each position combination and frequency, then divided by the difference limen for that parameter. In this way
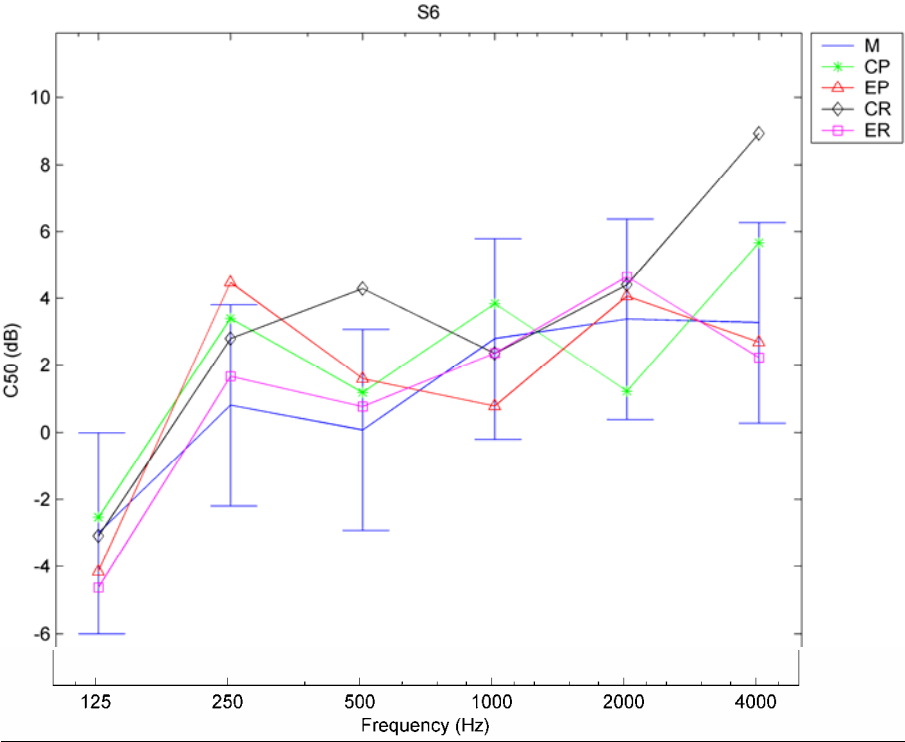
Figure 7.7. C50 comparison (with DL=3dB) between measured (M), CATT™ preliminary (CP), EASE™ preliminary (EP), CATT™ refined (CR), and EASE™ refined (ER) for S6.

119

the predicted values could be expressed in terms of the number of difference

limens they deviated by. These results were then averaged over all positions to

produce the values given in Table 7.1 through Table 7.4. Although these values

do not indicate which position combinations have better predictions than

others, they are useful in establishing how well each model predicts the

parameters overall.

Table 7.1. Number of difference limens each model differs from measurements averaged over the hall for C50.

	125 Hz	250 Hz	500 Hz	1000 Hz	2000 Hz	4000 Hz
CP	2.45	1.78	1.61	1.31	1.38	1.56
EP	1.45	1.34	0.94	1.07	1.06	1.08
CR	2.14	1.65	1.56	1.35	1.52	2.02
ER	1.37	1.30	1.31	1.46	1.50	1.33

Table 7.2. Number of difference limens each model differs from measurements averaged over the hall for C80.

	125 Hz	250 Hz	500 Hz	1000 Hz	2000 Hz	4000 Hz
CP	6.77	4.76	4.56	3.63	3.74	4.26
EP	3.41	3.25	2.58	2.74	2.55	2.69
CR	6.40	4.73	4.55	3.67	4.34	5.59
ER	3.31	3.48	3.62	4.04	3.81	3.63

Table 7.3. Number of difference limens each model differs from measurements averaged over the hall for EDT.

	125 Hz	250 Hz	500 Hz	1000 Hz	2000 Hz	4000 Hz
CP	10.33	8.82	7.46	7.13	6.94	6.86
EP	8.60	5.80	6.05	6.77	5.92	6.88
CR	9.74	8.10	7.44	6.66	7.38	8.17
ER	7.43	5.85	7.29	7.10	7.25	8.35

Table 7.4. Number of difference limens each model differs from measurements averaged over the hall for T30.

	125 Hz	250 Hz	500 Hz	1000 Hz	2000 Hz	4000 Hz
CP	4.97	5.99	2.33	2.67	2.70	1.21
EP	3.82	1.80	3.15	4.36	3.87	2.44
CR	5.63	5.64	3.31	3.26	3.55	3.53
ER	1.95	1.69	4.28	5.09	4.97	4.09

Section 5.5 mentioned that Vorländer[18] used a difference of twice the subjective limen as a cutoff for accuracy in the modeling packages. He considered values greater than this cutoff to suggest inaccurate modeling. With this in mind, it can be seen from Table 7.1 through Table 7.4 that on average C50 is predicted well by all of the models at most frequencies, C80 and EDT are not predicted well by any models, and T30 is predicted well for some of the models at a few frequencies.

Slight differences in the parameters are seen between the preliminary and the refined models from Table 7.1 through Table 7.4. Since the differences vary greatly from parameter to parameter, they do not seem to show a significant improvement in the refined model predictions over the preliminary model predictions. This is summarized in Table 7.5, which gives an average of the four parameters for all frequencies for each model. It is seen that on average the preliminary models actually provide slightly better results than the refined models. The table also shows that on average, the EASE™ models seem to predict the four parameters a little better than the CATT™ models.

Table 7.5. Average number of difference limens for all parameters and all frequencies.

	Avg # DLs
CP	4.38
EP	3.49
CR	4.66
ER	3.98

In order to visualize which source-receiver combinations have better predictions than others, it is necessary to look at the number of difference limens each prediction differs from the measured values for each. In order to simplify the tables, averages over frequency are given in Table 7.7 through Table 7.9.

Highlighted values in the tables correspond to combinations wherein the average number of difference limens is less than two. It can be seen that most positions predict C50 within two difference limens. However, receiver positions 9 and 10 tend to have poorer C50 predictions than other positions. Other parameters do not show such obvious trends.

Table 7.6. Number of difference limens each model differs from measurements averaged over frequency for C50.

C50	S1	S2	S3	S4	S5	S6	S7	S8	S9	S10	S11	S12
CP	1.94	1.82	0.98	0.57	0.65	0.54	0.69	0.46	2.54	4.25	1.22	1.34
EP	1.40	1.00	0.82	1.10	0.73	0.54	0.28		3.19	2.40	0.66	2.12
CR	1.99	2.12	0.73	0.67	0.29	0.75	0.30	0.38	2.79	4.18	1.70	1.62
ER	1.61	1.25	0.60	0.94	1.22	0.33	0.50	0.89	3.08	2.40	1.35	2.76
C50	A1	A2	A3	A4	A5	A6	A7	A8	A9	A10	A11	A12
CP	1.23	1.18	2.12	0.78	1.67	0.86	0.62	0.61	5.40	3.72	1.30	1.32
EP	0.60	0.75	0.77		0.60	0.69	1.00	0.78	1.90	1.72	0.95	1.34
CR	1.40	1.46	2.23	0.82	0.95	0.79	0.89	0.61	5.81	4.02	1.33	1.70
ER	1.03	1.28	0.81	0.61	0.96	1.06	1.13	0.74	2.10	1.33	1.48	1.86
C50	T1	T2	T3	T4	T5	T6	T7	T8	T9	T10	T11	T12
CP	2.53	1.60	1.60	1.32	1.79	1.09	1.37	0.89	6.62	1.29	0.73	1.32
EP	1.68	0.95	1.24	0.76	0.83	0.68	0.81	0.86	2.26	0.85	1.32	1.54
CR	2.62	1.77	1.30	0.89	1.61	0.92	0.85	0.95	6.71	1.08	1.48	1.33
ER	2.15	1.39	2.06	0.73	1.12	1.10	0.85	1.04	2.70	0.99	1.21	1.83
C50	B1	B2	B3	B4	B5	B6	B7	B8	B9	B10	B11	B12
CP	1.35	1.59	1.26	1.02	1.55	1.23	1.63	0.90	3.13	4.22	1.12	1.72
EP	0.99	0.59	1.14	0.75	0.94	0.62	0.73	0.63	2.46	2.37	1.21	1.76
CR	1.14	1.69	1.03	0.84	1.26	0.70	1.91	1.15	3.21	4.43	1.73	1.88
ER	1.22	1.04	1.05	1.12	1.39	0.83	1.04	0.93	2.76	2.79	1.32	2.15

Table 7.7. Number of difference limens each model differs from measurements averaged over frequency for C80.

C80	S1	S2	S3	S4	S5	S6	S7	S8	S9	S10	S11	S12
CP	5.66	5.01	1.97	2.02	4.23	2.62	1.72	1.82	8.76	7.53	4.02	3.00
EP	2.33	3.28	1.47	2.85	1.95	1.13	2.83		7.28	1.89	1.86	5.04
CR	5.95	6.38	1.91	1.66	4.61	2.98	1.77	1.80	9.34	7.32	5.84	3.63
ER	2.98	4.18	1.40	2.68	3.75	0.93	2.32	3.46	7.51	1.89	3.51	7.07
C80	A1	A2	A3	A4	A5	A6	A7	A8	A9	A10	A11	A12
CP	2.51	1.82	4.90	2.71	4.86	1.57	1.72	1.52	12.13	8.46	3.14	6.46
EP	1.97	1.57	1.07		1.15	1.83	2.72	2.28	3.96	2.65	2.21	5.08
CR	3.35	2.22	4.92	1.88	3.21	2.45	2.08	2.00	13.83	9.33	3.37	7.06
ER	2.10	2.19	1.52	1.58	2.34	2.10	3.39	2.53	4.69	1.97	3.54	7.07
C80	T1	T2	T3	T4	T5	T6	T7	T8	T9	T10	T11	T12
CP	5.61	4.44	3.15	3.80	4.54	2.14	4.29	2.69	16.68	3.05	1.76	5.31
EP	2.62	2.74	2.83	2.07	1.75	1.52	1.37	3.94	4.57	3.98	3.99	4.83
CR	6.18	5.28	2.41	2.87	4.08	1.58	3.52	1.45	16.73	3.58	3.87	5.90
ER	2.99	3.67	4.88	1.88	2.57	2.98	1.62	3.77	6.85	6.09	3.56	6.84
C80	B1	B2	B3	B4	B5	B6	B7	B8	B9	B10	B11	B12
CP	3.61	5.14	2.53	2.50	4.98	3.62	4.86	2.77	10.79	12.94	4.30	6.07
EP	2.14	2.55	2.83	1.65	2.44	1.15	2.00	2.50	7.47	3.01	4.07	5.66
CR	3.52	5.54	3.13	2.45	4.71	2.01	5.29	4.26	10.97	13.56	6.29	6.13
ER	2.65	3.04	3.09	2.20	4.19	2.66	2.51	2.12	8.42	8.28	4.68	6.89

Table 7.8. Number of difference limens each model differs from measurements averaged over frequency for EDT.

EDT	S1	S2	S3	S4	S5	S6	S7	S8	S9	S10	S11	S12
CP	8.19	7.17	3.65	8.70	11.04	7.62	6.22	6.07	13.29	10.75	10.04	6.90
EP	1.01	4.09	3.08	2.94	3.45	6.20	19.78		6.74	4.48	4.67	7.06
CR	10.56	8.65	5.06	7.12	9.60	6.62	4.46	5.24	12.78	11.12	10.34	6.25
ER	2.44	5.07	2.87	4.21	6.93	3.90	5.76	11.89	7.54	4.49	4.97	10.30
EDT	A1	A2	A3	A4	A5	A6	A7	A8	A9	A10	A11	A12
CP	8.25	8.23	5.38	6.65	6.25	8.09	9.25	9.13	11.06	8.41	11.35	10.90
EP	6.42	6.63	3.55		4.23	8.10	4.15	11.29	7.30	5.93	13.34	8.33
CR	8.83	4.13	4.03	4.38	4.63	5.96	8.20	7.67	11.99	8.65	10.16	12.07
ER	5.66	8.08	2.82	3.17	3.98	7.70	6.64	13.44	8.51	6.04	13.83	11.88
EDT	T1	T2	T3	T4	T5	T6	T7	T8	T9	T10	T11	T12
CP	9.06	6.45	2.05	5.49	4.70	5.37	5.70	10.16	9.40	4.52	10.46	20.37
EP	6.01	3.74	4.40	3.88	4.79	8.65	6.16	12.30	2.06	7.17	9.56	23.05
CR	9.83	7.27	2.34	6.12	6.89	6.58	5.90	8.86	9.65	5.42	9.95	20.89
ER	7.93	3.97	4.46	3.13	5.27	6.51	8.65	8.94	2.59	8.74	12.12	19.92
EDT	B1	B2	B3	B4	B5	B6	B7	B8	B9	B10	B11	B12
CP	8.45	6.37	2.94	3.29	5.04	5.73	7.02	4.19	8.17	9.96	8.73	14.18
EP	8.38	4.27	3.94	3.83	2.10	3.64	3.58	8.76	5.07	4.08	13.51	11.19
CR	8.95	7.05	2.82	2.82	4.57	5.04	6.31	7.14	8.44	12.97	11.66	13.93
ER	9.26	5.32	3.04	4.31	7.73	5.59	3.79	9.55	5.10	12.81	11.41	13.79

Table 7.9. Number of difference limens each model differs from measurements averaged over frequency for T30.

T30	S1	S2	S3	S4	S5	S6	S7	S8	S9	S10	S11	S12
CP	2.33	2.84	2.59	1.79	1.60	3.67	4.44	8.61	2.50	3.22	1.59	1.24
EP	3.26	2.34	2.97	3.04	3.22	2.69	3.04		3.95	3.14	3.07	3.40
CR	2.28	2.92	3.57	2.73	2.62	4.87	4.81	7.11	4.01	2.90	2.13	2.66
ER	4.19	2.79	4.12	3.76	3.89	3.29	4.47	2.95	4.11	2.33	3.76	3.65
T30	**A1**	**A2**	**A3**	**A4**	**A5**	**A6**	**A7**	**A8**	**A9**	**A10**	**A11**	**A12**
CP	2.53	3.01	2.62	2.82	1.61	3.03	3.05	11.57	2.21	3.47	1.89	1.18
EP	3.32	3.73	3.74		2.33	1.61	6.14	4.69	1.83	3.91	3.78	3.31
CR	3.43	2.77	4.31	3.34	3.25	3.93	3.93	13.78	1.32	3.36	3.86	3.11
ER	4.92	4.11	4.32	2.98	4.63	3.29	5.51	3.06	2.35	3.31	3.36	4.38
T30	**T1**	**T2**	**T3**	**T4**	**T5**	**T6**	**T7**	**T8**	**T9**	**T10**	**T11**	**T12**
CP	2.48	3.35	2.73	2.83	2.31	3.20	2.14	10.79	2.76	3.94	2.29	2.36
EP	2.93	3.06	3.15	2.54	1.88	4.08	2.87	2.73	2.99	3.02	5.17	3.13
CR	2.89	3.29	3.85	3.25	3.65	3.52	3.60	10.12	4.07	4.08	4.57	4.26
ER	3.83	3.00	5.17	3.37	3.16	3.18	3.71	2.90	3.35	3.13	4.38	3.28
T30	**B1**	**B2**	**B3**	**B4**	**B5**	**B6**	**B7**	**B8**	**B9**	**B10**	**B11**	**B12**
CP	1.95	2.20	3.02	3.84	3.46	2.08	3.02	9.11	3.27	5.00	2.98	2.54
EP	2.92	2.87	2.74	3.40	3.84	2.01	3.56	2.33	4.11	3.99	3.16	4.10
CR	2.59	2.76	3.53	3.23	3.71	4.84	3.73	9.96	4.38	6.70	4.65	5.16
ER	3.42	3.44	2.99	3.47	5.12	1.88	4.96	2.46	4.07	5.38	3.76	3.69

7.3   *Comparison of Auralizations*

In general, the EASE™ auralizations tend to have more low-frequency content, and the CATT™ auralizations tend to have more high-frequency content than auralizations based on measured monaural impulse responses. This happened despite the fact that the omnidirectional sources in the models were equalized to correspond to the measured free-field response of the dodecahedron loudspeaker used in the measurements.   Because of the assumptions of geometric acoustics, it is expected that the models should not be able to predict the low-frequency content accurately. Thus, in order to make an

accurate comparison of the auralizations the low-frequency content should be somehow ignored in the CATT™ and EASE™ auralizations when comparing to the measured auralizations.

Listening tests demonstrated that there were definitely some similarities between the measured and modeled auralizations. For example, one would expect auralizations in the choir loft to be clear, with a strong direct sound component because of the proximity of the source in the choir loft. This is apparent in the auralizations. In contrast, receiver positions located farther away in the main seating area have a more reverberant sound, picking up more of the characteristics of the hall.

When comparing auralizations for positions on the rostrum (receivers 9 and 10) it was noticed that the modeled and the measured auralizations had significant differences. The modeled auralizations were much clearer than the measured auralizations. The also failed to produce the perceived echoes that the measured auralizations had.

There is not a significant difference between the auralizations produced by the preliminary and refined models in both CATT™ and EASE™. The refined models did not seem to improve the auralizations noticeably.

Differences between the CATT™ and EASE™ models were hard to discern in the auralizations because of the large differences in frequency

content. With the frequency content as it is, the EASE™ auralizations tend to sound a little more similar to the measured auralizations than the CATT™ auralizations.

8   Conclusions

The primary objective of this research was to accurately model the existing acoustical characteristics of the Conference Center auditorium using the numerical acoustic packages CATT-Acoustic™ and EASE™. Preliminary models were created with this objective in mind, using the best-known techniques available. Geometries were modeled, keeping in mind details that set the hall apart from other halls, while not including so much detail that the models became too cumbersome to use. A thorough analysis was done to determine the number of rays to use in the packages in order to produce reliable results.

The results have shown that the models have been successful at representing characteristics of the hall at some positions but less successful at representing them at other positions. Comparisons of impulse responses, acoustic parameters, and auralizations showed that positions on the rostrum (receivers 9 and 10) were especially difficult positions to model in this hall for the single omnidirectional source and selected source positions. The results suggest that more work should be done to improve the quality and consistency of these software packages.

A secondary objective of this research was to use physical principles to find accurate absorption and scattering coefficients to input into the models. Random-incidence absorption coefficients were measured for two key surfaces in the hall (seats and absorptive panels) using actual hall samples. Results from comparing total predicted absorption curves to a measured curve from the hall showed that the measured absorption coefficients improved predictions at high frequencies. Two methods for determining scattering coefficients of seating areas based on physical principles were also investigated, but these methods did not lead to significant results. Nevertheless, it was shown that the models were not sensitive to scattering coefficients of the seating areas for most parameters of concern. Thus, including coefficients that had been based on physical principles probably would not have strongly affected the modeling results.

Refined models were created that included the new measured absorption coefficients. Significant differences were not found between the preliminary models and the refined models when impulse responses, acoustic parameters, and auralizations were compared. This suggests a need to investigate the sensitivity of the models to absorption coefficients.

When comparing broadband early impulse response characteristics and auralizations, there was not significant evidence showing that either the EASE™

128

or the CATT™ model was more accurate in representing the acoustical conditions of the hall. It was seen that the EASE™ models were a little better overall at predicting certain acoustic parameters (C50, C80, T30, and EDT) than the CATT™ models, but both models showed differences greater than two difference limens for an average of all parameters.

A confidence factor might be placed on the models to describe their effectiveness at predicting the acoustic properties of the hall. After comparing the results between models and measurements for impulse responses, acoustic parameters, and auralizations, the author believes that a subjective confidence factor of about 40% would be appropriate. While these models are effective at predicting some of the acoustic properties of the hall, there is still much room for improvement.

This research has contributed meaningful results to the field of geometric acoustic modeling. It has demonstrated the capabilities of existing software packages to model a very large auditorium. It has suggested that more work must be done to improve the modeling capabilities of these packages for this application. A method has been presented to assess the number of rays needed in these packages to adequately model a hall. A procedure to determine the sensitivity of a model to scattering coefficients of seating areas was also presented and can be applied to other models. In addition, a thorough

literature review has been presented on papers that deal with geometric acoustic modeling. The references have been categorized and included in the bibliography section of this thesis (Chapter 0).

Future research could be done to further optimize the number of curved surfaces and the level of detail in the models. More materials from the conference center could be measured in the reverberation chamber to determine their absorption coefficients to include in the models. More work is needed to determine the cause of the measured audience absorption coefficients being greater than one at high frequencies. The sensitivity of the model to absorption coefficients could be studied. The sensitivity of the model to scattering coefficients could be further studied, through analyzing the impulse responses and auralizations when scattering coefficients are varied, and to determine whether some source and receiver positions are more sensitive than others. A reliable echo criterion could be developed and the sensitivity of that parameter to seat scattering coefficients could be studied. More source positions and types could be studied. A source equalization procedure could be developed for equitable comparison between model outputs. Optimization of scattering coefficients used in the models could be done by comparing measured and modeled impulse responses, or one or more acoustic parameters. More work is

also needed to determine scattering coefficients of seating areas based on physical principles.

References

[1] T. Leishman, "A comprehensive survey and refinement of the Conference Center acoustics, results and conclusions for phases I, II, and III (Part A)," 2003 (unpublished).

[2] http://www.lds.org/newsroom/showpackage/0,15367,3899-1---10-111,00.html (October 2004).

[3] H. Kuttruff, "Digital simulation of concert hall acoustics and its applications," Proc. Inst. of Acoust., **13**, 27-35 (1991).

[4] N. Xiang, J. Blauert, "Computer-aided tenth-scale modeling for binaural auralization in room acoustic design," 90th Convention of AES, preprint 3120 (1991).

[5] N. Xiang, J. Blauert, "Binaural scale modeling for auralisation and prediction of acoustics in auditoria," Appl. Acoust., **38**, 267-290 (1993).

[6] M. Kleiner, R. Orlowski, J. Kirszenstein, "A comparison between results from a physical scale model and a computer image source model for architectural acoustics," Appl. Acoust., **38**, 245-265 (1993).

[7] M. Schroeder, B. Atal, C. Bird, "Digital computers in room acoustics," Proc. 4th Inter. Cong. Acoust., Copenhagen, Paper M21 (1962).

[8] A. Krokstad, S. Strøm, S. Sørsdal, "Calculating the acoustical room response by the use of a ray tracing technique," J. Sound Vib., **8**, 118-125 (1968).

[9] J. Rindel, "Computer simulation techniques for acoustical design of rooms," Acoustics Australia, **23**, 81-86 (1995).

[10] H. Kuttruff, *Room Acoustics, 4th Edition* (Spon Press, London, 2000), pp. 300.

[11] H. Kuttruff, *Room Acoustics, 4th Edition* (Spon Press, London, 2000), pp. 89-90.

[12] H. Lehnert and J. Blauert, "Principles of binaural room simulation," Appl.

Acoust., **36**, 259-291 (1992).

[13] A. Krokstad, A. Strom, S. Sorsdal, "Fifteen years' experience with computerized ray tracing" Appl. Acoust., **16**, 291-312 (1983).

[14] A. Pierce, *Acoustics: An Introduction to its Physical Principles and Applications* (McGraw-Hill Book Co., New York, 1981), pp. 106.

[15] K. Kuttruff, "Auralization of impulse responses modeled on the basis of ray-tracing results," J. Audio Eng. Soc., **41**, 876 – 877 (1993).

[16] M. Vorländer, "Recent progress in room acoustical computer simulations," Building Acoustics, **4**, 229-246 (1997).

[17] B. Dalenbäck, "The importance of diffuse reflection in computerized room acoustic prediction and auralization," Proc. Inst. Acoust., **17**, 27-34 (1995).

[18] M. Vorländer, "International round robin on room acoustical computer simulations," Proc. 15th Int. Cong. Acoust., Trondheim, Norway, **II**, 689-692 (1995).

[19] J. Rindel, "Scattering in room acoustics and the related activities in ISO and AES," Proc. 17th Inter. Cong. Acoust., Rome, Paper 6KN1.02, (2001).

[20] J. Embrechts, D. Archambeau, G. Stan, "Determination of the scattering coefficient of random rough diffusing surfaces for room acoustics applications," Acustica, **87**, 82-494 (2001).

[21] T. Cox, P. D'Antonio, "Contrasting surface diffusion and scattering coefficients," Proc. 17th Inter. Cong. Acoust., Rome, Paper 6B.09.01, (2001).

[22] M. Vorlander, E. Mommertz, "Definition and measurement of random-incidence scattering coefficients," Appl. Acoust., **60**, 187-199 (2000).

[23] http://www.rpginc.com/research/r002a.htm (October, 2004).

[24] B. Dalenbäck, "Room acoustic prediction based on a unified treatment of diffuse and specular reflection," J. Acoust. Soc. Am., **100**, 899-909 (1996).

[25] B. Dalenbäck, M. Kleiner, P. Svensson, "A macroscopic view of diffuse reflection," J. Audio Eng. Soc., **42**, 793-807 (1994).

[26] H. Kuttruff, *Room Acoustics*, *4th Edition* (Spon Press, London, 2000), pp. 110-114.

[27] T. Cox, P. D'Antonio, *Acoustic Absorbers and Diffusers Theory, Design and Application* (Spon Press, London, 2004), pp. 107.

[28] Y. Lam, "A comparison of three diffuse reflection modeling methods used in room acoustics computer models," J. Acoust. Soc. Am., **100**, 2181-2192 (1996).

[29] B. Dalenbäck, CATT-Acoustic™ v8.0 user's manual, (2002).

[30] C. Christenson, Odeon Room Acoustics Program, Version 6.5, User Manual, August (2003).

[31] G. Gehrke, "Computer supported construction of a model room for determining room acoustic parameters of a concert hall," 1997 (unpublished).

[32] J. Rindel, "Diffusion of sound in rooms – an overview," Proc. 15th Inter. Cong. Acoust., 633-636 (1995).

[33] T. Cox, P. D'Antonio, *Acoustic Absorbers and Diffusers Theory, Design and Application* (Spon Press, London, 2004), pp. 349-352.

[34] M. Kleiner, B. Dalenbäck, P. Svensson, "Auralization – an overview," J. Audio Eng. Soc., **41**, 861-875 (1993).

[35] H. Møller, "Interfacing room simulation programs and auralisation systems," Appl. Acoust., **38**, 333-347 (1993).

[36] http://www.ramsete.com/aurora/crostalk.htm (October 2004).

[37] H. Smith, "Numerical modeling of whizzer cone loudspeakers," Senior Thesis, Brigham Young University (2002).

[38] LMS North America, "Sound radiation of two engine blocks by the BEM and the rayleigh method," http://www.lmsna.com (July 2004).

[39] SYSNOISE Rev 5.0 Theoretical Manual, Numerical Integration Technologies, Leuven (1993) pp. 53-61.

[40] I. Bork, "A comparison of room simulation software – The 2nd round robin on room acoustical computer simulation," Acustica, **86**, 943-956 (2000).

[41] B. Dalenbäck, CATT-Acoustic™ v8.0 User's Manual, (2002) pp. 2-38 – 2-39.

[42] B. Dalenbäck, CATT-Acoustic™ v8.0 User's Manual, (2002) pp. 2-78 – 2-79.

[43] B. Dalenbäck, CATT-Acoustic™ v8.0 User's Manual, (2002) pp. 2-69 – 2-82.

[44] G. Ballou, Editor, *Handbook for Sound Engineers*, *3rd Edition* (Focal Press, Boston, 2002), Ch. 35 (W. Ahnert).

[45] B. Dalenbäck (private communication).

[46] B. Dalenbäck, CATT-Acoustic™ v8.0 User's Manual, (2002) pp. 7-39 – 7-42.

[47] O. Schmitz, S. Feistel, W. Ahnert, M. Vorländer, "Merging software for sound reinforcement systems and for room acoustics," 110th Convention of AES, preprint 5352 (2001).

[48] Acoustic Design Ahnert, EASE 4.1 Users Manual, (2003).

[49] Renkus-Heinz, EASE 4.0 for Windows Tutorial, (2002).

[50] EASE Teacher Seminar, ADA, Berlin, 16th-18th June 2003.

[51] http://www.rpginc.com/index.htm (February 2004).

[52] ASTM C423-00 "Standard test method for sound absorption and sound absorption coefficients by the reverberation room method," (2000).

[53] ISO 354, "Acoustics – measurement of sound absorption in a reverberation

room," (2003).

[54] ISO 9613-1, "Acoustics – attenuation of sound during propagation outdoors – part 1: calculation of the absorption of sound by the atmosphere," (1993).

[55] L. Beranek, T. Hidaka, "Sound absorption in concert halls by seats, occupied and unoccupied, and by the hall's interior surfaces," J. Acoust. Soc. Am., **104**, 3169-3177 (1998).

[56] W. Davies, R. Orlowski, Y. Lam, "Measuring auditorium seat absorption," J. Acoust. Soc. Am., **96**, 879-888 (1994).

[57] U. Kath, W. Kuhl, "Messungen zur schallabsorption von personen auf ungepolsterten stuhlen," Acustica, **14**, 49-55 (1964).

[58] U. Kath, W. Kuhl, "Messungen zur schallabsorption von polsterstuhlen mit und ohne personen," Acustica, **15**, 127-131 (1965).

[59] J. Bradley, "Predicting theatre chair absorption from reverberation chamber measurements," J. Acoust. Soc. Am., **91**, 1514-1524 (1992).

[60] J. Bradley, "The sound absorption of occupied auditorium seating," J. Acoust. Soc. Am., **99**, 990-995 (1996).

[61] T. Cox, P. D'Antonio, *Acoustic Absorbers and Diffusers Theory, Design and Application* (Spon Press, London, 2004), pp. 71-74

[62] Draft: ISO/DIS 17497-1, "Acoustics – measurement of the sound scattering properties of surfaces – Part 1: measurement of the random-incidence scattering coefficient in a reverberation room," International Organization for Standardization, In Process (2001).

[63] M. Gomes, "Determination of the acoustical random-incidence scattering coefficient," PhD. Thesis, Universidade Federal De Santa Catarina Brasil/Aachen University (2002).

[64] D. Bradley, L. Wang, "Effect of model detail level on room acoustic computer simulations," J. Acoust. Soc. Am., **111**, 2389(A) (2002).

[65] G. Naylor, J. Rindel, "Predicting room acoustical behavior with the ODEON computer model," J. Acoust. Soc. Am. **92**, 2346(A) (1992).

[66] L. Beranek, *Concert and Opera Halls: How They Sound* (AIP Press, Woodbury, NY, 1996), Appendix 5.

[67] D. Davis, C. Davis, *Sound System Engineering, 2nd Edition* (H.W. Sams, Indianapolis, IN, 1987), pp. 158-160.

[68] F. Everest, M. Shea, *How to Build a Small Budget Recording Studio from Scratch: with 12 Tested Designs, 2nd Edition* (TAB Books, Blue Ridge Summit, PA, 1988), Appendix A.

[69] A. Kulowski, "Error investigation for the ray tracing technique," Appl. Acoust., **15,** 263-274 (1982).

[70] J. Giner, C. Militello, A. Garciá, "Ascertaining confidence within the ray-tracing method," J. Acoust. Soc. Am., **106,** 816-822 (1999).

[71] Acoustic Design Ahnert, EASE 4.1 Users Manual, (2003), pp. 327, 336, 466.

[72] B. Dalenbäck, CATT-Acoustic™ v8.0 User's Manual, (2002), pp. 2-24.

[73] B. Dalenbäck, CATT-Acoustic™ v8.0 User's Manual, (2002), pp. 2-73.

[74] M. Gomes, S. Gerges, R. Tenenbaum, "On the accuracy of the assessment of room acoustics parameters using MLS technique and numerical simulation," Acta Acust., **86,** 891-895 (2000).

[75] T. Cox, W. Davies, Y. Lam, "The sensitivity of listeners to early sound field changes in auditoria," Acustica, **79**, 27-41 (1993).

[76] I. Bork, "Simulation and measurement of auditorium acoustics – The round robins on room acoustical simulation," Proc. Inst. of Acoust., **24,** (2002).

[77] A. Farina, "Verification of the accuracy of the pyramid rracing algorithm by comparison with experimental measurements of objective acoustic parameters," Proc. 15th Inter. Cong. Acoust., Trondheim, Norway, **II**, 445 (1995).

[78] M. Howarth, Y. Lam, "An assessment of the accuracy of a hybrid room acoustics model with surface diffusion facility," Appl. Acoust., **60,** 237-251 (2000).

[79] J. Bradley, R. Reich, S. Norcross, "A just noticeable difference in C-50 for speech," Appl. Acoust., **58**, 99-108 (1999).

[80] S. Bistafa, J. Bradley, "Predicting speech metrics in a simulated classroom with varied sound absorption," J. Acoust. Soc. Am., **109**, 1474-1482 (2001).

[81] D. Moore, G. McCabe, *Introduction to the Practice of Statistics, 4th Edition* (W. H. Freeman and Co., New York, 2003). pp. 494.

[82] J. Rathsam, L. Wang, "Sensitivity of room acoustic parameters to changes in scattering coefficients," J. Acoust. Soc. Am., **115,** 2515(A) (2004).

[83] E. Mommertz, "Determination of scattering coefficients from the reflection directivity of architectural surfaces," Appl. Acoust., **60**, 201-203 (2000).

[84] H. Kuttruff, *Room Acoustics*, *4th Edition* (Spon Press, London, 2000), pp. 49.

Bibliography

Auralization and Binaural Room Simulation

1. J. Rindel, C. Christensen "Room acoustic simulation and auralization – how close can we get to the real room?" 8th Western Pacific Acoustics Conference, Melbourne (2003).

2. T. Lokki, V. Pulkki, "Evaluation of geometry-based parametric auralization," 22nd International Conference on Virtual, Synthetic and Entertainment Audio, AES, 367-376 (2002).

3. L. Savioja, T. Lokki, and J. Huopaniemi, "Auralization applying the parametric room acoustic modeling technique - the diva auralization system," Proceedings of the International Conference on Auditory Display (ICAD'2002), Kyoto, Japan, 219-224 (2002).

4. C. Weitze, J. Rindel, C. Christensen, A. Gade, "Comparison between in-situ recordings and auralizations for mosques and Byzantine Churches," Proceedings of the Joint Baltic-Nordic Acoustics Meeting, Copenhagen, **II**, 53-57 (2002).

5. T. Lokki, "Physically-based auralization – design, implementation, and evaluation," PhD thesis, Helsinki University of Technology, Telecommunications Software and Multimedia Laboratory (2002).

6. D. Begault, E. Wenzel, M. Anderson, "Direct comparison of the impact of head tracking, reverberation, and individualized head-related transfer functions on the spatial perception of a virtual speech source," J. Audio Eng. Soc., **49**, 904-916 (2001).

7. T. Lokki, H. Järveläinen, "Subjective evaluation of auralization of physics-based room acoustics modeling," Proceedings of the 7th International Conference on Auditory Display, Espoo, Finland, 26-31 (2001).

8.	L. Tronchin, A. Farina, M. Pontillo, V. Tarabusi, "The calculation of the impulse response in the binaural technique," 7th International Congress on Sound and Vibration, Germany (2000).

9.	L. Savioja, "Modeling techniques for virtual acoustics," Doctorate thesis, Helsinki University of Technology (1999).

10.	J. Sendra, Editor, *Computational Acoustics in Architecture* (Wit Press, Southampton, England, 1999). Chapter 3 (D. Begault).

11.	B. Dalenbäck, M. Kleiner, P. Svensson, "Auralization, virtually everywhere," 100th Convention of AES, preprint 4228 (1996).

12.	E. Granier, M. Kleiner, B. Dalenbäck, P. Svensson, "Experimental auralization of car audio installations," J. Audio Eng. Soc., **44**, 835-849 (1996).

13.	D. Begault, "Audible and inaudible early reflections: thresholds for auralization system design," 100th Convention of AES, preprint 4244 (1996).

14.	E. Granier, M. Kleiner, B. Dalenbäck, P. Svensson, "Experimental auralization of car audio installations," 98th Convention of AES, preprint 3952 (1995).

15.	B. Dalenbäck, D. McGrath, "Narrowing the gap between virtual reality and auralization," Proc. 15th Inter. Cong. Acoust., Norway, 429-432 (1995).

16.	W. Ahnert, R. Feistel, "Comparison of auralized impulse responses acquired by both measurement and simulation," Proc. 15th Inter. Cong. Acoust., Norway, 353-356 (1995).

17.	M. Kleiner, E. Granier, B. Dalenbäck, P. Svensson, "Coupling of low and high frequency models in auralization," Proc. 15th Inter. Cong. Acoust., **IV**, 533-536 (1995).

18.	A. Reilly, D. McGrath, B. Dalenbäck, "Using auralisation for creating animated 3-D Sound fields across multiple speakers," 98th Convention of AES, preprint 4127 (1995).

19. J. Huopaniemi, "Real-time binaural room simulation," 1995 Finnish Signal Processing Symposium (FINSIG'95), Finland (1995).

20. J. Rindel, C. Christensen, "The use of a digital audio mainframe for room acoustical auralizations," 96th Convention of AES, preprint 3860 (1994).

21. M. Kleiner, P. Svensson, B. Dalenbäck, P. Linusson, "Audibility of individual characteristics in reverberation tails of a concert hall," Proc. Wallace Clement Sabine Centennial Symposium, 227-230 (1994).

22. B. Dalenbäck, M. Kleiner, P. Svensson, "Audibility of changes in geometric shape, source directivity, and absorptive treatment – experiments in auralization," J. Audio Eng. Soc., **41**, 905-913 (1993).

23. K. Kuttruff, "Auralization of impulse responses modeled on the basis of ray-tracing results," J. Audio Eng. Soc., **41**, 876-880 (1993).

24. M. Kleiner, B. Dalenbäck, P. Svensson, "Auralization – an overview," J. Audio Eng. Soc., **41**, 861-875 (1993).

25. W. Ahnert, "EARS auralization software," J. Audio Eng. Soc., **41**, 894-904 (1993).

26. A. Mochimaru, "A study of the practicality and accuracy of impulse response calculations for the auralization of sound system design," J. Audio Eng. Soc., **41**, 881-893 (1993).

27. A. Farina, "Convolution of anechoic music with binaural impulse response," Proceedings of PARMA-CM Users Meeting, Parma (1993).

28. K. Iida, M. Morimoto, "Basic study on sound field simulation based on running interaural cross-correlation," Appl. Acoust., **38**, 303-317 (1993).

29. H. Møller, "Interfacing room simulation programs and auralisation systems," Appl. Acoust., **38**, 333-347 (1993).

30. H. Møller, "Fundamentals of binaural technology," Appl. Acoust., **36**, 171-218 (1992).

31. H. Lehnert, J. Blauert, "Principles of binaural room simulation," Appl. Acoust., **36**, 259-291 (1992).

32. H. Gierlich, "The application of binaural technology," Appl. Acoust., **36**, 219-243 (1992).

33. J. Vian, J. Martin, "Binaural room acoustics simulation: practical uses and applications," Appl. Acoust., **36**, 293-305 (1992).

34. H. Lehnert, "Aspects of auralization in binaural room simulation," 92nd Convention of AES, preprint 3390 (1992).

35. D. Hammershoi, H. Moller, M. F. Sorensen, "Head-related transfer functions: measurements on 40 human subjects," 92nd Convention of AES, preprint 3286 (1992).

36. M. Kleiner, B. Dalenbäck, P. Svensson, "Auralization – an overview," 91st Convention of AES, preprint 3119 (1991).

37. M. Kleiner, P. Svensson, B. Dalenbäck, "Influence of auditorium reverberation on the perceived quality of electroacoustic reverberation enhancement systems – experiments in auralization," 90th Convention of AES, preprint 3015 (1991).

38. B. Dalenbäck, M. Kleiner, P. Svensson, "The audibility of changes in geometric shape, source directivity and absorptive treatment: experiments in auralization," 91st Convention of AES, preprint 3123 (1991).

39. K. Kotorynski, "Digital binaural/stereo conversion and crosstalk canceling," 89th Convention AES, preprint 2949 (1990).

40. J. Blauert, H. Lehnert, W. Pompetzki, N. Xiang, "Binaural room simulation," Acustica, **72**, 295-296 (1990).

41. W. Pompetzki, "Binaural recording and reproduction for documentation and evaluation," AES 8th Inter. Conf. (The Sound of Audio), Paper 8-029 (1990).

42. M. Kleiner, P. Svensson, B. Dalenbäck, "Auralization: experiments in acoustical CAD," 89th Convention AES, preprint 2990 (1990).

43. B. Delage, D. Fortier, "The 'audiosphere' a three-dimensional audio computer-assisted simulation system," 82nd Convention AES, preprint 2461 (G-6) (1987).

Background for Architectural Acoustic Design

44. G. Ballou, Editor, *Handbook for Sound Engineers, Third Edition* (Focal Press, Boston, MA, 2002), Chapter 6 (W. Ahnert, H. Tennhardt).

45. G. Ballou, Editor, *Handbook for Sound Engineers, Third Edition* (Focal Press, Boston, MA, 2002), Chapter 9 (D. Chéenne).

46. G. Ballou, Editor, *Handbook for Sound Engineers, Third Edition* (Focal Press, Boston, MA, 2002), Chapter 35 (W. Ahnert).

47. H. Kuttruff, *Room Acoustics, 4th Edition* (Spon Press, London, 2000), Chapter 9.

Computer Modeling Techniques

48. J. Rindel, "Modelling in auditorium acoustics from ripple tank and scale models to computer simulations," Revista de Acustica, **XXXIII**, 31-35 (2003).

49. M. Vorländer, "Recent progress in room acoustical computer simulations," Building Acoustics, **4**, 229-246 (1997).

50. J. Rindel, "Computer simulation techniques for acoustical design of rooms – how to treat reflections in sound field simulation," Proceedings of the International Symposium on Simulation, Visualization, and Auralization for Acoustics Research and Education (ASVA 97'), Tokyo, Japan, 201-208 (1997).

51.   J. Rindel, "Computer simulation techniques for acoustical design of rooms," Acoustics Australia, **23**, 81-86 (1995).

52.   O. Warusfel, "Predictive acoustics software and computer aided optimization in room acoustics," Proc. 15th Inter. Cong. Acoust., **II**, 693-696 (1995).

53.   H. Kuttruff, "Digital simulation of concert hall acoustics and its applications," Proc. Institute of Acoust., **13**, 27-35 (1991).

54.   E. Tzekakis, "Geometrical acoustics design software," Proc. 13th Inter. Cong. Acoust., Yugoslavia, 257-260 (1989).

55.   J. Blauert, C. Pösselt, "Application of modeling tools in the process of planning electronic room acoustics," AES 6th Inter. Conf. Sound Reinforcement, Paper 6-034 (1988).

56.   J. P. Vian, "Different computer modeling methods – their merits and their applications," Proc. 12th Inter. Cong. Acoust., Paper E4-10 (1986).

57.   M. Schroeder, "Computer models for concert hall acoustics," Amer. J. of Physics, **41**, 461-471 (1973).

58.   A. Krokstad, S. Strøm, S. Sørsdal, "Calculating the acoustical room response by the use of a ray tracing technique," J. Sound Vib., **8**, 118-125 (1968).

59.   M. Schroeder, B. Atal, C. Bird, "Digital computers in room acoustics," Proc. 4th Inter. Cong. Acoust., Copenhagen, Paper M21 (1962).

Defining and Determining Scattering Coefficients

60.   J. Jeon, S. Lee, M. Vorländer, "Development of scattering surfaces for concert halls," Appl. Acoust., **65**, 341-355 (2004).

61.   J. Embrechts, L. Geetere, G. Vermeir, "Calculation of the scattering coefficient of a sine-shaped surface by solving the Helmholtz integral," Proc. IOA (UK) Research Symp., **25**, 67-74 (2003).

62.   L. Geetere, J. Embrechts, G. Vermeir, "Calculation of the scattering coefficient of a sine-shaped surface by using the 3D BEM method," Proc. IOA (UK) Research Symp., **25**, 75-83 (2003).

63.   M. Gomes, "Determination of the acoustical random-incidence scattering coefficient," PhD. Thesis, Universidade Federal De Santa Catarina Brasil/Aachen University (2002).

64.   J. J. Embrechts, "Practical aspects of the ISO procedure for measuring the scattering coefficient in a real-scale experiment," Paper RBA-06-001-IP Presented at Forum Acusticum Sevilla 2002, Acta Acustica united with Acustica, **88 Suppl. 1**, S32 (A) (2002).

65.   M. Gomes, M. Vorländer, S. Gerges, "Aspects of the sample geometry in the measurement of the random-incidence scattering coefficient," Paper RBA-06-002-IP Presented at Forum Acusticum Sevilla 2002, Acta Acustica united with Acustica, **88 Suppl. 1**, S32 (A) (2002).

66.   L. De Geetere, G. Vermeir, K. Leuven, "Investigations on real-scale experiments for the measurement of the ISO scattering coefficient in the reverberation room," Paper RBA-06-004-IP Presented at Forum Acusticum Sevilla 2002, Acta Acustica united with Acustica, **88 Suppl. 1**, S32 (A) (2002).

67.   Draft International Standard, "Acoustics -- measurement of the sound scattering properties of surfaces -- Part 1: Measurement of the random-incidence scattering coefficient in a reverberation room," 2001 Draft: ISO/DIS 17497-1.

68.   A. Farina, L. Tronchin, "Comparison between measurements of the scattering and diffusion coefficients" Proc. 17th Inter. Cong. Acoust., Rome, (2001).

69.   T. Cox, P. D'Antonio, "Contrasting surface diffusion and scattering coefficients," Proc. 17th Inter. Cong. Acoust., Rome, Paper 6B.09.01, (2001).

70. J. Embrechts, D. Archambeau, G. Stan, "Determination of the scattering coefficient of random rough diffusing surfaces for room acoustics applications," Acustica, **87**, 82-494 (2001).

71. J. Rindel, "Scattering in room acoustics and the related activities of ISO and AES," Proc. 17th Inter. Cong. Acoust., Rome, Paper 6KN1.02, (2001).

72. A. Farina, "Measurement of the surface scattering coefficient: comparison of the Mommertz/Vorlander approach with the new Wave Field Synthesis method" International Symposium on Surface Diffusion in Room Acoustics, Liverpool (2000).

73. Y. Lam, "Editorial: Surface diffusion," Appl. Acoust., **60,** 111-112 (2000).

74. E. Mommertz, "Determination of scattering coefficients from the reflection directivity of architectural surfaces," Appl. Acoust., **60**, 201-203 (2000).

75. M. Vorländer, E. Mommertz, "Definition and measurement of random-incidence scattering coefficients," Appl. Acoust., **60**, 187-199 (2000).

76. A. Farina, M. Zanolin, E. Crema, "Measurement of sound scattering properties of diffusing panels through the Wave Field Synthesis approach" 108th Convention AES, preprint 5091 (2000).

77. T. Hargreaves, T. Cox, Y. Lam, P. D'Antonio, "Standard diffusion coefficients", Proc. Inst. Acoust., **21**, 195-200 (1999).

78. E. Mommertz, M. Vorländer, "Measurement of scattering coefficients of surfaces in the reverberation chamber and in the free field," Proc. 15th Inter. Cong. Acoust., Trondheim, Norway, 577-580 (1995).

79. RPG Diffusers, "Scattering coefficient part I" http://www.rpginc.com/research/5i4.htm (October 2004).

80. RPG Diffusers, "Scattering coefficient part II" http://www.rpginc.com/research/6i1.htm (October 2004).

Determining the Accuracy of Room Acoustic Software Packages

81. I. Bork, "Simulation and measurement of auditorium acoustics – the round robins on room acoustical simulation," Proc. Inst. of Acoust., **24**, (2002).

82. G. Cammarata, A. Fichera, A. Pagano, G. Rizzo, "Acoustical prediction in some Italian theatres," Applied Research Letters Online, **2**, 61-66 (2001).

83. S. Bistafa, J. Bradley, "Predicting speech metrics in a simulated classroom with varied sound absorption," J. Acoust. Soc. Am., **109**, 1474-1482 (2001).

84. I. Bork, "A comparison of room simulation software – the 2nd round robin on room acoustical computer simulation," Acustica, **86**, 943-956 (2000).

85. M. Gomes, S. Gerges, R. Tenenbaum, "On the accuracy of the assessment of room acoustics parameters using MLS technique and numerical simulation," Acta Acustica united with Acustica, **86**, 891-895 (2000).

86. M. Howarth, Y. Lam, "An assessment of the accuracy of a hybrid room acoustics model with surface diffusion facility," Appl. Acoust., **60,** 237-251 (2000).

87. J. Suh, P. Nelson, "Measurement of transient response of rooms and comparison with geometrical acoustic models," J. Acoust. Soc. Am., **105**, 2304-2317 (1999).

88. A. Farina, "Verification of the accuracy of the pyramid tracing algorithm by comparison with experimental measurements of objective acoustic parameters," Proc. 15th Inter. Cong. Acoust., Trondheim, Norway, **II**, 445 (1995).

89. M. Vorländer, "International round robin on room acoustical computer simulations," Proc. 15th Inter. Cong. Acoust., Trondheim, Norway, **II**, 689-692 (1995).

90. S. Dance, B. Shield, "The effect on prediction accuracy of reducing the number of rays in a ray-tracing model," Inter-Noise '94, 2127-2130, (1994).

91. G. Naylor, J. Rindel, "Predicting room acoustical behavior with the ODEON computer model," J. Acoust. Soc. Am. **92**, 2346(A) (1992).

92. W. Ahnert, "Comparison between simulated and measured time energy curves," 90th Convention of AES, preprint 3028 (1991).

93. http://www.ptb.de/en/org/1/17/173/roundrobin.htm (October 2004).

Diffuse Reflection in Room Acoustic Prediction

94. T. Cox, P. D'Antonio, "Surface characterization for room acoustic modeling and design," Intern. Symp. Room Acoust.: Design and Science (2004).

95. J. Rathsam, L. Wang, "Sensitivity of room acoustic parameters to changes in scattering coefficients," J. Acoust. Soc. Am., **115,** 2515(A) (2004).

96. B. Dalenbäck, "The rediscovery of diffuse reflection in room acoustics prediction" J. Acoust. Soc. Am., **112**, 2225 (2002).

97. R. Torres, M. Kleiner, "Audibility of 'diffusion' in room acoustics auralization: an initial investigation," Acustica, **86**, 919-927 (2000).

98. J. Embrechts, "Modeling sound diffusion in ray tracing programs," Acústica 2000, EAA Symposium on Architectural Acoustics, Madrid (2000).

99. J. Embrechts, "Broad spectrum diffusion model for room acoustics ray-tracing algorithms," J. Acoust. Soc. Am., **107**, 2068-2081 (2000).

100. A. Farina, "Validation of the numerical simulation of the scattered sound field with a geometrical pyramid tracing approach" ACOUSTICS 2000 - IOA Conf., Liverpool (2000).

101. A. Farina, "Introducing the surface diffusion and edge scattering in a pyramid-tracing numerical model for room acoustics" 108th Convention of AES, preprint 5145 (2000).

102. J. Embrechts, "Modelization of Kirchoff scattering by a sound ray algorithm," Proc. 16th Inter. Cong. Acoust., Seattle, Washington, 2329-2330 (1998).

103. Y. Lam, "On the modeling of diffuse reflections in room acoustics prediction", Proceedings of the BEPAC & EPSRC Conference on Sustainable Building, 106-113 (1997).

104. Y. Lam, "The dependence of diffusion parameters in a room acoustics prediction model on auditorium sizes and shapes," J. Acoust. Soc. Am., **100**, 2193-2203 (1996).

105. Y. Lam, "A comparison of three diffuse reflection modeling methods used in room acoustics computer models," J. Acoust. Soc. Am., **100**, 2181-2192 (1996).

106. W. Ahnert, R. Feistel, "Use of different methods to calculate scattering effects," Proc. 15th Inter. Cong. Acoust., Trondheim, Norway, 357-360 (1995).

107. B. Dalenbäck, "The importance of diffuse reflection in computerized room acoustic prediction and auralization," Proc. Inst. Acoust., **17**, 27-34 (1995).

108. Y. Lam, "On the description of partially diffused reflections in a room acoustics computer model," Proc. 15th Inter. Cong. Acoust., Trondheim, Norway, **IV**, 461-464 (1995).

109. B. Dalenbäck, M. Kleiner, P. Svensson, "A macroscopic view of diffuse reflection," J. Audio Eng. Soc., **42**, 793-807 (1994).

110. Y. Lam, "On the parameters controlling diffusion calculation in a hybrid computer model for room acoustic prediction," Proc. Inst. Acoust., **16**, 537-544 (1994).

111. B. Dalenbäck, M. Kleiner, P. Svensson, "A macroscopic view of diffuse reflection," 95th Convention of AES, preprint 3726 (1993).

112. M. Hodgson, "Evidence of diffuse surface reflections in rooms" J. Acoust. Soc. Am., **89**, 765-771 (1991).

113. B. Dalenbäck, "Reverberation time, diffuse reflection, Sabine, and computerized prediction – part I" Online Paper, http://www.rpginc.com/research/reverb01.htm (October 2004).

114. B. Dalenbäck, "Reverberation time, diffuse reflection, Sabine, and computerized prediction – part II" Online Paper, http://www.rpginc.com/research/reverb02.htm (October 2004).

Diffusers

115. K. Fujiwara, K. Nakai, H. Torihara, "Visualization of the sound field around a Schroeder diffuser" Appl. Acoust., **60**, 225-235 (2000).

116. T. Wu, T. Cox, Y. Lam, "From a profiled diffuser to an optimized absorber," J. Acoust. Soc. Am., **108**, 643-650 (2000).

117. J. Angus, "Using grating modulation to achieve wideband large area diffusers," Appl. Acoust., **60**, 143-165 (2000).

118. P. D'Antonio, T. Cox, "Diffusor application in rooms," Appl. Acoust., **60,** 113-142 (2000).

119. P. D'Antonio, T. Cox, "Two decades of sound diffusor design and development part 1: applications and design," J. Audio. Eng. Soc., **46**, 955-975 (1998).

120. P. D'Antonio, T. Cox, "Two decades of sound diffusor design and development part 2: prediction, measurement, and characterization," J. Audio. Eng. Soc., **46**, 1075-1091 (1998).

121. D. Takahashi, "Development of optimum acoustic diffusers," J. Acoust. Soc. Jpn. (E), **16**, 51-58 (1995).

122. M. Kleiner, H. Gustafsson, J. Backman, "Measurement of directional scattering coefficients using near-field acoustic holography and spatial transformation of sound fields," 98th Convention of AES, preprint 4118 (1995).

123. J. Angus, A. Marvin, J. Clegg, J. Dawson, "A practical metric for evaluating sound diffusers," 98th Convention of AES, preprint 3955 (1995).

124. T. Cox, "The optimization of profiled diffusers," J. Acoust. Soc. Am., **97**, 2928-2936 (1995).

125. H. Kuttruff, "Sound absorption by pseudostochastic diffusers (Schroeder diffusers)," Appl. Acoust., **42**, 215-231 (1994).

126. W. Ten Kate, "Analysis of the diffusor" 14th Inter. Cong. Acoust., paper F8-6 (1992).

127. P. D'Antonio, J. Konnert, "The role of reflection phase grating diffusors in critical listening and performing environments," 78th Convention of AES, preprint 2255 (1985).

128. P. D'Antonio, J. Konnert, "The reflection phase grating diffusor: design theory and application," J. Audio Eng. Soc., **32**, 228-238 (1984).

Diffusion Coefficients

129. AES, "AES information document for room acoustics and sound reinforcement systems – characterization and measurement of surface scattering uniformity," Audio Engineering Society, Inc. (2001)

130. M. Kleiner, H. Gustafsson, J. Backman, "Measurement of directional scattering coefficients using near-field acoustic holography and spatial transformation of sound fields," J. Audio Eng. Soc. Am., **45**, 331-346 (1997).

131. P. D'Antonio, J. Konnert, P. Kovitz "The DISC project: experimental measurement of the directional scattering properties of architectural acoustic surfaces," Proc. Wallace Clement Sabine Centennial Symposium, 141-144 (1994).

132. P. D'Antonio, "The DISC project: directional scattering coefficient determination and auralization of virtual environments," Proc. Noise-Con 93', 259-264 (1993).

133. P. D'Antonio, P. Kovitz, "DISC project: auralization using directional scattering coefficients," 95th Convention of AES, preprint 3727 (1993).

134. P. D'Antonio, J. Konnert, "The directional scattering coefficient: experimental determination," J. Audio Eng. Soc., **40,** 997-1017 (1992).

135. A. Kulowski, "Remarks on a limit value of the sound directional diffusion coefficient in rooms," Appl. Acoust., **32**, 93-105 (1991).

136. P. D'Antonio, J. Konnert, "The directional scattering coefficient: experimental determination," 91st Convention AES, preprint 3117 (1991).

137. RPG Diffusers, "Diffusion coefficient" http://www.rpginc.com/research/5i3.htm (October 2004).

138. RPG Diffusers, "The evolution of the diffusion coefficient" http://www.rpginc.com/research/ (October 2004).

Error Analysis for Ray-tracing

139. Z. Xiangyang, C. Ke'an, S. Jincai, "On the accuracy of the ray-tracing algorithms based on various sound receiver models," Appl. Acoust., **64**, 433-441 (2003).

140. J. Giner, C. Militello, A. Garciá, "The Monte Carlo method to determine the error in calculation of objective acoustic parameters within the ray-tracing technique," J. Acoust. Soc. Am., **110,** 3081-3085 (2001).

141. J. Giner, C. Militello, A. Garciá, "Ascertaining confidence within the ray-tracing method," J. Acoust. Soc. Am., **106,** 816-822 (1999).

142. H. Lehnert, "Systematic errors of the ray-tracing algorithm," Appl. Acoust., **38**, 207-221 (1993).

143. A. Kulowski, "Error investigation for the ray tracing technique," Appl. Acoust., **15,** 263-274 (1982).

Geometrical Acoustic Prediction Algorithms

144. T. Funkhouser, N. Tsingos, I. Carlbom, G. Elko, M. Sondhi, J. West, G. Pingali, P. Min, A. Ngan, "A beam tracing method for interactive architectural acoustics," J. Acoust. Soc. Am., **115**, 739-756 (2004).

145. Z. Xiangyang, C. Ke-an, S. Jincai, "Development of a hybrid computer model for simulating the complicated virtual sound field in enclosures," Appl. Acoust., **63**, 481-491 (2002).

146. Z. Xiangyang, C. Ke'an, S. Jincai, "Modeling the sound fields in rooms with multiple sources using a hybrid image method including phase," Acta Acustica United with Acustica, **88**, 88-92 (2002).

147. O. Schmitz, S. Feistel, W. Ahnert, M. Vorländer, "Merging software for sound reinforcement systems and for room acoustics," 110th Convention of AES, preprint 5352 (2001).

148. C. Christensen, "ODEON – a design tool for auditorium acoustics, noise control and loudspeaker systems," Proc. Inst. Acoust., **23**, 137-144 (2001).

149. I. Drumm, Y. Lam, "The adaptive beam-tracing algorithm," J. Acoust. Soc. Am., **107,** 1405-1412 (2000).

150. N. Campo, P. Rissone, M. Toderi, "Adaptive pyramid tracing; a new technique for room acoustics," Appl. Acoust., **61**, 199-221 (2000).

151. G. Mahalingam, "A new algorithm for the simulation of sound propagation in spatial enclosures," Proceedings of Building Simulation, **3**, 1383-1387 (1999).

152. T. Funkhouser, I. Carlbom, G. Elko, G. Pingali, M. Sondhi, J. West, "A beam tracing approach to acoustic modeling for interactive virtual environments," Computer Graphics (SIGGRAPH `98), Orlando, Florida, 21-32 (1998).

153. B. Dalenbäck, "Room acoustic prediction based on a unified treatment of diffuse and specular reflection," J. Acoust. Soc. Am., **100**, 899-909 (1996).

154. U. Stephenson, "Quantized pyramidal beam tracing – a new algorithm for room acoustics and noise immission prognosis," Acustica, **82,** 517-525 (1996).

155. A. Farina, "RAMSETE: A new pyramid tracer for medium and large scale acoustic problems," Proc. EURO-NOISE 95 Conference (1995).

156. A. Farina, "Pyramid tracing vs. ray tracing for the simulation of sound propagation in large rooms," Proceedings of the International Conference on Computational Acoustics Environmental Applications, Southampton, England (1995).

157. B. Dalenbäck, "Room acoustic prediction and auralization based on a unified treatment of diffuse and specular reflection," 15th Inter. Cong. Acoust., Trondheim, Norway, 425-428 (1995).

158. B. Dalenbäck, "A new model for room acoustic prediction and auralization," Doctoral Thesis, Chalmers University of Technology (1995).

159. D. Maercke, J. Martin, "The prediction of echograms and impulse responses within the Epidaure software," Appl. Acoust., **38**, 93-114 (1993).

160. K. Nakagawa, T. Miyajima, Y. Tahara, "An improved geometrical sound field analysis in rooms using scattered sound and an audible room acoustic simulator," Appl. Acoust., **38**, 115-129 (1993).

161. G. Naylor, "ODEON – another hybrid room acoustical model," Appl. Acoust., **38**, 131-143 (1993).

162. R. Heinz, "Binaural room simulation based on an image source model with addition of statistical methods to include the diffuse sound scattering of walls and to predict the reverberant tail," Appl. Acoust., **38**, 145-159 (1993).

163. H. Staffeldt, "Modeling of room acoustics and loudspeakers in JBL's complex array design program CADP2," Appl. Acoust., **38**, 179-193 (1993).

164. T. Lewers, "A combined beam tracing and radiant exchange computer model of room acoustics," Appl. Acoust., **38**, 161-178 (1993).

165. U. Kristiansen, A. Krokstad, T. Follestad, "Extending the image method to higher-order reflections," Appl. Acoust., **38**, 195-206 (1993).

166. B. Dalenbäck, P. Svensson, M. Kleiner, "Prediction and auralization based on a combined image source/ray-model," Proc. 14th Inter. Cong. Acoust., Beijing, China, Paper F2-7 (1992).

167. A. Kulowski, "Optimization of a point-in-polygon algorithm for computer models of sound field in rooms," Appl. Acoust., **35**, 63-74 (1992).

168. O. Warusfel, R. Denayrou, J. Jullien, "Validation of a computer model environment for room acoustics prediction," Proc. 14th Inter. Cong. Acoust., Beijing, China, Paper F6-5 (1992).

169. U. Stephenson, "Comparison of the mirror image source method and the sound particle simulation method," Appl. Acoust., **29**, 35-72 (1990).

170. W. Ahnert, R. Feistel, "Ray-tracing or sound imaging," 89th Convention of AES, preprint 2993 (1990).

171. M. Vorländer, "Simulation of the transient and steady-state sound propagation in room using a new combined ray-tracing/image-source algorithm," J. Acoust. Soc. Am., **86**, 172-178 (1989).

172. J. Martin, J. P. Vian, "Binaural sound simulation of concert halls by a beam tracing method," Proc. 13th Int. Cong. Acoust., 253-256 (1989).

173. H. Lee, B-H. Lee "An efficient algorithm for the image model technique," Appl. Acoust., **24**, 87-115 (1988).

174. D. Maercke, "Simulation of sound fields in time and frequency," Proc. 12th Inter. Cong. Acoust., Paper E11-7 (1986).

175. M. Merkle, M. Mijic, "Some ray tracing algorithms and their comparison," Proc. 12th Inter. Cong. Acoust., Paper E12-4 (1986).

176. J. Vian, D. Maercke, "Calculation of room impulse response using a ray tracing method," Proceedings of the Vancouver Symposium of Acoustics and Theatre Planning for Performing Arts, 74-78 (1986).

177. K. Iida, Y. Ando, "Expansion of the image source method for acoustical design of auditoria," Proc. 12th Inter. Cong. Acoust., Paper E11-3 (1986).

178. A. Kulowski, "Algorithmic representation of the ray tracing technique," Appl. Acoust., **18**, 449-469 (1985).

179. J. Kirszenstein, "An image source computer model for room acoustics analysis and electroacoustic simulation," Appl. Acoust., **17**, 275-290 (1984).

180. J. Borish, "Extension of the image model to arbitrary polyhedra," J. Acoust. Soc Am., **75**, 1827-1836 (1984).

181. A. Krokstad, S. Strøm, S. Sørsdal, "Fifteen years' experience with computerized ray tracing," Appl. Acoust., **16**, 291-312 (1983).

182. J. Embrechts, "Sound field distribution using randomly traced sound ray techniques," Acustica, **51**, 288-295 (1982).

183. J. Walsh, "The design of Godot: a system for computer-aided room acoustics modeling and simulation," Proc. 10th Inter. Cong. Acoust., Paper E15.3 (1980).

184. J. Allen, D. Berkley, "Image method, for efficiently simulating small-room acoustics," J. Acoust. Soc. Am., **65**, 943-950 (1979).

185. M. Gensane, F. Santon, "Prediction of sound fields in rooms of arbitrary shape: validity of the image sources method," J. Sound. Vib., **63**, 97-108 (1979).

186. S. Strøm, "Computerized sound ray tracing in rooms," Proc. 9th Inter. Cong. Acoust., Paper B6 (1977).

187. B. Gibbs, D. Jones, "A simple image method for calculating the distribution of sound pressure levels within an enclosure," Acustica, **26**, 24-32 (1972).

188. S. Strøm, "Investigation of room shapes by use of a computer model," Proc. 7th Inter. Cong. Acoust., **2,** 133-136 (1971).

Geometric Acoustics Theory

189. J. Polack, "Playing billiards in the concert hall: the mathematical foundations of geometric room acoustics," Appl. Acoust., **38**, 235-244 (1993).

190. H. Kuttruff, *Room Acoustics, 4th Edition* (Spon Press, London, 2000), Chapter 4

Layman Papers on Geometric Acoustics and Auralization

191. N. Shaw, "Acoustical design and auralization: going to school for EASE and EARS," Sound & Communications, 44-51, 60 (1994).

192. M. Klasco, "Software review, EASE Version 1.0 from Renkus-Heinz, part I," Sound & Communications, 64-66, 75 (1991).

193. M. Klasco, "Software review, part II, performance simulations and selecting speakers with EASE," Sound & Communications, 62-65 (1991).

194. M. Klasco, "Bose modeler revisited, part 1: the sound system software series ships its annual update," Sound & Communications, 66-69 (1990).

Level of Detail in Geometric Acoustic Models

195. D. Bradley, L. Wang, "Effect of model detail level on room acoustic computer simulations," J. Acoust. Soc. Am., **111**, 2389(A) (2002).

196. M. Yuge, H. Shiokawa, J. Rindel, C. Christensen, A. Gad, M. Itamoto, "Comparisons between computer simulations of room acoustical parameters and those measured in concert halls part 2: Göteborgs Konserthus and Barbican concert hall," 17th Inter. Cong. Acoust., Rome, Paper 3P.43 (2001).

197. J. Rindel, H. Shiokawa, C. Christensen, A. Gade, "Comparisons between computer simulations of room acoustical parameters and those measured in concert halls," Proc. Joint Meeting of the Acoust. Soc. of Am. and the European Acoust. Assoc., (1999).

198. W. Pompetzki, J. Blauert, "A study on the perceptual authenticity of binaural room simulation," Proc. Wallace Clement Sabine Centennial Symposium, 81-84 (1994).

Measuring Audience Seating Absorption Coefficients

199. T. Cox, P. D'Antonio, *Acoustic Absorbers and Diffusers Theory, Design and Application* (Spon Press, London, 2004), Sections 3.4.1 and 7.1

200. J. Summers, "Measurement of audience seat absorption for use in geometrical acoustics software," Applied Research Letters Online, **4**, 77-82 (2003).

201. N. Nishihara, T. Hidaka, L. Beranek, "Mechanism of sound absorption by seated audience in halls," J. Acoust. Soc. Am., **110**, 2398-2411 (2001).

202. M. Barron, S. Coleman, "Measurements of the absorption by auditorium seating – a model study," J. Sound Vib., **239**, 573-587 (2001).

203. L. Beranek, T. Hidaka, "Sound absorption in concert halls by seats, occupied and unoccupied, and by the hall's interior surfaces," J. Acoust. Soc. Am., **104**, 3169-3177 (1998).

204. L. Beranek, T. Hidaka, "Sound absorption in concert halls by seats, occupied and unoccupied, and by the hall's interior surfaces," J. Acoust. Soc. Am., **101**, 3134(A) (1997).

205. J. Bradley, "The sound absorption of occupied auditorium seating," J. Acoust. Soc. Am., **99**, 990-995 (1996).

206. W. Davies, R. Orlowski, Y. Lam, "Measuring auditorium seat absorption," J. Acoust. Soc. Am., **96**, 879-888 (1994).

207. J. Bradley, "Reply to: 'comments on 'predicting theatre chair absorption from reverberation chamber measurements' [J. Acoust. Soc. Am. **93,** 2238-2240 (1993)]," J. Acoust. Soc. Am., **95**, 1155-1157 (1994).

208. W. Davies, Y. Lam, R. Orlowski, "Comment on 'predicting theatre chair absorption from reverberation chamber measurements' [J. Acoust. Soc. Am. 91, 1514-1524 (1992)]," J. Acoust. Soc. Am., **93**, 2238-2240 (1993).

209. J. Bradley, "Predicting theatre chair absorption from reverberation chamber measurements," J. Acoust. Soc. Am., **91**, 1514-1524 (1992).

210. L. Beranek, "Audience and chair absorption in large halls. II," J. Acoust. Soc. Am., **45**, 13-19 (1969).

211. L. Beranek, "Audience and seat absorption in large halls," J. Acoust. Soc. Am., **32**, 661-670 (1960).

Using Room Acoustic Software Packages to Design Rooms

212. N. Bayazit, "An approach for the geometrical design of rectangular concert halls with good acoustics," Architectural Science Review, **46**, 125-134 (2003).

213. S. Strøm, H. Dahl, A. Krokstad, E. Eknes, "Acoustical design of the Grieg memorial hall in Bergen," Appl. Acoust., **18**, 127-142 (1985).

214. Krokstad, S. Strøm, "Acoustical design of the multi-purpose 'Hjertnes' hall in Sandefjord," Appl. Acoust., **12**, 45-63 (1979).

215. S. Strøm, "Acoustical design of a multi-purpose hall in Ibsen house," Proc. 8th Inter. Cong. Acoust., **II**, 605 (1974).

Appendix A

Absorption Coefficients (values listed are percentages)

Material Symbol	Description	α 125	α 250	α 500	α 1K	α 2K	α 4K	Reference:
MainCarp	Main floor carpeted areas	2	5	11	29	48	53	Average of "Carpet, heavy, cemented to concrete[66]" and "Carpet, thin, cemented to concrete[66]"
MainAud	Main floor audience areas	54	62	68	70	68	66	"Seats, unoccupied, medium upholstered[55]"
DoorbyTerr	Door by side of terrace	15	11	10	7	6	7	"Floors, wood[67]"
MainBack	Main floor back wall	27	51	59	56	53	52	Average of "Owens-Corning Fiberglass 2" 703[68]" and "Ordinary window glass[67]"
MainDoors	Main floor doors on back wall	15	11	10	7	6	7	"Floors, wood[67]"
MainWall	Wall on side of terrace near main floor back wall	25	8	5	4	7	9	"Gypsum Board, 1/2" nailed to 2x4", 16" o.c. (adjusted the low end to change to 5/8")[67]"
MainCeil	Main floor ceiling above vestibule	25	8	5	4	7	9	"Gypsum Board, 1/2" nailed to 2x4", 16" o.c. (adjusted the low end to change to 5/8")[67]"
TerrAud	Terrace audience areas	54	62	68	70	68	66	"Seats, unoccupied, medium upholstered[55]"
TerrCarp	Terrace carpeted areas	2	5	11	29	48	53	Average of "Carpet, heavy, cemented to concrete[66]" and "Carpet, thin, cemented to concrete[66]"
TerrFasc	Terrace fascia	25	8	5	4	7	9	"Gypsum Board, 1/2" nailed to 2x4", 16" o.c. (adjusted the low end to change to 5/8")[67]"
TerrBack	Terrace back wall	18	76	99	99	99	99	"Owens-Corning Fiberglass 2" 703[68]"
TerrDoors	Terrace doors on back wall (in vestibule)	15	11	10	7	6	7	"Floors, wood[67]"
RostPanel	Rostrum front panelling	15	11	10	7	6	7	"Floors, wood[67]"
RostAud	Rostrum general authorities audience area	70	76	81	84	84	81	"Seats, unoccupied, heavily upholstered[55]"

Name	Description							Reference
RostCarp	Rostrum carpet areas	30	14	9	17	26	30	Average of "Average of 'Carpet, heavy, cemented to concrete[66]' and 'Carpet, thin, cemented to concrete[66]'" and "Hardwood plywood paneling 1/4" thick, wood frame[68]"
RostSideEntries	Rostrum side entry ways	15	11	10	7	6	7	"Floors, wood[67]"
ChoirAud	Choir audience areas	54	62	68	70	68	66	"Seats, unoccupied, medium upholstered[55]"
RostChoirPanel	Rostrum & choir side paneling	15	11	10	7	6	7	"Floors, wood[67]"
ChoirFloor	Floor in front and behind choir	58	22	7	4	3	7	"Hardwood plywood paneling ¼" thick, wood frame[68]"
OrganCase	Organ casing	20	20	20	20	20	20	Estimated – pipes are resonators so they absorb sound. There are all sizes of pipes so absorption is roughly flat across the frequency range
WoodBaffles	Wooden baffles behind choir	15	11	10	7	6	7	"Floors, wood[67]"
RostSideWalls	Rostrum side walls	25	8	5	4	7	9	"Gypsum Board, 1/2" nailed to 2x4", 16" o.c. (adjusted the low end to change to 5/8")[67]"
TechCols	Technical columns	99	99	99	99	98	98	"Owens-Corning Fiberglass 4" 703[68]"
SideTechCols	Opposite side of Technical columns (near treated side walls)	3	3	3	4	5	7	"Unglazed Brick[67]"
HangBaffles	Hanging baffles	25	8	5	4	7	9	"Gypsum Board, 1/2" nailed to 2x4", 16" o.c. (adjusted the low end to change to 5/8")[67]"
FloorUpOrgan	Floor of upper organ cavity	15	15	15	15	15	15	Estimated - This room is actually closed off, but I accidently included it
SideOrganCav	Side of organ cavity	20	9	8	5	6	8	Average "Floors, wood[67]" and "Gypsum Board, 1/2" nailed to 2x4-in, 16-in o.c. (adjusted the low end to change to 5/8")[67]"
FrontWallOrgan	Front wall facing lower middle organ cavity	25	8	5	4	7	9	"Gypsum Board, 1/2" nailed to 2x4", 16" o.c. (adjusted the low end to change to 5/8")[67]"
CeilLowOrgan	Ceiling of lower middle organ cavity	1	1	2	2	2	2	"Concrete Floor[66]"
WallsUpOrgan	Walls of upper organ cavity	15	15	15	15	15	15	Estimated - This room is actually closed off, but I accidently included it
WallsLowOrgan	Walls of lower organ cavity	1	1	2	2	2	2	"Concrete Floor[66]"

Name	Description							Material
Walls2SideCav	Walls of two small side cavities	1	1	2	2	2	2	"Concrete Floor[66]"
WallsBackMainCav	Back walls of main large cavity behind rostrum	5	20	26	26	26	26	Average "Concrete Floor[66]" and "Owens-Corning Fiberglass 2" 703[68]" weighted concrete:3/4 fiberglass:1/4
WallsSideMainCav	Side walls of main large cavity behind rostrum	1	1	2	2	2	2	"Concrete Floor[66]"
Ceil2SideCav	Ceilings of two small side cavities	1	1	2	2	2	2	"Concrete Floor[66]"
PartWallMainCav	Partial wall of main large cavity	25	8	5	4	7	9	"Gypsum Board, 1/2" nailed to 2x4", 16" o.c. (adjusted the low end to change to 5/8")[67]"
FloorCavRost	Floor cavity behind rostrum	1	1	2	2	2	2	"Concrete Floor[66]"
LowCeilRost	Lower ceiling over rostrum entrance	1	1	2	2	2	2	"Concrete Floor[66]"
BackWallCav	Back wall cavity underneath balcony	1	1	2	2	2	2	"Concrete Floor[66]"
BalcBackWall	Balcony back wall	18	76	99	99	99	99	"Owens-Corning Fiberglass 2" 703[68]"
BalcDoorsBack	Balcony doors on back wall (in vestibule)	15	11	10	7	6	7	"Floors, wood[67]"
TerrCeilCan	Terrace ceiling canopies	5	5	5	5	5	5	Estimated – not much energy is actually "absorbed" by these canopies, it is just transmitted back into the room
BalcAud	Balcony audience seating	54	62	68	70	68	66	"Seats, unoccupied, medium upholstered[55]"
BalcFasc	Balcony fascia	25	8	5	4	7	9	"Gypsum Board, 1/2" nailed to 2x4", 16" o.c. (adjusted the low end to change to 5/8")[67]"
BalcCarp	Balcony carpet area	2	5	11	29	48	53	Average of "Carpet, heavy, cemented to concrete[66]" and "Carpet, thin, cemented to concrete[66]"
BalcCeilCan	Balcony ceiling canopies	5	5	5	5	5	5	Estimated – not much energy is actually "absorbed" by these canopies, it is just transmitted back into the room
BalcCeilBack	Balcony ceiling back wall	1	1	2	2	2	2	"Concrete Floor[66]"
CeilSkyCones	Ceiling skylight cones	25	8	5	4	7	9	"Gypsum Board, 1/2" nailed to 2x4", 16" o.c. (adjusted the low end to change to 5/8")[67]"

ChoirCan	Canopies above choir	5	5	5	5	5	5	Estimated – not much energy is actually "absorbed" by these canopies, it is just transmitted back into the room
Ceiling	Ceiling	1	1	2	2	2	2	"Concrete Floor[66]"
SideWalls	Side walls (treated façade)	39	53	55	54	54	54	Average of "Plywood panels, ¼-in., mounted over 3" air space, with 1" glassfiber batts right behind the panel[67]" and "Owens-Corning Fiberglass 2" 703[68]"
SideWallsTop	Concrete lid over side walls	1	1	2	2	2	2	"Concrete Floor[66]"
TerrCeilBack	Cavity under balcony and above ceiling in back	1	1	2	2	2	2	"Concrete Floor[66]"
TerrCeilFront	Cavity under balcony and above ceiling in front	25	8	5	4	7	9	"Gypsum Board, 1/2" nailed to 2x4", 16" o.c. (adjusted the low end to change to 5/8")[67]"
CeilingTreat	Absorptive ceiling treatment	5	11	19	23	24	22	Noise baffles, 2'x4' for factories, gymnasiums – data in Sabins/unit. Divide by 8 to get sabins/ft^2. Divide by 3 because panels cover approximately 1/3 of the ceiling. Divide by 2 because panels are double-sided.

Appendix B

Scattering Coefficients (values listed are percentages)

Material Symbol	Description	δ 125	δ 250	δ 500	δ 1K	δ 2K	δ 4K	Edge?	Ref.:
MainCarp	Main floor carpeted areas	15	15	15	15	15	15	No	Mostly Flat
MainAud	Main floor audience areas	30	40	50	60	70	70	No	Dalenbäck and CATT™ user's web page
DoorbyTerr	Door by side of terrace	10	10	10	10	10	10	Yes	Hard and Flat
MainBack	Main floor back wall	20	20	20	20	20	20	Yes	Curved with windows so a little higher than normal
MainDoors	Main floor doors on back wall	10	10	10	10	10	10	Yes	Hard and Flat
MainWall	Wall on side of terrace near main floor back wall	10	10	10	10	10	10	Yes	Hard and Flat
MainCeil	Main floor ceiling above vestibule	10	10	10	10	10	10	Yes	Hard and Flat
TerrAud	Terrace audience areas	30	40	50	60	70	70	No	Dalenbäck and CATT™ user's web page
TerrCarp	Terrace carpeted areas	15	15	15	15	15	15	No	Mostly Flat
TerrFasc	Terrace fascia	15	15	15	15	15	15	Yes	Mostly Flat
TerrBack	Terrace back wall	20	20	20	20	20	20	No	Curved so a little higher than normal
TerrDoors	Terrace doors on back wall (in vestibule)	10	10	10	10	10	10	Yes	Hard and Flat
RostPanel	Rostrum front panelling	30	60	70	80	80	80	Yes	Scatters mainly due to the height
RostAud	Rostrum general authorities audience area	30	40	50	60	70	70	No	Dalenbäck and CATT™ user's web page
RostCarp	Rostrum carpet areas	15	15	15	15	15	15	No	Mostly Flat
RostSideEntries	Rostrum side entry ways	10	10	10	10	10	10	No	Flat
ChoirAud	Choir audience areas	30	40	50	60	70	70	No	Dalenbäck and CATT™ user's web page

RostChoirPanel	Rostrum & choir side paneling	15	15	15	15	15	15	No	Mostly Flat
ChoirFloor	Floor in front and behind choir	10	10	10	10	10	10	No	Flat
OrganCase	Organ casing	10	15	30	65	80	80	No	the organ pipe surfaces will range from roughly .4 m in diameter to <.1 m in diameter. Mostly the frequency scattering will be at high frequencies, but there will be some minimal low frequency as well.
WoodBaffles	Wooden baffles behind choir	10	10	10	10	10	10	No	Flat
RostSideWalls	Rostrum side walls	15	15	15	15	15	15	no	Mostly Flat
TechCols	Technical columns	10	10	10	10	10	10	No	Flat
SideTechCols	Opposite side of Technical columns (near treated side walls)	10	10	10	10	10	10	No	Flat
HangBaffles	Hanging baffles	15	15	15	15	15	15	yes	Curved so a little higher than normal
FloorUpOrgan	Floor of upper organ cavity	10	10	10	10	10	10	No	Flat
SideOrganCav	Side of organ cavity	15	15	15	15	15	15	No	Mostly Flat
FrontWallOrgan	Front wall facing lower middle organ cavity	15	15	15	30	60	80	No	Some scattering due to irregularities underneath rostrum (beams, etc)
CeilLowOrgan	Ceiling of lower middle organ cavity	10	10	10	10	10	10	No	Flat
WallsUpOrgan	Walls of upper organ cavity	10	10	10	10	10	10	No	Flat
WallsLowOrgan	Walls of lower organ cavity	10	10	10	10	10	10	No	Flat
Walls2SideCav	Walls of two small side cavities	10	10	10	10	10	10	No	Flat
WallsBackMainCav	Back walls of main large cavity behind rostrum	10	10	10	10	10	10	No	Flat
WallsSideMainCav	Side walls of main large cavity behind rostrum	10	10	10	10	10	10	No	Flat
Ceil2SideCav	Ceilings of two small side cavities	10	10	10	10	10	10	No	Flat

PartWallMainCav	Partial wall of main large cavity	10	10	10	10	10	10	No	Flat
FloorCavRost	Floor cavity behind rostrum	10	10	10	10	10	10	No	Flat
LowCeilRost	Lower ceiling over rostrum entrance	10	10	10	10	10	10	No	Flat
BackWallCav	Back wall cavity underneath balcony	10	10	10	10	10	10	No	Flat
BalcBackWall	Balcony back wall	20	20	20	20	20	20	No	Curved so a little higher than normal
BalcDoorsBack	Balcony doors on back wall (in vestibule)	10	10	10	10	10	10	Yes	Hard and Flat
TerrCeilCan	Terrace ceiling canopies	20	20	20	20	20	20	Yes	Curved so a little higher than normal
BalcAud	Balcony audience seating	30	40	50	60	70	70	No	Dalenbäck and CATT™ user's web page
BalcFasc	Balcony fascia	15	15	15	15	15	15	Yes	Mostly Flat
BalcCarp	Balcony carpet area	15	15	15	15	15	15	No	Mostly Flat
BalcCeilCan	Balcony ceiling canopies	20	20	20	20	20	20	Yes	Curved so a little higher than normal
BalcCeilBack	Balcony ceiling back wall	10	10	10	10	10	10	No	Flat
CeilSkyCones	Ceiling skylight cones	20	20	20	20	20	20	No	Curved so a little higher than normal
ChoirCan	Canopies above choir	20	20	20	20	20	20	Yes	Curved so a little higher than normal
Ceiling	Ceiling	70	70	70	70	70	70	No	Lots of irregularities up there
SideWalls	Side walls (treated façade)	25	25	40	70	90	90	No	Scattering due to depth and impedance change
SideWallsTop	Concrete lid over side walls	10	10	10	10	10	10	No	Flat
TerrCeilBack	Cavity under balcony and above ceiling in back	10	10	10	10	10	10	No	Flat
TerrCeilFront	Cavity under balcony and above ceiling in front	10	10	10	10	10	10	No	Flat
CeilingTreat	Absorptive ceiling treatment	10	10	10	10	10	10	No	Flat

Appendix C

Definitions of Acoustic Parameters

The clarity factor C50 describes the intelligibility of speech and is expressed in decibels. It is calculated by determining the ratio of the early energy (arriving before 50 ms) to the late energy (arriving after 50 ms) and is given by:

$$C50 = 10\log_{10}\left\{\frac{\int\limits_{0ms}^{50ms}[h(t)]^2\,dt}{\int\limits_{50ms}^{\infty}[h(t)]^2\,dt}\right\}, \qquad (C.1)$$

where $h(t)$ is the impulse response measured with an omni-directional receiver. Good intelligibility of speech is usually given when C50 > 0 dB.

The "Deutlichkeit" or definition, D50, describes the same perceived quantity as the C50, but is given as a percentage:

$$D50 = \frac{\int\limits_{0ms}^{50ms}[h(t)]^2\,dt}{\int\limits_{0ms}^{\infty}[h(t)]^2\,dt}. \qquad (C.2)$$

Good intelligibility of speech is usually given when D50 > 50%.

C80 is a clarity factor for music and is also expressed in decibels. It is calculated by determining the ratio of the early energy (arriving before 80 ms) to the late energy (arriving after 80 ms), and is given by:

$$C80 = 10\log_{10}\left\{ \frac{\int_{0ms}^{80ms}[h(t)]^2\,dt}{\int_{80ms}^{\infty}[h(t)]^2\,dt} \right\}. \qquad (C.3)$$

The optimum value for C80 depends strongly on the genre of music. Good C80 values for romantic music range from -3 dB to +4 dB while classic and modern music will allow C80 values up to +8 dB.

The lateral fraction, LF, describes the fraction of energy that arrives from the lateral directions within the first 80 ms and is expressed as a decimal or percentage value. The LF is related to the perceived width of the sound source and the amount the listener feels enveloped by the sound. It is calculated as the ratio of the energy measured by a figure-of-eight pattern receiver (with its null direction aimed at the source) to the energy measured by an omni-directional receiver, and is given by:

$$LF = \frac{\int_{5ms}^{80ms}[h_L(t)]^2\,dt}{\int_{0ms}^{80ms}[h(t)]^2\,dt}, \qquad (C.4)$$

where $h_L(t)$ is the impulse response measured with a figure-of-eight microphone. The time integration for the figure-of-eight microphone is evaluated started at 5 ms in order to make certain that the direct sound is eliminated. Because the directivity of a figure-of-eight microphone is essentially a cosine pattern and the impulse response is squared, the LF is often calculated in computer modeling packages by:

$$LF = \frac{\int\limits_{5ms}^{80ms} [h(t)]^2 |\cos^2(\theta)| dt}{\int\limits_{0ms}^{80ms} [h(t)]^2 dt},$$ (C.5)

where (θ) is the reflection angle related to the ear to ear axis on an assumed listener looking towards the main source. Good values for LF fall in the range of 10% to 25%.

A similar quantity, but one that is thought to be subjectively more accurate is the lateral fraction coefficient, LFC. This parameter is given by:

$$LFC = \frac{\int\limits_{5ms}^{80ms} |h_L(t) \cdot h(t)| dt}{\int\limits_{0ms}^{80ms} [h(t)]^2 dt}.$$ (C.6)

Rather than varying with the square of the cosine of the angle of incidence, the contributions now vary with the cosine of the angle. This is apparent in the form used by computer modeling packages to calculate this parameter:

$$LFC = \frac{\int\limits_{5ms}^{80ms} [h(t)]^2 |\cos(\theta)| dt}{\int\limits_{0ms}^{80ms} [h(t)]^2 dt}.$$ (C.7)

The sound strength factor G describes the strength of the sound source in the hall relative to the strength of the same sound source in a free-field and is expressed in decibels. It is calculated as the ratio of the integrated squared impulse response at a position in the hall to the integrated squared impulse response measured at a distance of 10 m from the same source located in a free-field, and is given by:

$$G = 10 \log_{10} \left[\frac{\int\limits_{0}^{\infty} [h(t)]^2 dt}{\int\limits_{0}^{\infty} [h_{10}(t)]^2 dt} \right],$$ (C.8)

where $h_{10}(t)$ is the impulse response of a source measured by an omni-directional microphone at a distance of 10 m in the free field. Optimum values for G for music and speech are within the range +1 dB to +10 dB which means that the loudness at all seats in a hall should be equal to or twice as loud as in the open at 10 m distance from the sound source.

SPL is a measure of the direct sound pressure level at a given receiver location with a given source. SPL is expressed in decibels.

The early decay time, EDT, is subjectively related to the perceived reverberance of a hall. It is obtained by backward integrating the impulse response to acquire a decay curve. Then a line is fit to the initial 10 dB of the decay curve and the time is calculated from this slope as the time required to decay 60 dB.

The reverberation time T30 is related to the physical properties of the auditorium or hall and is not as subjectively related to reverberance as the EDT. It is obtained in the same way as the EDT but fitting a line to the decay curve between -5 dB and -35 dB below the direct sound rather than the initial 10 dB of the decay.

The inter-aural cross correlation coefficient, IACC, gives an estimate of the similarity between the left and the right ear. It is measured from the inter-aural cross correlation function IACF, which is defined as:

$$IACF_{t_1 t_2}(\tau) = \frac{\left[\int_{t_1}^{t_2} h_L(t) h_R(t+\tau) dt \right]}{\left[\int_{t_1}^{t_2} [h_L(t)]^2 dt \int_{t_1}^{t_2} [h_R(t)]^2 dt \right]^{1/2}}$$ (C.9)

where $h_L(t)$ is the impulse response measured at the entrance to the left ear canal and $h_R(t)$ is the impulse response measured at the entrance to the right ear canal. The inter-aural cross correlation coefficient is then given by:

$$IACC_{t_1 t_2} = \max \left| IACF_{t_1 t_2}(\tau) \right|, \qquad\qquad (C.10)$$

where τ ranges from -1 to +1 ms because this is the approximate time it takes for a sound wave to travel from one side of the head to the other. The integration limits t_1 and t_2 depend on the subjective quantity of interest. The early IACC ($t_1 = 0$ and $t_2 = 80\,\text{ms}$) gives a measure of the apparent source width (1-IACC) or the spaciousness of the hall. The late IACC ($t_1 = 80\,\text{ms}$ and $t_2 = 1000\,\text{ms}$) is a measure of the amount the listener feels enveloped by the hall.

The speech transmission index, STI, indicates the effect of a transmission system on speech intelligibility and is expressed as a decimal value between 0 and 1. The determination of the STI is based on measuring the reduction of the signal modulation between the location of the sound source and the measurement position. Modulation transfer functions (MTFs) are measured at octave center frequencies with sine-wave amplitude modulation of a random noise signal. Modulation reduction indices are computed from the MTFs at modulation frequencies that are associated with the human voice. These modulation reduction indices are then converted to a single index, the speech transmission index (STI). Excellent STI values range from 0.75 to 1.0, very good values range from 0.6 to 0.75, good values range from 0.45 to 0.6, poor values range from 0.3 to 0.45, and unsatisfactory values range from 0 to 0.3.

Definitions are taken from the following references:

1. G. Ballou, Editor, *Handbook for Sound Engineers, Third Edition* (Focal Press, Boston, MA, 2002), Chapter 6 (W. Ahnert, H. Tennhardt).

2. ISO 3382, "Acoustics – Measurement of the reverberation time of rooms with reference to other acoustical parameters," (1997).

3. B. Dalenbäck, CATT-Acoustic™ v8.0 user's manual, (2002).

Appendix D

Sensitivity of Model to Scattering Coefficients

Seat 2

Seat 3

Seat 4

Seat 5

Seat 6

Seat 7

Seat 8

Seat 9
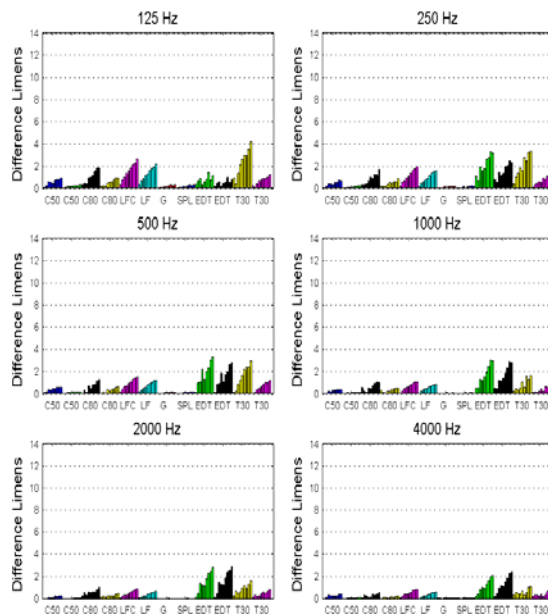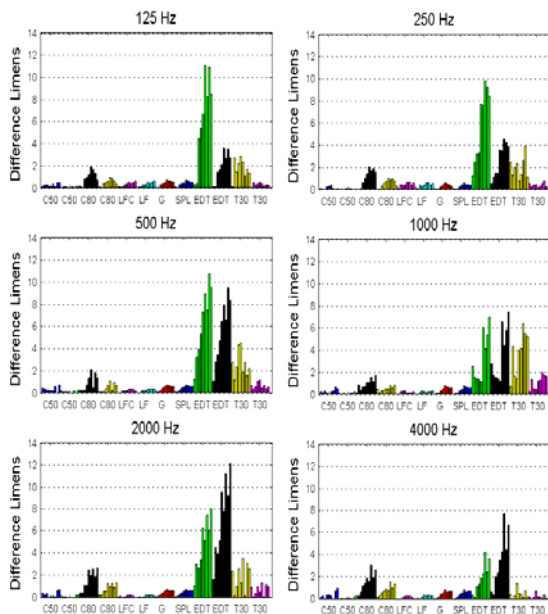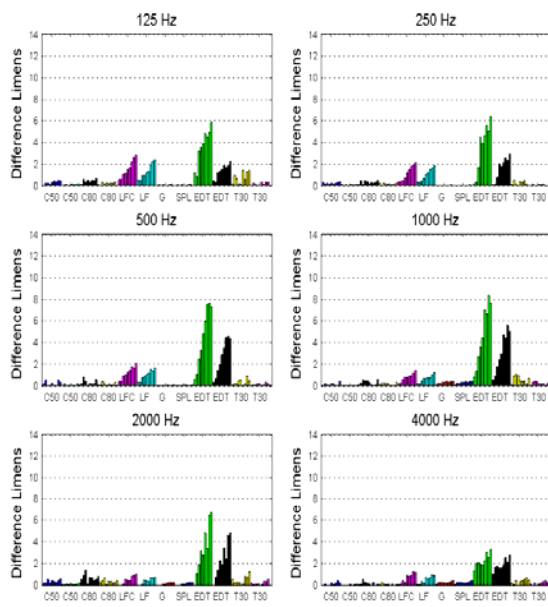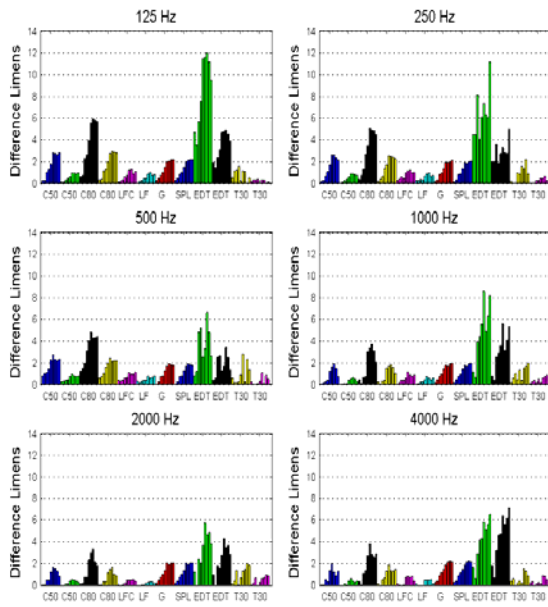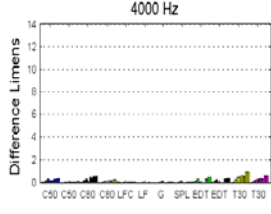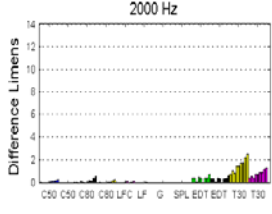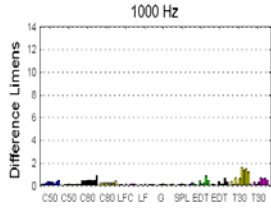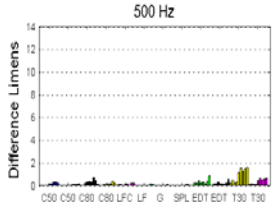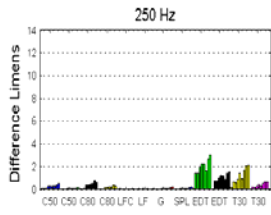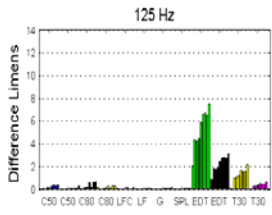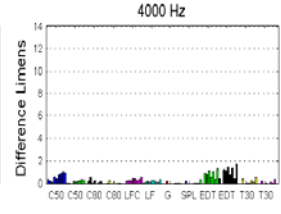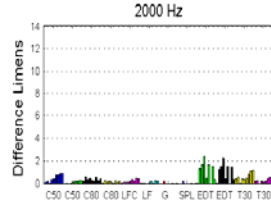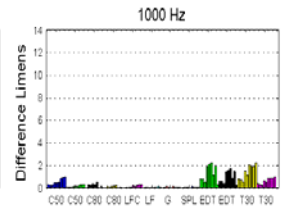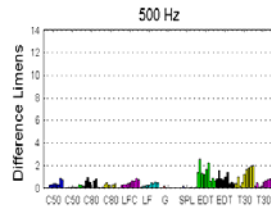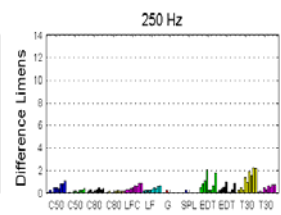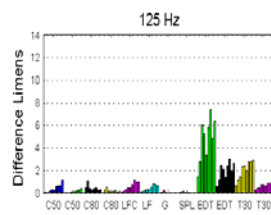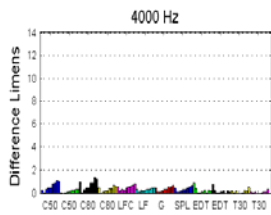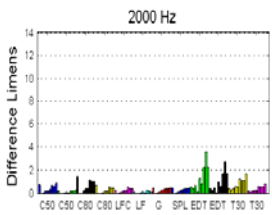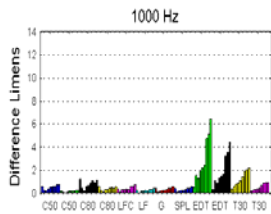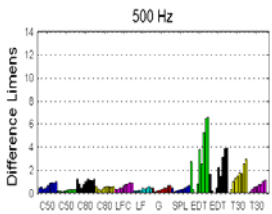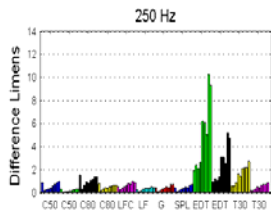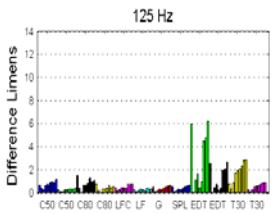
Seat 10

Seat 11

Seat 12

Appendix E

Temperature and Humidity measurements for empty room

Microphone #	Source Position	Temperature (°C)	Humidity (%)
1	A	21.61	33.54
2	A	21.6	33.53
3	A	21.57	33.6
4	A	21.55	33.61
5	A	21.54	33.61
7	A	21.54	33.62
1	B	21.5	31.22
2	B	21.49	31.46
3	B	21.54	31.56
4	B	21.51	31.8
5	B	21.52	32.36
7	B	21.52	32.36

Temperature and Humidity measurements for empty seats without carpet

Mic #	Source Position	Temp both baffles (°C)	Humidity both baffles (%)	Temp side baffle (°C)	Humidity side baffle (%)	Temp rear baffle (°C)	Humidity rear baffle (%)
1	A	21.46	34.2	21.53	34.36	21.49	34.11
2	A	21.47	34.36	21.52	34.41	21.49	34.12
3	A	21.47	34.36	21.52	34.45	21.49	34.12
4	A	21.48	34.41	21.49	34.51	21.51	34.09
5	A	21.48	34.25	21.49	34.58	21.5	34.07
7	A	21.48	33.99	21.49	34.58	21.52	34.1
1	B	21.49	34.03	21.47	34.61	21.58	34.36
2	B	21.49	34.03	21.46	34.61	21.59	34.42
3	B	21.47	33.94	21.48	34.58	21.57	34.51
4	B	21.46	33.89	21.49	34.54	21.54	34.57
5	B	21.45	33.95	21.49	34.53	21.53	34.61
7	B	21.46	33.92	21.49	34.52	21.53	34.6

Temperature and Humidity measurements for empty seats with carpet

Mic #	Source Position	Temp both baffles (°C)	Humidity both baffles (%)	Temp side baffle (°C)	Humidity side baffle (%)	Temp rear baffle (°C)	Humidity rear baffle (%)
1	A	21.63	28.8	21.65	27.91	21.74	28.07
2	A	21.64	28.84	21.65	27.98	21.74	28.08
3	A	21.63	28.84	21.65	27.92	21.72	28.06
4	A	21.64	28.83	21.65	27.92	21.71	28.11
5	A	21.63	28.89	21.68	27.98	21.7	28.08
7	A	21.63	28.89	21.66	28.01	21.71	28.05
1	B	21.64	28.82	21.69	28.5	21.65	27.65
2	B	21.64	28.81	21.68	28.45	21.66	27.7
3	B	21.64	28.88	21.68	28.47	21.66	27.57
4	B	21.65	28.88	21.66	28.36	21.68	27.81
5	B	21.65	28.93	21.67	28.34	21.68	27.93
7	B	21.65	28.95	21.67	28.37	21.68	27.99

Temperature and Humidity measurements for audience in seats

Mic #	Source Position	Temp both baffles (°C)	Humidity both baffles (%)	Temp side baffle (°C)	Humidity side baffle (%)	Temp rear baffle (°C)	Humidity rear baffle (%)
1	A	22.26	29.05	22.34	28.77	22.6	30.08
2	A	22.25	28.82	22.37	29.5	22.59	29.95
3	A	22.25	28.69	22.37	29.36	22.59	30.02
4	A	22.22	28.45	22.38	29.48	22.6	30.03
5	A	22.21	28.47	22.38	29.59	22.59	29.95
7	A	22.16	28.35	22.39	29.65	22.58	29.84
1	B	21.95	27.14	22.41	29.95	22.51	29.82
2	B	22.02	27.58	22.39	29.6	22.52	29.75
3	B	22.04	27.79	22.4	29.88	22.53	29.71
4	B	22.09	27.98	22.39	29.64	22.53	29.72
5	B	22.1	28.19	22.39	29.74	22.56	29.89
7	B	22.13	28.37	22.38	29.38	22.55	29.69

Appendix F

Consent to be a Research Subject

Introduction
This research study is being conducted by Heather Smith and Dr. Tim Leishman to determine the amount of sound an audience will absorb.

Procedures
You will be seated in a chair in a reverberation chamber for approximately 1-1/2 to 2 hours. You will have adequate breaks to stand and stretch. A sound source will send noise into the room at levels which will be well within the OSHA guidelines for hearing protection even without ear plugs. As an extra precaution, however, hearing protection will be provided for all participants. The sound field will be measured with microphones in order to determine the amount of sound the audience absorbs.

Risks/Discomforts
There are no risks or discomforts associated with your participation in this research study.

Benefits
There are no direct benefits to subjects. This study will, however, aid the researchers in a better understanding of the absorptive properties of an audience.

Confidentiality
No personal information is needed for your participation in this study. A photograph will be taken of the group seated in the chairs as a means of documenting the research done and may be published in a journal article in the future. No other documentation will link you to participation in this research study.

Participation
Participation in this research study is voluntary. You have the right to withdraw at anytime or refuse to participate entirely without jeopardy to your standing in the acoustics research group or with the university.

Questions about the Research

If you have questions regarding this study you may contact Heather Smith at 422-4612, hm73@email.byu.edu or Tim Leishman at 422-1748, tim_leishman@byu.edu.

Questions about your Rights as Research Participants

If you have questions you do not feel comfortable asking the researchers, you may contact Dr. Reana Beckstrand, IRB Chair, 422-3873, 422 SWKT, reana_beckstrand@byu.edu.

I have read, understood, and received a copy of the above consent and desire of my own free will and volition to participate in this study.

Name (Please Print):_____

Signature: _____   Date:_____

Appendix G

C50 Parameter Code

```
function C50=C50(WavData,time) %WavData=IR, time=IR time

num=0;     %num is numerator
denom=0;   %denom is denominator
for iter=1:length(WavData)
   if time(iter)<=.05
      num=num+(WavData(iter))^2;
   end
   if time(iter)>=.05
      denom=denom+(WavData(iter))^2;
   end
end
C50=10*log10(num/denom);
```

C80 Parameter Code

```
function C80=C80(WavData,time) %WavData=IR, time=IR time

num=0;     %num is numerator
denom=0;   %denom is denominator
for iter=1:length(WavData)
   if time(iter)<=.08
      num=num+(WavData(iter))^2;
   end
   if time(iter)>=.08
      denom=denom+(WavData(iter))^2;
   end
end
C80=10*log10(num/denom);
```

EDT Parameter Code

```
function EDT=EDT(data,FS,ts)%data=IR, Fs=sampling freq, ts=IR time

data=data+.000000001;%keeps from getting the log of zero error
endtime=length(data);%assumes the impulse response ends before the noise
impdata=data.^2;
schrint(endtime:-1:1)=cumsum(impdata(endtime:-1:1));
pschr=10*log10(schrint./max(abs(schrint)));%+.9*max(plsqimp);
%Calculate the EDT from Schroeder curve between 0 dB down and 10 dB down
%**REF: ISO 3382:1997(E), pp 14**
dBdown0=max(pschr);
dBdown10=max(pschr)-10;
%Find the 0 dB down point
for k=1:length(pschr)
   if pschr(k)<dBdown0
     zerodB=k-1;
     break;
   end
end
%Find the 10 dB down point
for k=1:length(pschr)
   if pschr(k)<dBdown10
     tendB=k-1;
     break;
   end
end
%Calculate EDT from Schroeder integration curve
%Find a and b for the least squares regression line
x=ts(zerodB:tendB);
y=pschr(zerodB:tendB);
N=length(x);%different N from index 'n' above
a=(mean(y)*sum(x.^2)-mean(x)*sum(x.*y))/(sum(x.^2)-N*mean(x)^2);
b=(sum(x.*y)-N*mean(x)*mean(y))/(sum(x.^2)-N*mean(x)^2);
regline=a+b*x;
EDT=(max(pschr)-60-a)/b;
```
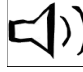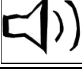
T30 Parameter Code
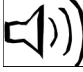
```
function T30=T30(data,FS,ts) %data=IR, Fs=sampling freq, ts=IR time

data=data+.000000001;  %keeps from getting the log of zero error
endtime=length(data); %assumes the impulse response ends before the noise
impdata=data.^2;
schrint(endtime:-1:1)=cumsum(impdata(endtime:-1:1));
pschr=10*log10(schrint./max(abs(schrint)));%+.9*max(plsqimp);
%Calculate the T30 from Schroeder curve between 5 dB down and 35 dB down
%**REF: ISO 3382:1997(E), pp 9,14**
dBdown5=max(pschr)-5;
dBdown=max(pschr)-35;
%Find the 5 dB down point
for k=1:length(pschr)
   if pschr(k)<dBdown5
      fivedB=k-1;
      break;
   end
end
%Find the 35 dB down point
for m=1:length(pschr)
   if pschr(m)<dBdown
      tfivedB=m-1;
      break;
    end
end
%Calculate T30 from Schroeder integration curve
%Find a and b for the least squares regression line
x=ts(fivedB:tfivedB);
y=pschr(fivedB:tfivedB);
N=length(x);%different N from index 'n' above
a=(mean(y)*sum(x.^2)-mean(x)*sum(x.*y))/(sum(x.^2)-N*mean(x)^2);
b=(sum(x.*y)-N*mean(x)*mean(y))/(sum(x.^2)-N*mean(x)^2);
regline=a+b*x;
T30=(max(pschr)-60-a)/b;
```

190

Appendix H

Auralization Comparisons

Position	Measured	CATT™ Preliminary	CATT™ Refined	EASE™ Preliminary	EASE™ Refined
B12	🔊		🔊		🔊
A3	🔊	🔊	🔊	🔊	🔊
A9	🔊		🔊		🔊